Controlling Mast Cell Inflammatory Mediators Secretion with Botulinum Neurotoxins

A Thesis Submitted for the degree of Doctor of Philosophy

Huria Omar Alarouse

MBBCH, MSc

Supervised by Dr. Elizabeth Seward

The University of Sheffield

School of Bioscience

2026

Acknowledgement

First and foremost, Alhamdulillah, all praises to Allah S.W.T., who is the most gracious and most compassionate for giving me the strength and perseverance to endure all the challenges encountered during my Ph.D. journey. I thank God for making my dream possible.

My deepest appreciation and gratitude must go to my supervisor, Dr. Elizabeth Seward for their invaluable continuous academic guidance, unwavering support and encouragement throughout my research project. Her expertise and constructive feedback have been invaluable in outcome of my study. I appreciate her patience and dedication, which where vital to finishing my thesis. Your advice had a good impact on my research and academic life. I have learned so much from you. Thank you for providing me with so many amazing experiences.

I would like to thank my second supervisor Dr. Andrew Peden and my advisor Proof. Elizabeth Smith and my pastoral supervisor Dr. Mohammed Nassar for their professional guidance and insightful advice and continued support that significantly improved the quality of my research.

Thank you to every member of the Andrew lab: Charlotte Leese, Ceyda Caliskan and my friend Oula El Atat and Haneen Alsehli, Sarah, Nora, they helped me throughout my research. Thanks all for your support. I wish to express my gratitude to my friend Tamara J Allcock for her assistance during my studies, especially for her support and

aid in some difficult phases of my research. Many thanks to Beka Armstrong and all her colleague in G-floor for killing mice, this will not be possible be without their help.

The work contained in this thesis may have never come together without the help, continual support, and encouragement of so many people.

A huge thanks and appreciation to my close friend Reham Filfilan for her positively and for having supported me throughout all study years that we worked together. Your friendship has meant so much to me, not only for the academic support you provided, but also for the positivity and comfort you brought to my daily life. I will always value the time we spent together during my studies, coffee breaks, and snakes we share with each other, and for the way you consistently encouraged me and reminded me to keep going during challenging times.

My heartfelt thanks to my family, especially my father for including me in his prayers all the time and believe in me in everything I do. My stepmother, my sisters, and my brothers for their constant support and love all my project. True, despite the distance between us, their belief in me has been a constant source of strength and motivation, and they were never far away from me.

I want to express my heartful gratitude to my husband, Salah, whose unwavering support, patience, and encouragement have sustained me throughout my PhD journey. His understanding and constant belief in me gave me the strength to overcome challenges and remain committed completing this work. To my dear son, Abdelrahman, thank you for being such a wonderful boy and for always trying to cheer me up.

Finally, special thanks to everyone who supported me on my journey.

Dedication

This work is dedicated to the memory of my mother (Lutfiya Ibrahim), whose love and belief in me remain the foundation of everything I achieve

Abstract

Mast cells are key mediators of allergic and inflammatory responses that exert their actions through the regulated exocytosis of preformed mediators stored in secretory granules and, the *de novo* synthesis of cytokines which are sorted into vesicles and secreted via constitutive exocytosis. Exocytosis of mast cell mediators requires the function of SNARE complexes. Botulinum neurotoxins, bacterial proteases that inhibit vesicular fusion by cleaving specific SNARE proteins.

The aim of my research was to evaluate the ability of botulinum neurotoxin serotypes B and D to inhibit mediator secretion from mast cells. I hypothesized that through their cleavage of VAMP3, these proteases could indirectly inhibit antigen-evoked degranulation by interfering with IgE receptors trafficking and directly inhibit the secretion of cytokines by inhibiting vesicular fusion. The light chain protease domains of the toxins BoNT.LC/B and D tagged with eGFP, were transfected into bone marrow derived mast cells (BMMCs). The BMMCs were then sensitised with anti-DNP-IgE, before being stimulated with either the antigen DNP or in a receptor-independent manner. Degranulation was assessed by quantifying secreted β-hexosaminidase and by flow cytometry analysis of plasma membrane levels of CD107a. Proteolysis of VAMP3 in transfected BMMCs was confirmed by western blotting. The results from these experiments showed that expression of eGFP-BoNT.LC/B and D did not significantly inhibit degranulation. Furthermore, flow cytometry analysis of cellular levels of the cytokine TNF-α, as well as ELISA quantification of secreted TNF-α, IL-6 and IL-13 from transfected BoNT.LC/B and D BMMCs showed that these cytokines

was also not impaired by the loss of VAMP-3. Taken together the results of my research indicate that the VAMP isoforms affected by these serotypes are not essential for mast cell mediator secretion and that novel engineered proteases with altered SNARE specificity will be required if these toxins are to be used to control inflammation and hypersensitivity.

Declaration

I hereby certify that all my written content and scientific figures presented in this thesis are the original work of the author, unless otherwise stated in the figure legends. All research shown was conducted and processed by the author, except where explicitly specified. All research findings, concepts, and diagrams taken from other sources have been clearly referenced, with no known infringement of copyright. This statement is true as of the date of submission.

Huria Omar Alarouse

February 2026

List of Abbreviations

Ab	Antibody
ACD	Allergic contact dermatitis
AD	Atopic dermatitis
AERD	Aspirin Exacerbated Respiratory Diseases
ALS	Amyotrophic Lateral Sclerosis
BCG	Bacillus Calmette-Guerin
BFA	Brefeldin A
BoNTs	Botulinum neurotoxins
BMMCs	Bone Marrow-Derived Mast Cells
BSA	Bovine serum albumin
Ca^{2+}	Calcium
CCL2	C-C motif chemokine ligand 2
CD	Glycosylated transmembrane protein
COX	Cyclooxygenase
DAPI	4',6-diamidino-2-phenylindole
DNP	Dinitrophenyl
ELISA	Enzyme-linked Immunosorbent Assay
ER	Endoplasmic Reticulum
FcεRI	Fc epsilon high affinity receptor for IgE
GFs	Growth factors
FGF	Fibroblast Growth Factor
eGFP	Enhanced Green Fluorescent Protein
FGRs	Fibroblast Growth Factor Receptors
HC	Heavy Chain

IBS	Irritable Bowel Syndrome
IHC	Immunohistochemistry
IgE	Immunoglobulin E
ITAM	Immune-receptor tyrosine-based activation motif
IL	Interleukin
IL-3	Interleukin-3
IL-6	Interleukin-6
IL-13	Interleukin-13
IL-33	Interleukin-33
IBS	Irritable bowel syndrome
LAD2	Cells derived from CD34+ from patient with aggressive mastocytosis
LAT1	L-type amino acid transporter 1
LAT2	L-type amino acid transporter 2
LC	Light Chain
MAPK	Mitogen-Activated Protein Kinase
MCs	Mast cells
MCp	Mast cells progenitor
MFI	Mean Fluorescent Intensity
MIP1	Macrophage Inflammatory Protein-1
MRGPRX2	Mas-related G protein-coupled receptor X2
Mut	Mutant type
PAF	Platelet-activating factor
PDGFs	Platelet Derived Growth Factors
PKC	Protein Kinase C
PLC	Phospholipase C
PMA	Phorbol 12-myristate 13-acetate
PGE2	Prostaglandin E2
RBL	Rat Basophilic Leukaemia Cell Line

SCF	Stem cell factor
SNAP	Soluble N-ethylmaleimide-sensitive factor Attachment protein
SNAP23	Soluble N-ethylmaleimide-sensitive factor Attachment protein 23
SNAP25	Soluble N-ethylmaleimide-sensitive factor Attachment protein 25
SNAREs	Soluble N-ethylmaleimide-sensitive factor attachment protein receptors
TGN	Trans-Golgi Network
TNF-α	Tumour necrosis factor-alpha
t-SNARE	Target membrane bound SNARE proteins
VAMP	Vesicle-associated membrane protein
VAMP1	Vesicle-associated membrane protein 1
VAMP2	Vesicle-associated membrane protein 2
VAMP3	Vesicle-associated membrane protein 3
VAMP7	Vesicle-associated membrane protein 7
VAMP8	Vesicle-associated membrane protein 8
VEGF	Vascular endothelial Growth Factor
v-SNARE	Vesicle bound SNARE proteins
WB	Western blot
WT	Wild type

List of figures

List of tables

Table of contents

Chapter 1: Introduction

1.1. Mast Cells

Mast cells (MCs) are long-lived, highly granular cells mainly found in tissues and rarely in the bloodstream. MCs were first discovered by Friedrich von Recklinghausen and Paul Ehrlich100 years ago. They have described MCs as fattening cells due to the presence of a large number of granules (Xu and Chen, 2015). MCs originate from hematopoietic, myeloid progenitor stem cells derived in the bone marrow which circulate to tissues where they subsequently undergo maturation and tissue-specific differentiation in response to growth factors, particularly stem cell factor (SCF) and Interleukin-3 (IL-3). MCs are concentrated in mucosal surfaces, where their proximity to the interface with the external environment makes them one of the first cells of the immune system to detect foreign antigens and pathogens. MCs are an integral part of both acquired and innate immunity, contributing to host defence and combating parasitic infections, inactivation of venoms, wound healing, pain, chronic inflammatory and autoimmune disorders. Recent research has also highlighted their complicated involvement in tumour biology, where they may exert both pro- or anti-tumour effects depending on the microenvironment (Theoharides et al., 2012) (Costela-Ruiz et al., 2018). MCs exert their functions through the secretion of a plethora of mediators with diverse biological actions. Some mediators are pre-stored in granules for rapid secretion. In contrast, others are *de novo* synthesized, and their secretion depends on the activation of receptors and signaling pathways. Best characterized amongst these receptors is the high-affinity IgE receptor (FcεRI), whose signaling leads to both degranulation and *de novo* mediator secretion. MCs are best known for their role in allergic reactions, where they are activated by the high-affinity IgE receptor FcεRI. However, inappropriate activation of MCs by innocuous antigens causes allergic reactions associated with a range of disorders, including hay fever, asthma, IBS, atopic dermatitis, and life-threatening anaphylaxis; a role for MCs in autoimmune and non-allergic inflammatory diseases is also emerging. In addition to FcεRI-mediated activation, C-KIT (CD117) regulates mast cell growth, survival, and homeostasis (Moon et al., 2014).

Current therapies are aimed either at blocking the downstream receptors for secreted MC mediators (e.g. antihistamines) or inhibiting their synthesis (e.g. anti-inflammatory steroids), both with limited success and unwanted side-effects, particularly for patients with chronic disease. Controlling MC mediator secretion could provide an important alternative approach for treating these conditions (Boyce, 2003) (Hofmann and Abraham, 2009) (Valent et al., 2022).

1.1.1 Origin and development of MCs

MCs originate initially as immature cells, i.e., mast cells progenitors (MCp) in the bone marrow. Once the progenitors migrate to the mucosal or connective tissue, they undergo a final differentiation into mature MCs located in peripheral tissue (figure1.1). During haematopoiesis, the growth of MCp is markedly controlled by transcription factors such as stem cell factor (SCF) and Interleukin-3 (IL-3) (Dahlin et al., 2015). SCF has an essential role in the biology of MCs through regulating the development and migration of MCs (Reber et al., 2015). Migration of MCp to tissues may be stimulated by inflammation, leading to an increase in the number of MC in the tissues, in chronic disease and exacerbation of symptoms (Grizzi et al., 2013). The phenotype of MCs, either mucosal or connective tissue type, is determined by the final differentiation stages. Therefore, MCs can be basically divided into connective Tissue MCs (CTMC), which express tryptases and chymase, and mucosal MCs (MMC), which express tryptases only (Kubo, 2018).

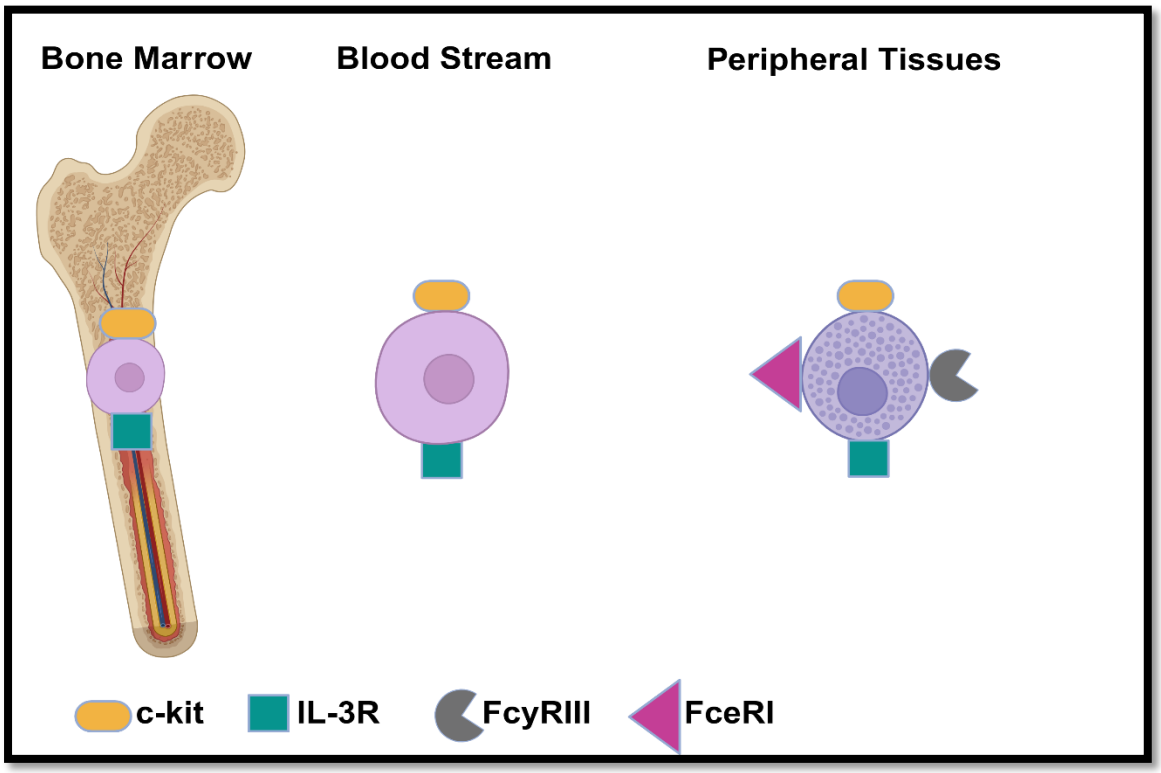

Figure 1.1: Origin and differentiation of mast cells. MCs originate from Multipotential hematopoietic progenitor cells (MHPC) in bone marrow, which are released into the bloodstream for distribution throughout the body. They then undergo terminal differentiation in the tissues. Interleukin: IL-3R, Receptor: c-Kit, High-affinity IgE receptor: FcεRI, Low affinity receptors: FcγRIII (Adapted from Grizzi et al., 2013). And created with BioRender.com.

MCs express a diverse group of receptors on their cell surface enabling them to respond to a wide variety of stimuli. Best characterised is the high-affinity receptor for IgE, FcεRI. The degranulation and *de novo* synthesis of MCs mediators occurs due to the cross-linking of FcεRI (figure 1.2) (Theoharides and Kalogeromitros, 2006). The FcεRI receptor is made up of three subunits: α,β and disulphide bonded ɣ units. The α subunit binds IgE but does not trigger downstream signalling. The β subunit contains an immune-receptor tyrosine-based activation motif (ITAM) that serves to amplify signalling. Whereas the ɣ subunits include motifs that initiate downstream signalling. Antigen-induced receptor cross linking leads to phosphorylation of the ITAMs through Lyn, Fyn, and Syc family kinases (Wu, 2011). Then the phosphorylated ITAMs provide a scaffold, recruiting adaptors and enzymes such as phosphatidyl 3-OH kinase (Siraganian et al., 2002). Besides the IgE receptor, MCs have several receptors that participate in the ability of MCs to respond to different stimuli, such as Interleukin-3R (IL-3R), C-kit, low affinity IgG receptors (FcɣRIII) and Toll like receptors (Schaefer et al., 2004); (Table 1.1).

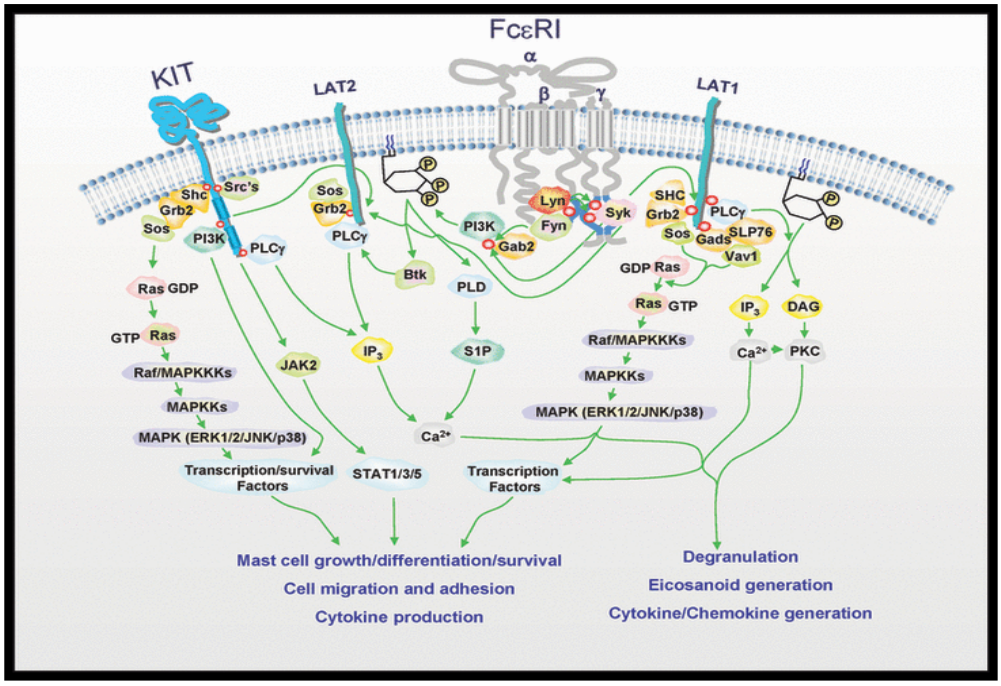

Figure 1.2: Signalling by IgE receptor in mast cells leads to the synthesis and secretion of inflammatory mediators. Diagram summarising key signalling pathways and molecules activated upon antigen-cross linking of IgE receptors. Lyn, Syk and Fyn are tyrosine kinases which initiate the signalling through phosphorylation of ITAMs on the receptor b and g subunits. Degranulation and the secretion of pre-synthesized mediators is subsequently triggered by rises in calcium and PKC signalling downstream of PLC activation. Synthesis of de novo mediators is controlled by the activation of transcription factors (adapted from (Gilfillan and Rivera, 2009).

Stimulus	Mechanism	Mediators	MC Types	References
DEGRANULATION AND *DE NOVO* SYNTHESIZED MEDIATOR RELEASE				
Antigen	FcεRI	Histamine	BMMC[a], RBL-2H3	(Burd et al., 1989),(Wang et al., 2006))
		cysLTs, PGD_2, cytokines, chemokines, NO, ROS	hPBDMC, LAD2, HMC-1, rat PMC	
Neuropeptides (substance P, CGRP, capsaicin, etc.)	NKRs	β-Hexosaminidase, cytokines, chemokines	LAD2, hPBDMC	(Kulka et al., 2008)
		cysLTs, PGD_2	BMMC	(Karimi et al., 2004),(Ogasawara et al., 1997)
		5-HT	Rabbit MC	(Reynier-Rebuffel et al., 1994)
Compound 48/80	MrgprX2	β-Hexosaminidase, cytokines, chemokines, PGD_2	BMMC	(Ogasawara et al., 1997), (McNeil et al., 2015)
Cathelicidin	GPCR	Histamine	Rat PMC	(Niyonsaba et al., 2001)
		Cytokines, chemokines, PGE_2, LTC_4	LAD2, hPBDMC	(Niyonsaba et al., 2010)
Defensins	GPCR	Histamine	Rat PMC	(Niyonsaba et al., 2001),(Befus et al., 1999),(Subramanian et al., 2013)
		Cytokines, chemokines, PGD_2, PGE_2, LTC_4	LAD2, hPBDMC	(Niyonsaba et al., 2010)
Pleurocidin	FPRL1 (GPCR)	β-Hexosaminidase, PGD_2, cysLTs, cytokines, chemokines	hPBDMC, LAD2	(Pundir et al., 2014)

Stimulus	Mechanism	Mediators	MC Types	References
A23187	Ca^{2+} ionophore	Histamine	huMC, hPBDMC	(Wang et al., 2006),(Behrendt et al., 1978)
		β-Hexosaminidase	HMC-1	(Balletta et al., 2013)
		Cytokines	FLMC	(Hosokawa et al., 2013)
Morphine, codeine	Opioid receptors	β-Hexosaminidase, cytokines, chemokines	hPBDMC, LAD2	(Sheen et al., 2007),(Shalit et al., 1987)
Monomeric IgE	FcεRI	Cytokines,	BMMC	(Kalesnikoff et al., 2001)–(Matsuda et al., 2005)
		β-Hexosaminidase	RBL-2H3	
			hCBDMC	
Nerve growth factor	Trk receptor	Histamine, PGD_2, PGE_2 cytokines	Rat PMC, BMMC	(Marshall et al., 1999),(Tomioka et al., 1988)
***DE NOVO* SYNTHESIZED MEDIATOR RELEASE WITHOUT DEGRANULATION**[b]				
Zymosan, PGN, LTA	TLR2	GM-CSF, IL-1β, cysLTs	huMC	(McCurdy et al., 2003)
	Dectin-1 receptor	ROS	BMMC	(Yang and Marshall, 2009)
PolyI:C, viral particles	TLRs	Cytokines	huMC progenitor	(Sundstrom et al., 2009)
			LAD2, HMC-1, hPBDMC, BMMC	(Kulka et al., 2004)
			KU-812	(King et al., 2000)
LPS	TLR4, CD14	Cytokines, chemokines	BMMC[c]	(McCurdy et al., 2001)
SCF	F-actin polymerization	Cytokines	hPBDMC	(Smrž et al., 2013)
	MAP kinase kinase 3	Cytokines	BMMC	(MacNeil et al., 2014)
Lectins (ex: galectins)	TIM-3	Cytokines	HMC-1	(Kojima et al., 2014)

Stimulus	Mechanism	Mediators	MC Types	References
DEGRANULATION WITHOUT *DE NOVO* SYNTHESIZED MEDIATOR RELEASE EXCEPT ROS[d]				
Complement peptides (C3a, C5a)	Complement receptors	Histamine	Human skin MC	(Erdei et al., 2004)– (el-Lati et al., 1994)
Insect venoms	Guanylate cyclase	Histamine	Rat PMC	(Mendes and Palma, 2006)
Pollutants (i.e. acrolein)		Histamine, ROS	RBL-2H3	(Hochman et al., 2014)
Persulfate salts		Histamine, ROS	LAD2, KU-812	(Pignatti et al., 2013)
Advanced glycation endproducts (AGEs)		Histamine, ROS	Rat PMC	(Sick et al., 2010)
UV radiation		Tryptase	Human skin MC	(Iddamalgoda et al., 2008)
Particulates (sodium sulfite, titanium dioxide nanoparticles, silver nanoparticles)	Non-FcεRI-mediated	Histamine, ROS	RBL-2H3 Rat MC	(Collaco et al., 2006),(Yang et al., 2010) (Wang et al., 2013)
NEITHER DEGRANULATION NOR *DE NOVO* SYNTHESIZED MEDIATOR RELEASE EXCEPT ROS				
IgG	FcγRI, RIIA, RIII	ROS	BMMC, rat PMC, hPBDMC	(Swindle et al., 2007)
Mercuric chloride ($HgCl_2$)		ROS	Rat PMC	(Wolfreys and Oliveira, 1997)
Gold compounds		ROS	Rat PMC	(Wolfreys and Oliveira, 1997)
D-penicillamine		ROS	Rat PMC	(Wolfreys and Oliveira, 1997)
Mechanical stretch		??	RBL-2H3	(Komiyama et al., 2014)
Gamma radiation		??	BMMC, hPBDMC	(Soule et al., 2007)

Table 1.1: Summary of representative receptors stimulating mediator secretion from MCs. Different receptors stimulate the release of distinct mediators. Degranulation and secretion of pre-synthesized mediators require activation of signalling pathways that causes increases in cytosolic calcium and degranulation. Secretion of *de novo* synthesized mediators is determined by the activation of transcription factors. Notably the expression of receptors varies between various sources of mast cells and mast cell models. (Table adapted from Moon et al. 2014).

1.2 MC in health and disease

MCs are known to be involved in allergic responses, and they have important roles in both immunological and non-immunological reactions as well as in different inflammatory and immunoregulatory reactions (Kumar and Sharma, 2010). MCs and their mediators are associated with different physiological and inflammatory reactions such as wound healing, angiogenesis, bone remodelling, AD, asthma, and tumour growth (Roy et al., 2021). Some studies highlighted the participation of MCs in homeostasis (Weller et al., 2011). The rapid release of inflammatory mediators following degranulation leads to immediate hypersensitivity reactions which, if localised to the skin, lead to wheal and flare reaction and if localised in airways result in mucus secretion and contraction of airway smooth muscle (Olivera et al., 2018). If systemic, as in anaphylaxis, the result can involve fatal hypotension caused by vasodilation of blood vessels. These immediate reactions are followed hours later by late-stage reactions, induced by the secretion of *de novo* synthesized cytokines and chemokines, and the influx of other circulating immune cells that amplify inflammation (Olivera et al., 2018). Chronic activation of MCs, moreover, promotes the proliferation of fibroblast and epithelial cells by the synthesis and secretion of GFs such as FGFs and PDGFs. MCs functions become harmful when they respond to prolonged stimuli which increase their number within the tissues, as in chronic inflammatory diseases such as asthma and IBS (Lyons and Pullen, 2020).

The adverse consequences of uncontrolled MC activation require mechanisms that maintain MC haemostasis. One of these mechanisms might involve PGE2, which is the most common metabolite of arachidonic acid. It is believed that PGE2 plays a significant role in maintaining airways stability in patients diagnosed with AERD (Boyce, 2022). Boyce et al 2022 concluded that the ability of endogenous PGE2 to inhibit MC activation in vivo may help alleviate some of the reinforcing effects of COX inhibitors in cases of hypersensitivity.

1.3 MCs activation

MCs are known by their main pathway of activation: IgE- mediated hypersensitivity reactions through FcεRI receptors. IgE antibodies are produced by mature B cells and most of them bind to the FcεRI receptor on the MCs' surface and cross-linking of FcεRI leads to degranulation (Gilfillan and Beaven, 2011). The FcεRI receptor for IgE has a 100 times greater affinity than IgG for the Fc of IgE. And for this reason, IgE is found binding to the FcεRI receptors on the MCs even when there are no antigens detected. Subsequently, this makes MCs response to antigen very fast (Krystel-Whittemore et al., 2015). The intensity of stimulus regulates which mediator is supplied to the area and the intensity of degranulation response; for example, low occupancy of antigen response causes chemokine release over cytokine due to various signalling pathways being stimulated: L neutral amino acid transporter 2 (LAT2) regulated signalling leads to chemokine exocytosis, whereas L neutral amino acid transporter 1 (LAT1) regulated signalling and Ca^{2+} signals are needed for MCs' degranulation response. In addition to IgE-dependent signalling and exocytosis, MCs may also be activated through IgE-independent pathways (Choi and Abraham, 2015). For example, activation of Toll-like receptors, leads to the production of *de novo* synthesised mediators without degranulation (Blank et al., 2014). As summarised in table 1 previously, there is good evidence for differential mediator secretion through activation of different receptors expressed on MCs.

1.4 MC mediators

MCs are characterised by synthesis and release of pharmacologic-active substances known as mediators (Varricchi et al., 2019). These mediators are classified into three main groups: the first group consists of pre-formed mediators which include histamine, serotonin, and heparin, and the second group, which are *de novo* synthesised includes

leukotrienes, prostaglandins, and the third group are cytokines / chemokines (figure 1.3).

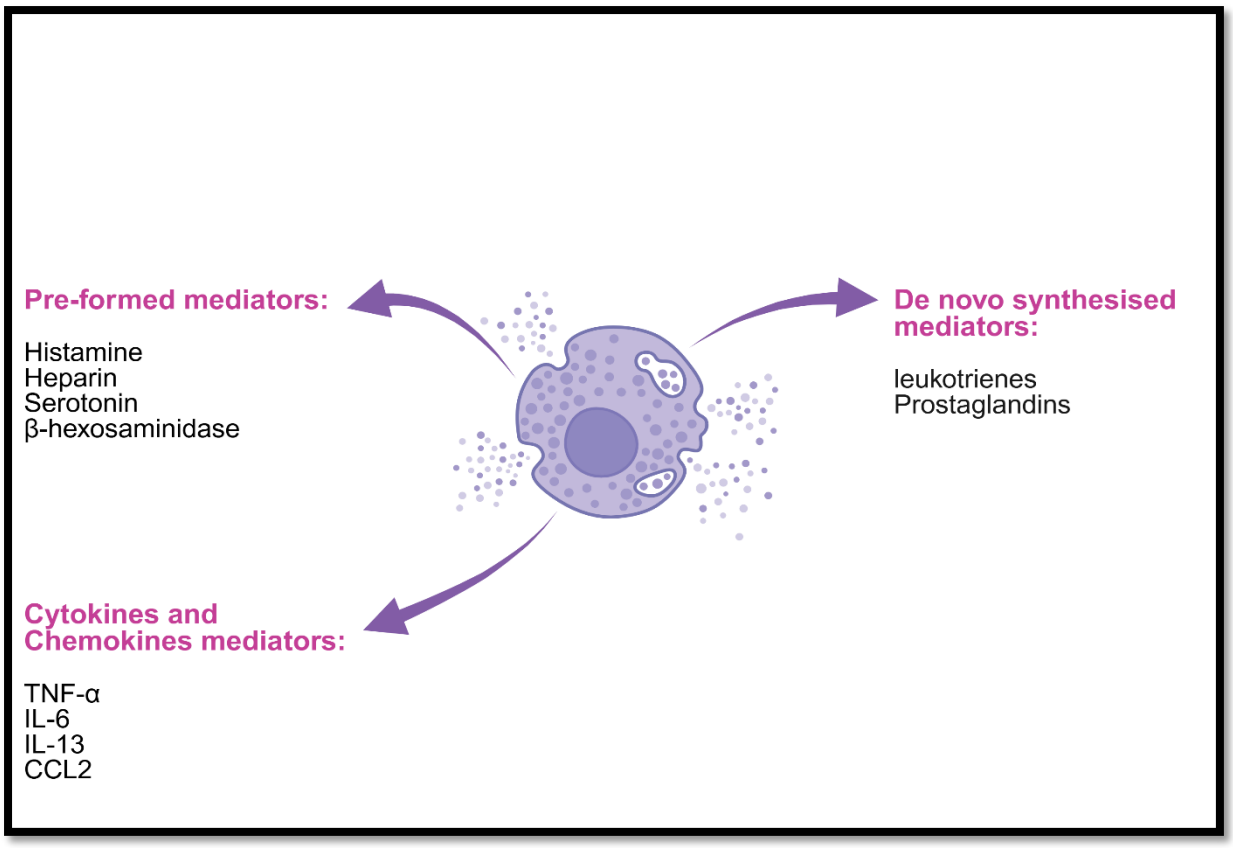

Figure 1.3: Different MCs mediators. Upon activation, MCs release a wide variety of mediators in a receptor-dependent manner, using distinct secretory pathways (adapted from Solimando et al 2022). (Solimando et al., 2022) and created with BioRender.com.

The release of pre-formed mediators into the surrounding tissues starts within seconds to minutes after the MCs activation. The sites of inflammation go through different cycles of degranulation followed by regranulation, by this pathway MCs are able to maintain the inflammatory reactions against pathogens (Choi and Abraham, 2015). Degranulation of a MC occurs as a result of increasing the level of Ca^{2+} influx (Amin, 2012). Although the terms 'degranulation' and 'exocytosis' are usually used interchangeably, there are slight differences in meaning. Degranulation is defined as the release of cell granules and when associated with MCs can be distinguished by the large intracellular granules. Meanwhile, exocytosis is known as a process in which the vesicles are released from the cell by fusion of the vesicle membrane with the plasma membrane (Moon et al., 2014). Constitutive exocytosis happens in the absence of distinguishable calcium triggers for moving the secretory vesicles to the cell membrane; secretion of chemokines, cytokines and growth factors are thought to be secreted from MC via this pathway. Two types of degranulation are observed in MCs: piecemeal and anaphylactic. Piecemeal degranulation is described as a selective release of part of the granules' content without granule to granule and/or granule to cell membrane fusion. In contrast, anaphylactic degranulation is the explosive secretion of granule contents after granule to granule and/or granule to plasma membrane fusions, processes triggered by a rise in intracellular calcium (figure 1.4) (Moon et al., 2014). For the purposes of my project, it is important to note that fusion of vesicle membranes with the plasma membrane is the final step required for the secretion of all non-lipid mediators from MCs irrespective of the stimulus activating the cells.

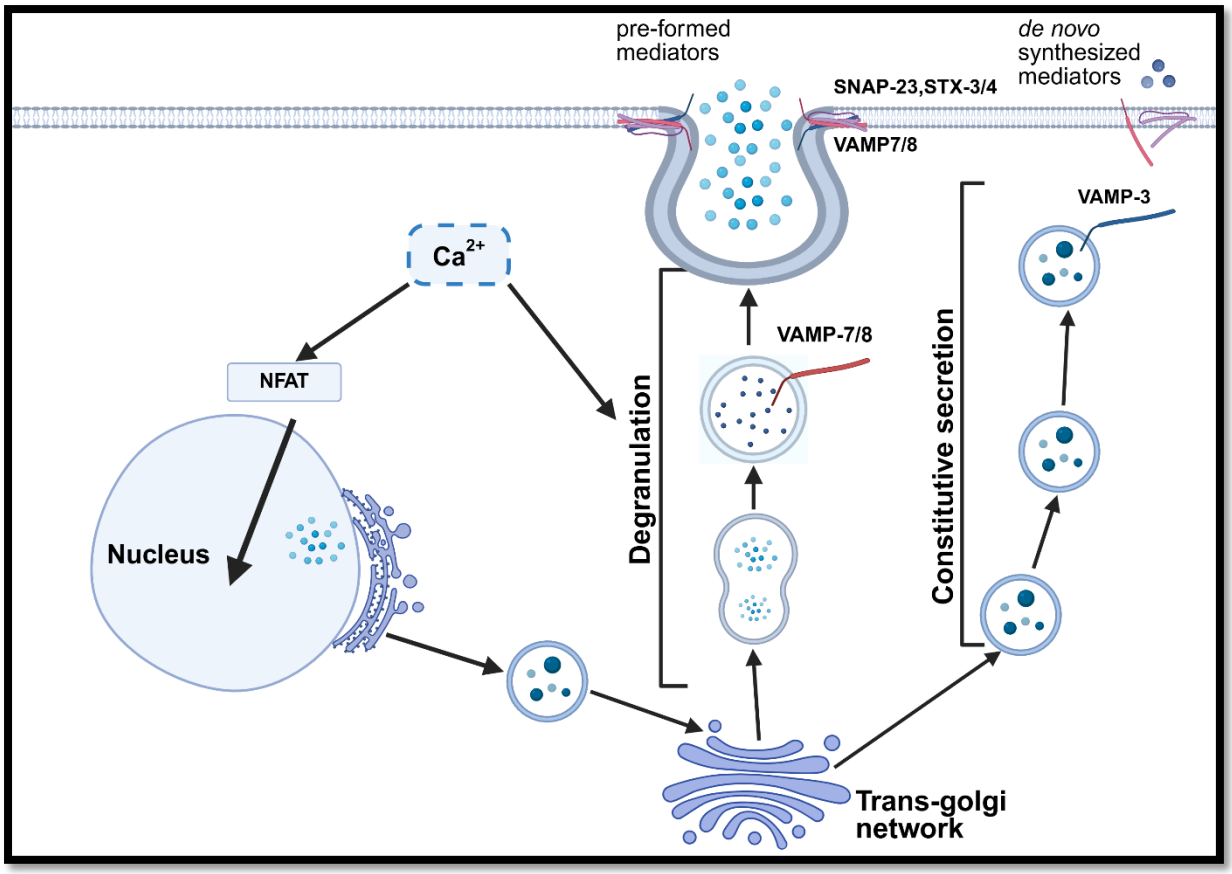

Figure 1.4: Different mediators released from various compartments in the MCs after different stimuli. MCs rapidly release prestored mediators from granules by anaphylactic degranulation or piecemeal degranulation. Mature and immature granules can fuse with endosomes and store lysosomal proteins. Exosomal secretion may also be used for secretion of some mediators. *De novo* synthesized chemokines and cytokines trafficked in secretory vesicles are released via constitutive exocytosis (adapted from Moon et al., 2014). And created with BioRender.com.

1.2. SNARE proteins

Approximately a decade ago, the SNARE superfamily became the most studied component of protein machinery that participates in intracellular trafficking and vesicle fusion (Ungar and Hughson, 2003). SNAREs are a group of proteins named (Soluble (NSF N-ethylmaleimide soluble fragment) Attachment receptor proteins that play an essential role in membrane fusion and the release of most of mediators requires the fusion of secretory vesicles with the plasma membrane (Yang et al., 2018). In humans there are approximately 38 SNARE proteins, which are of 150-300aa in length and differ in their subcellular membrane localization and control of distinct fusion reactions. All SNARE proteins are defined by having a coiled-coil domain known as the SNARE motif. This motif contains 50-70aa with hydrophobic repeats and helps in the formation of the SNARE complex. The SNARE complex is formed when 4 domains come together to make an antiparallel coiled coil (figure 1.5) (Han et al., 2017). For example, in neurons, the SNARE core complex includes 4-α helixes: (two from SNAP-25, one from syntaxin-1 and one from synaptobrevin and Syntaxin-1A) (Sauvola and Littleton, 2021). SNARE proteins classified into vesicular (v-SNAREs) including vesicular associated membrane protein (VAMP) and target (t-SNAREs) including syntaxins and soluble NSF attachment proteins (SNAP). Fusion proceeds when three Q-SNARE motifs donated by the syntaxin (Qa-SNARE) and SNAP (Qb,c-SNARE) t-SNAREs protein families, combine with an R-SNARE donated by a vesicle localised VAMP protein, from the v-SNARE family of proteins. Vesicles may be distinguished by the v-SNARE/VAMP isoform associated with them. SNAREs are essential for membrane fusion and the release of exocytotic mediators. It is now clear that SNARE proteins are essential for all types of membrane fusion within the cell, there are 36 mammalian SNAREs have been discovered (Lorentz et al., 2012). Synaptobrevin also known as vesicle associated membrane protein2 (VAMP-2), derives its name from the Latin term brevis (short) and has been identified in synaptic vesicles in rat brains, whereas VAMP-1 was purified from Torpedo californica. Additionally, two more proteins present on the neuronal plasma membrane were discovered, these known synapse-associated protein of 25 KDa (SNAP-25) and p35 (syntaxin). It became obvious that these

proteins were significantly conserved across species and thus though to be essential in neurotransmitter release (Raptis et al., 2005).

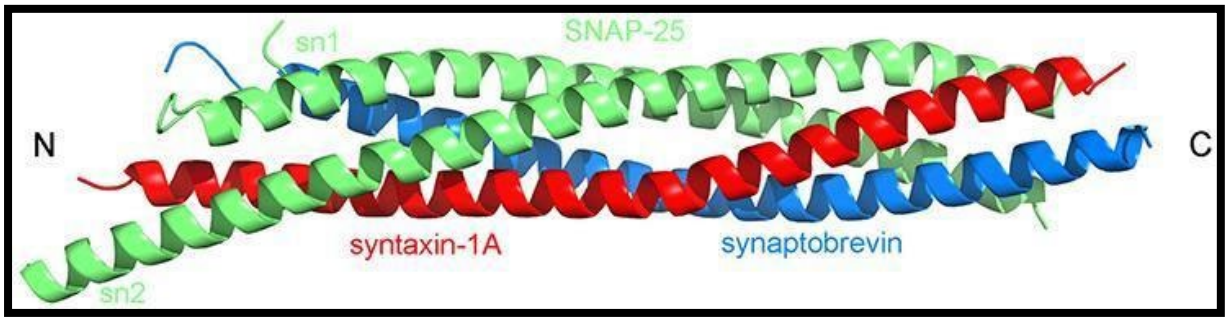

Figure 1.5: SNARE protein formation of the α helical core complex. 4 SNARE domains come together to form the core complex of a SNARE complex or SNARE pin as it is also referred to. In neurons, two SNARE domains are contributed by two SNAP-25 (green) found at the plasma membrane and one by the Synaptobrevin (blue) and Syntaxin-1A (red) found on the vesicle (adapted from Han et al., 2017).

The process of vesicle fusion contains three main phases: tethering, docking, and fusion (figure 1.6). In the tethering phase, the vesicle is brought into proximity of the target membrane, association of a vesicular VAMP with an acceptor complex of syntaxin and SNAP on the target membrane and initiation of SNARE complex formation, leads to tight docking of the vesicle to the target membrane. In the final third fusion phase, tight zippering of the SNARE complex leads to fusion of the membranes and opening of a fusion pore through which mediators stored in the vesicles may escape. Fusion of vesicle membranes with the plasma membrane may also serve to deliver integral proteins to the cell surface. Following fusion, the SNARE complex is disassembled by the action of triple-A ATPase NSF. The function and formation of SNARE complexes involved in secretion are controlled by various groups of proteins such as Sec1/Munc18- and Munc13- family members, as well as Rab GTPases. Rab proteins together with the v-SNAREs identify distinct vesicles (Dingjan et al., 2018). The mechanism of fusion is also controlled by different regulatory apparatus, such as cytoskeleton, that support the fusion and transport of granules through degranulation (Benhamou and Blank, 2010), (Menasche et al., 2021).

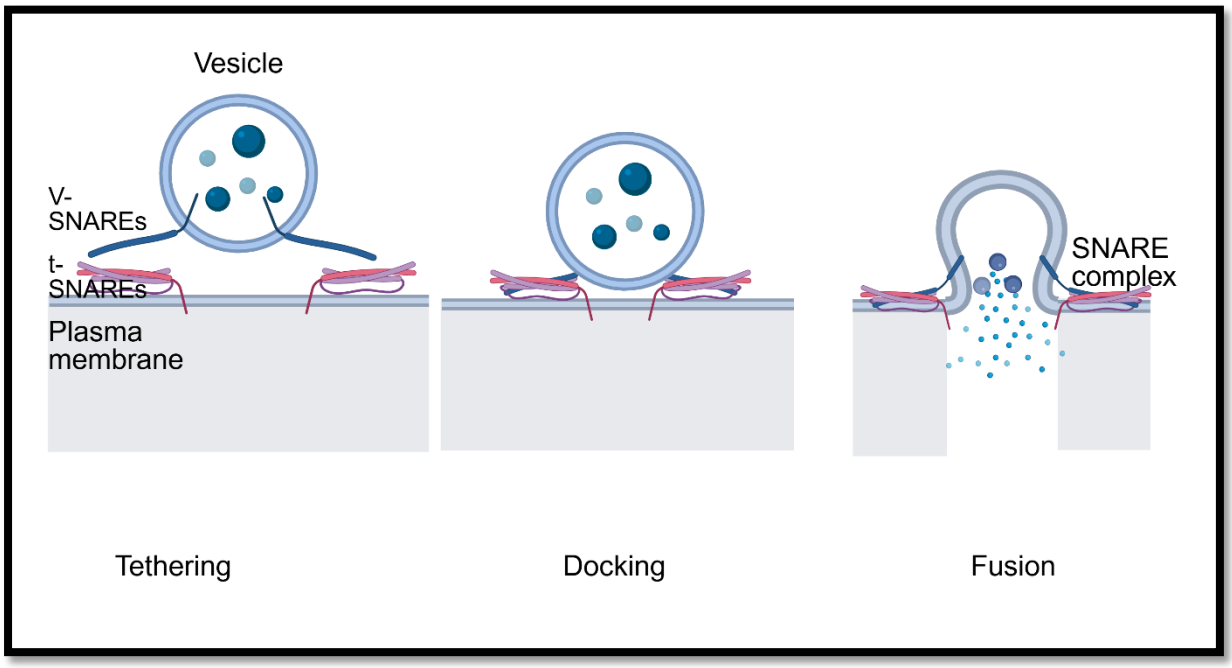

Figure 1.6: The process of fusion and formation of the SNARE complex. SNAREs function to tether, dock and promote fusion of vesicles with their target membranes. For secretion of mediators the last step must involve fusion with the plasma membrane, in order for mediators to be secreted (adapted from (Hatsuzawa and Sakurai, 2020). And created with BioRender.com.

1.2.1 SNAREs protein expression and function in MCs

The expression and function of SNARE proteins in controlling MC mediator secretion have been investigated previously using a variety of approaches (reviewed in Woska and Gillespie, 2012, Menasche et al. 2021). Previous studies have shown that MCs use t-SNAREs SNAP-23 and syntaxin-4 in IgE dependent degranulation and different VAMP proteins are expressed in MCs involving VAMP-2,VAMP-3, VAMP-7 and VAMP-8 (Tiwari et al., 2008a). The latter appear markedly colocalization with secretory granules, whereas for the others colocalization was less. Although, role of v-SNAREs in MCs degranulation is insufficient. Likewise, result regarding involvement of SNARE proteins in cytokines secretion are unavailable, with the exception that pre-formed TNF may be transferred into this site after re-endocytosis of newly synthesized mediators.

Analysis of the transcriptome of MCs for SNAREs indicates high expression of the v-SNAREs VAMP-2, VAMP-3, VAMP-8, Ykt-6 and VAMP-4, SNAP-23, syntaxin-3 and syntaxin-4 (figure 1.7). Western blot analysis of RBL-2H3 cells evidenced expression of VAMP-2, VAMP-3, VAMP-7 and VAMP-8, SNAP-23, and Syntaxin 2, 3, 4 (Paumet et al., 2000); a similar profile of expression is shown in BMMCs (Tiwari et al., 2008b) (Puri and Roche, 2008) (figure 1.8) and human mast cells (Sander et al., 2008) (figure 1.9). Immunohistochemistry experiments show that VAMP-8, and to some extent VAMP-7, are localised to granules, but not VAMP-3 (figures 1.9-1.11). VAMP-3 on the other hand has been reported by one study to co-localize with newly synthesized TNF-a (Tiwari et al., 2008b) (figure 1.11). In antigen- or calcium ionophore activated MCs, VAMP-8 is seen to move to the plasma membrane, consistent with fusion of the granules (figure 1.10). SiRNA knockdown experiments in RBL-2H3 cells (Woska and Gillespie, 2011) and studies performed on BMMCs (Puri and Roche, 2008) from VAMP-8 knockout mice confirm a functional requirement for VAMP-8 in degranulation, although notably only a partial inhibition is observed. VAMP-7 is also shown to function in degranulation, supporting the notion of subtypes of granules distinguished by their v-SNARE and mediator content (Sander et al. 2008, Puri and Roche, 2008, Tiwari & et al. 2008, Woska and Gillespie, 2011). Immunoprecipitation experiments indicate that VAMP-7 and VAMP-8 form complexes with Syntaxin-4 and SNAP-23 and that

interfering with their function either through siRNA knockdown or blocking antibodies partially inhibits degranulation (Sander et al. 2008, Woska and Gillespie, 2011). On the other hand, studies performed on mature MCs from a conditional knockout indicate a role for syntaxin-3 not syntaxin-4 in degranulation (Sanchez et al. 2019), with the implication that different SNARE complexes may regulate degranulation in several types of mast cells.

Researches have shown that human and murine mast cells contain different SNAREs including VAMP-8 suggesting VAMP-8 is important function in MC degranulation (Cao et al., 2018). The VAMP-8 is one of v-SNARE protein and known as endobrevin, is expressed in various organs involving lings, heart, kidneys, and salivary gland but not in nervous tissue. It was primarily described as v-SNARE contributed to homotypic fusion of early and late endosomes as well as in the heterotypic fusion between late endosomes and lysosomes. Recently, it has been shown to play essential role in regulated exocytosis in the pancreas and platelets. According to the previous data, underlying that MC secretory lysosomes have VAMP-8, other studies examine if this v-SNARE protein plays important role in degranulation of MC and cytokine secretion testing cells from VAMP-8 deficient mice and this study concluded that VAMP-8 is a significant fusion protein part in trafficking pathway that recognizes degranulation from cytokine secretion. Interestingly, VAMP-8 does not affect cytokine secretion, suggesting that cytokine trafficking use another trafficking pathways independent of VAMP-8 (Tiwari et al., 2008b).

Tiwari et al study describes that the v-SNARE VAMP-8 in MCs mediates the exocytosis of granular stored inflammatory mediators but has no role in the exocytosis of newly synthesized cytokines. In vitro findings indicate that IgE- stimulated release of β-hexosaminidase and histamine was inhibited by approximately 50% in VAMP-8 deficient MCs. These findings were further supported by passive systemic anaphylaxis tests, which detected a similar decrease in blood plasma histamine levels, it means a process dependent on MC activation. Conversely, TNF-α,IL-6 releases remained unaffected by the absence of VAMP-8. The findings show, VAMP-8, as a fusion protein in MCs that segregates the secretion of preformed mediators from cytokines trafficking pathways. Previous research has established that MC SGs are secretory lysosomes, which highlighting a strong connection between the endocytic and secretory pathways (Tiwari et al., 2008b). There are three obvious types of secretory granules: type I

granules: which consist from multivesicular bodies which are accessible to the endocytic pathway and its serotonin free, type II granules: contains of multivesicular and electron bodies and its accessible to the endocytic pathway and serotonin free, type III granules: consisting only electron body and inaccessible to endocytic pathway and its positive for serotonin (Tiwari et al., 2008b). Therefore, in addition to VAMP-8, there may also be other effective v-SNAREs, VAMP-2 and VAMP-7 are possible candidates as protein particles that partially colocalized with secretory granules in MCs. In macrophages the TNF-α, may involve the VAMP-3 containing recycling parts. This distinguishes between VAMP-3 containing cytokine occupied vesicle like structure versus VAMP-8 containing secretory vesicles allows interference to occur with intracellular trafficking signals controlled with VAMP-8 and other fusion proteins may potentially indicate a specific therapeutic target to selectively interfering with degranulation but not cytokine secretion in MCs (Sander et al., 2008).

Despite the crucial role of MCs exocytosis in health and disease, the underlying SNARE-SM mechanism has remained obscure (Adhikari et al., 2023). In BMMCs from VAMP-8 KO mice, one study found that VAMP-8 is partially involved in histamine release, in contrast, another study with the same approach showed the opposite result. It is possible that the VAMP-8 KO mice in the first study carried an additional mutation that interfered specifically with histamine release. Although less likely, that VAMP-8 KO mice in the second study might have carried mutations that somehow increased histamine release. Regardless, Adhikari et al study, they argue that at least in MCs, VAMP-8 is necessary for to achieve the highest levels of release for both histamine and serotonin. Knockout and rescue experiments are essential to confirm the exclusive role of VAMP-8 in the release of these amines. Furthermore, to VMAP-8, Knockdown of Munc18b leads to a marked decrease in histamine release in a way that could be reversed by adding exogenous RNAi resistant Munc18b (Lippert et al., 2007).

Unlike histamine, serotonin and β-hexosaminidase which are mediators pre-stored in secretory vesicles in resting MCs, TNF-α is both pre-stored and newly synthesized following MC activation. Adhikari et al study, showed that an increase in TNF-α levels can be measured within 10 minutes after allergen dependent stimulation, thereby making it hard to determine whether the release of TNF through the regulated secretory pathway or via the constitutive secretory way. Based on genetic analyses

of TNF release using primary MCs in KO mice, they seemed to exclude any role for syntaxin 3, 4, or VAMP-8, these three SNAREs are widely responsible for the exocytosis of MC granules. Furthermore, their research reinforced the view that VAMP-8 is dispensable in TNF-α secretion from MCs, which elicited the question of why depletion of VAMP-8 decreased serotonin secretion but not TNF-α release. Despite the knockout of VAMP-8 in BMMCs, did not completely reduce allergen induced degranulation, however expression of VAMP-3 increased, and the VAMP-3 is involvement in mediator release is conceivable. Therefore, reducing VAMP-3 could have dual effect on MC exocytosis, while this directly leads to decrease the level of MC exocytosis and degranulation via inhibiting vesicle fusion, furthermore, amplifies IgE dependent signalling and consequently indirectly promoting an increase in mediator synthesis and release. This observation explains why the secretion decrease in knockdown VAMP-3 cells was time dependent and it could also explain why Adhikari et al study has not found any VAMP-3 related defect of MCs exocytosis in their knockout studies.

In contrast to the many studies investigating SNARES regulating degranulation, very few is known about the SNAREs controlling secretion of *de novo* mediators from activated MCs. Decreasing expression of VAMP-3 has been reported to attenuate TNF-α but not IL-6 secretion (Tiwari et al., 2008b), (Mishima et al., 2022).

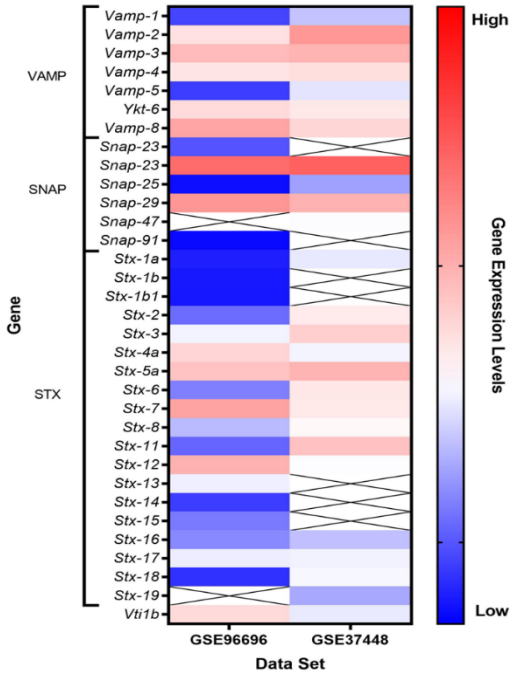

Figure 1.7: SNARE gene expression in mouse mast cells. Heat map displaying the expression levels of SNARE genes within murine mast cells from two separate data sets : GSE96696 and GSE37448 (log_2 transformed data). The 'X' marked boxes indicate no data was recorded for this gene within that data set. The GSE96696 samples are BMMCs harvested from C57BL/BJ mice and were analysed using Illumina Microarray Technology. The GSE37448 samples are skin MCs harvested from C57Bl/BJ mice and were analysed using Affymetrix Microarray technology. All samples are unstimulated/resting mast cells. The gene expression levels are presented using a colour scale, where blue represents low gene expression and red shows high. The highest level of gene expression within the colour scale is the highest log_2 transformed value across all the genes analysed from both data sets (GSE96696 resting BMMC: Fcεr1a, 14.68482). The lowest is the smallest log_2 transformed value across all the genes analysed (GSE96696 IgE 1 µg / ml BMMC: *Stx-1a*, 3.524967). Data analysis and figure from I Houton/Seward laboratory.

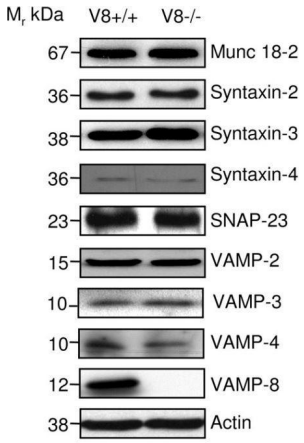

Figure 1.8: SNARE expression in rodent MCs. Western Blot image shows expression of SNARE proteins in BMMCs derived from wild type (V8+/+) and VAMP-8 knockout mice (V8-/-). (adapted from Tiwari et al. 2008).

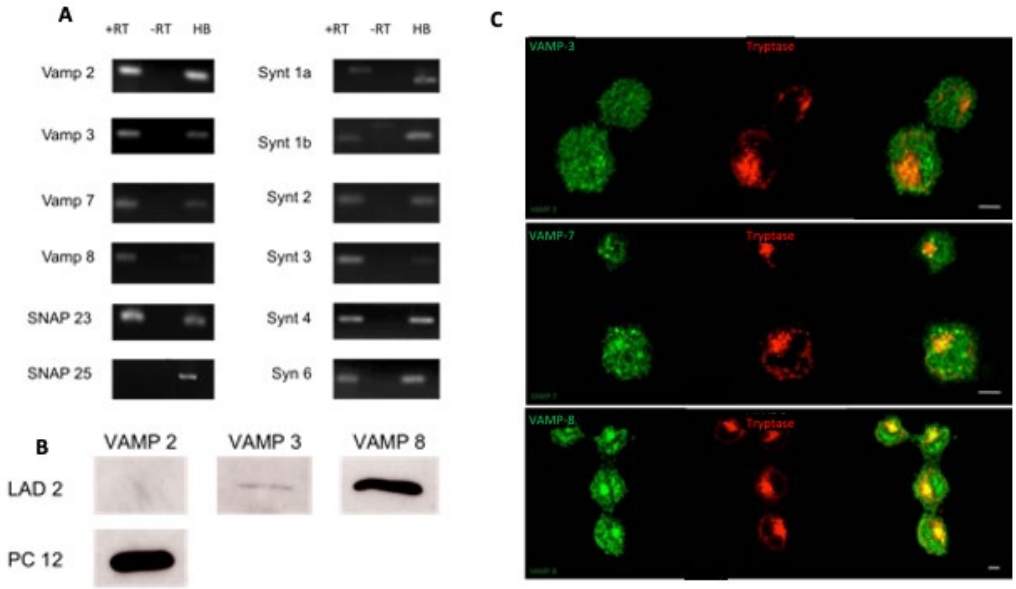

Figure 1.9: SNARE expression in human MCs. VAMP-8, and some VAMP-7 but not VAMP-3 localises to granules. (A) RT-PCR shows that the mRNA of all tested SNAREs apart from the neuronal SNAP-25 are present in the LAD2 human MC cell line. RT = Reverse transcriptase. HB = Human brain cDNA control. (B) Western blot analysis confirmed the expression of VAMP-3, VAMP-7 and VAMP-8. (C) Immunocytochemistry shows that VAMP-8, and some VAMP-7 but not VAMP-3 colocalizes with tryptase, a MC granule marker. The same SNAREs were also shown to be expressed in MCs isolated from human lungs. Data from R Friend, Seward lab.

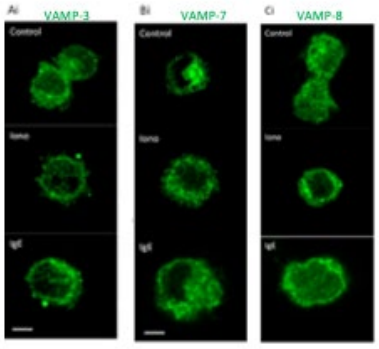

Figure 1.10: VAMP-3 and VAMP-8 relocate to the plasma membrane in activated MCs. Immunocytochemistry showing the distribution of VAMP-3 (A), VAMP-7 (B) and VAMP-8 (C) in representative resting LAD2 cells (control, top row) and after 20 min of activation with either 1 μM ionomycin (middle row) or 10 ug/ml anti-IgE (bottom row), to induce FcεRI crosslinking. VAMP-3 and VAMP-8, but not VAMP-7 were observed to redistribute to the plasma membrane following MC activation. Data from R Friend, Seward Lab.

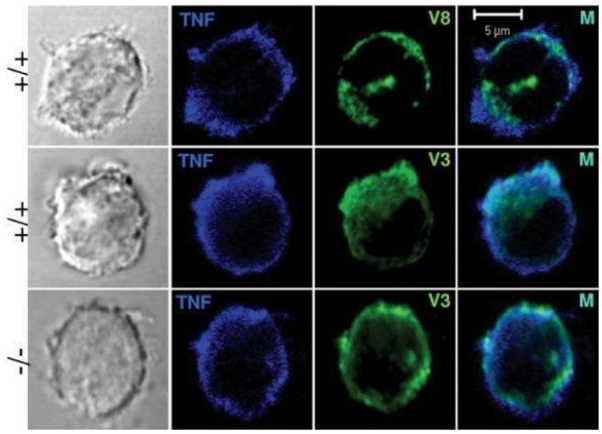

Figure 1.11: VAMP-8 and VAMP-3 identify distinct vesicular compartments in MCs. Fluorescent images of BMMCs immunolabeled with anti-VAMP-3 or anti-VAMP-8 and anti-TNF-α in cells isolated from wild type or VAMP-8 knockout mice. Cells were stimulated with IL-1β to synthesise TNF-α; colocalization of the cytokine is observed with VAMP-3, not VAMP-8. Data adapted from Tiwari et al. 2008.

1.2.2 SNAREs in diseases

SNARE proteins are essential for facilitating membrane fusion, a process vital to numerous biological activities. Due to its crucial function, the inhibition of SNARE proteins is hypothesized to be involved in the several illnesses. The role of SNARE proteins in several diseases, including immunological disorders, neurological conditions, and metabolic diseases, underscores their significance in preserving cellular homeostasis (Han et al., 2017).

It is not currently known the relation between the SNARE protein and different disorders by the effect of mediators released from activated MCs. For example, hyperpigmentation a major aesthetic issue for many patients has a limited effective treatment option often involving substantial recovery. However, recent research indicates that in addition to their muscle relax effects BoNTs can markedly influencing skin quality (Malik et al., 2025). One study describes that the BoNT/DC is a novel potential therapeutic agent for treating hyperpigmentation and their results shows that BoNT/DC effectively decrease intracellular melanin by interfering with melanosome maturation with VAMP-3 cleavage likely playing a key role. Significantly, BoNT/DC can markedly affect cellular biology in non-neuronal cells such as melanocytes through cleavage of one or more SNARE proteins when compared to BoNT/A serotype that can impact on non-neuronal cells such as fibroblast and macrophages through binding to cell membrane receptors such as FGFRs. It is important to expand the involving the SNARE proteins in melanogenesis as it has been previously shown that VAMP-2 is present in melanocytes. This study provides the first evidence that VAMP-3 is expressed in these cells and shows that the BoNT/DC cleaves both proteins within melanocyte (Malik et al., 2025). Briefly, for the first time, the data from this study that the non-neuronal effect of a native toxin through cleavage of a SNARE protein. Moreover, VAMP-3 was also identified as a novel target for hyperpigmentation treatments, which may be targeted SNARE blocking agents in combination with BoNT/DC (Malik et al., 2025).

VAMP-2 also known as synaptobrevin-2 Syb2, is an R-SNARE protein, highly expressed in neurons and localized to vesicles that play a crucial role in neurotransmitter release. VAMP-2 binds with SNAP-25 (a Qb-c SNARE) and syntaxin-1 (syn1, a Qa SANSRE) present on the plasma membrane to form SNARE complex. VAMP-2 is participated in both synaptic vesicle endocytosis and exocytosis, subsequently loss of VAMP-2 in Drosophila leads to neurodegeneration also, perturbations of the N-terminal domain of VAMP-2 inhibit neurotransmitter release (Margiotta, 2021). Recent studies highlighted the relationship between SNARE proteins and neurodegenerative diseases and most of them are listed in Table 1.2 as well as the molecules that targets by SNARE proteins and their functional in neurodegenerative disorders. Neurodegenerative diseases are often characterised by the accumulation of protein aggregates marked by the presence of ubiquitin. Liu et al have examined the impact of ubiquitination on SNARE complex consists of VAMP-2,SNAP-25 and syntaxin-1 in the spinal cord and brain of transgenic mice and the modification of this complex due to the alteration of VAMP-2 with a non-cleavable N-terminal ubiquitin molecule might cause adult-onset paralysis and neurodegeneration. This SNARE complex plays an essential in the chemical synaptic transmission. Despite this, VAMP-2 ubiquitination caused progressive synaptic transmission impairment at the neuromuscular junction and subsequently motor nerve ends degenerated. It is also interesting to note that VAMP-2 ubiquitination changed synaptic vesicle endocytosis and membrane trafficking. Although ubiquitination, syntaxin-1 did not show muscle denervation. In contrast, modulated VAMP-2 even when ubiquitinated was still able to bind with SNAP-25 and syntaxin-1. Consequently, a specific role for VAMP-2 in neurodegeneration in ALS has been established and involving altered endocytosis, retention at the TGN and /or ER and reduced synaptic transmission (Margiotta, 2021).

SNARE Type	Name of the SNARE Protein (Alternative Name)	Neurodegenerative Disease	References
Q_a (syntaxins)	Syntaxin-1 (HPC-1)	AD, PD, ALS	(Liu et al., 2015),(Pham et al., 2010),(Mingazov and Ugrumov, 2016),(Almandoz-Gil et al., 2018),(Darios et al., 2010),(Law et al., 2016),(Santos et al., 2017),(Yang et al., 2015),(Smith et al., 2000),(Burre et al., 2014),(Garcia-Reitbock et al., 2010),(Agliardi et al., 2021)
	Syntaxin-2 (Epimorphin)		
	Syntaxin-3		
	Syntaxin-4		
	Syntaxin-5	AD, PD	(Hernandez-Zimbron and Rivas-Arancibia, 2016),(Suga et al., 2015),(Suga et al., 2004),(Rendon et al., 2013),(Tomas et al., 2021)
	Syntaxin-7		
	Syntaxin-11		
	Syntaxin-13 (Syntaxin-12)		
	Syntaxin-16		
	Syntaxin-17	AD, PD	(McLelland et al., 2016),(Bustos et al., 2017)
	Syntaxin-18		
Q_b	GS-27		
	GS-28		
	Vti1a		
	Vti1b		
Q_c	BET1	AD	(Suga et al., 2015)
	GS-15		
	Slt1		
	Syntaxin-6	PD	(Beilina et al., 2020)
	Syntaxin-8		
	Syntaxin-10		
Q_{b-c}	SNAP-23 (Syndet)		
	SNAP-25	AD; PD; ALS	(Liu et al., 2015),(Pham et al., 2010),(McLelland et al., 2016),(Almandoz-Gil et al., 2018),(Darios et al., 2010),(Santos et al., 2017),(Burre et al., 2014),(Zhang et al., 2018),(Agliardi et al., 2019),(Yun et al., 2013)
	SNAP-29 (GS-32)		

SNARE Type	Name of the SNARE Protein (Alternative Name)	Neurodegenerative Disease	References
R	VAMP1 (Synaptobrevin 1)		
	VAMP2 (Syb 2)	AD; PD; ALS	(Liu et al., 2015),(Pham et al., 2010),(Almandoz-Gil et al., 2018),(Darios et al., 2010),(Burre et al., 2014),(Agliardi et al., 2021),(Kawamata et al., 2014),(Choi et al., 2013),(Choi et al., 2018),(Lou et al., 2017),(Sun et al., 2019),(Lai et al., 2014)
	VAMP3 (Cellubrevin)		
	VAMP4	PD	(Beilina et al., 2020),(Brown et al., 2021)
	VAMP5		
	VAMP7 (Ti-VAMP)	PD	(McLelland et al., 2016)
	VAMP8 (Endobrevin)	AD, PD	(Bustos et al., 2017),(Pilliod et al., 2020),(Emmanouilidou et al., 2016),(Benskey et al., 2016)
	YKT6P	PD	(Thayanidhi et al., 2010)
	SEC22b (ERS-24)	PD	(Thayanidhi et al., 2010)
Unclassified	SEC22a		
	SEC22c		
	SEC20 (Bnip1)		

Table 1.2: Human SNARE proteins, classification and relevance to neurodegenerative diseases. Table from (Margiotta, 2021).

A key feature of neurodegenerative diseases is the dysregulation of vesicle trafficking caused by changes in some proteins that control exocytosis, endocytosis and neuronal survival. However, the mechanism through which SNARE complex affect leads to neurodegeneration remains unclear. Targeting SNAREs to modulate neurotransmitter release and vesicle fusion indicates a potential therapeutic strategy. Moreover, regulating SNARE complex formation and activity may be essential for preventing the intracellular accumulation of specific proteins and/or release of neurotoxic particles (Margiotta, 2021).

1.3. Botulinum neurotoxins (BoNTs)

1.3.1 Structure

BoNTs are defined as protein substances produced by neurotologic species of spore-forming and gram-positive anaerobic bacteria of the genus Clostridium (Clostridium botulinum). Clostridium botulinum produces eight exotoxins that are antigenically distinct (A,B,C1,C2, D, E, F and G (Nigam and Nigam, 2010). All serotypes inhibit neural transmission by blocking acetylcholine release, the role of acetylcholine at the neuromuscular junction resulting in muscle paralysis.

BoNTs consist of ~150 KDa chain that includes heavy chain HC (100 KDa) and light chain LC (50 KDa), separated by a translocation domain (figure 1.12) (Pirazzini et al., 2017). From the chemical aspect, the BoNTs are contained in three main domains consisting of the catalytic, receptor binding, and translocation domain. The HC contains the receptor and translocation domains, whereas the LC contains the catalytic domain (Lim et al., 2019). The toxin is taken up into the cells through receptor-mediated endocytosis by binding to a protein receptor (Ben David et al., 2013). Various serotypes bind with different protein receptors. For example, BoNT/A binds to SV protein 2 (SV2) and BoNT/E binds to glycosylated variants of SV2 A and B (Ben David et al., 2013).

All BoNTs serotypes are produced in a relatively inactive form as a single polypeptide chains that have a molecular mass of 150KDa each with a highly similar amino acid sequences among the toxin serotypes (Nigam and Nigam, 2010).

Basically, despite the differences between serotypes A1 and B1 they are the only ones that are used in clinical application. Although both have a similar duration of actions, B1 is used less as an increased dose is needed to obtain the same results. The other BoNT serotypes have limited medical uses. Most research confirms that the pre-clinical results support the chemical variations between the BoNTs serotypes (Burgin et al., 2021). Some BoNTs serotypes, such as BoNT/A,B,F and E, cause botulism in humans, with the lethal dose being around 1 ng/kg body weight (Ben David et al.,

2013). Those cases show symptoms of peripheral neuromuscular blockade and flaccid paralysis, which is caused by inhibiting neurotransmitter release, commonly at peripheral cholinergic nerve terminals, of both the autonomic nervous and skeletal system (Masuyer et al., 2018).

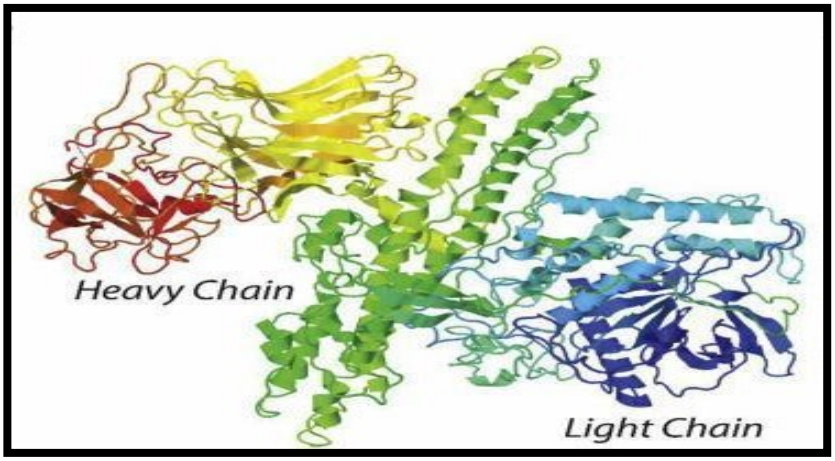

Figure 1.12: Structure of BoNT toxin. The schematic structure shows the heavy chain (green, yellow, and red) and light chain (blue) (Lim et al., 2019)

1.3.2 Mechanism of BoNTs action

When BoNTs are ingested, the accessory proteins are separate from HC and LC which are endocytosed by neuronal cells. The HC consists of two receptor binding domains which bind specific to synaptic proteins and gangliosides at the cell membrane of presynaptic space. The HC binds irreversible and selective to the high affinity receptors at the pre-synaptic part of cholinergic neurones. The toxins are then internalised by receptor mediated endocytosis (Fonfria et al., 2018a). The LC bind with various proteins such as SNAP-25, VAMPs and syntaxin in the nerve terminals to inhibit fusion of acetylcholine vesicles with the cell surface. After that, the pH inside the endocytic vesicle is decreased, resulting in changes in the toxins. The disulphide bonds that connect the HC to the LC are reduced. These changes then permit the LC to translocate into the cell cytoplasm. Subsequently, these toxins prevent neurotransmission by cleavage of SNARE proteins which are responsible for fusion of synaptic vesicles (Pirazzini et al., 2017).

The peak of the BoNTs paralytic effect appear from four to seven days after injection. The damaged nerve endings do not degenerate, but the inhibition of neurotransmitter release irreversible. Recovery of nerve function which typically takes two to three months occurs through sprouting of nerve ends and production of new synaptic contacts (Nigam and Nigam, 2010).

BoNTs target four specific sites within human body: autonomic ganglia, neuromuscular junction, postganglionic sympathetic nerve endings and postganglionic parasympathetic nerve endings. Different SNARE proteins are targeted by various serotypes of BoNTs; this property may be exploited to regulate mast cell degranulation and/or constitutive secretion. The LC of BoNTs that may selectively cleave SNARE proteins essential for MCs mediator secretion are summarised in (Table 3). For example, BoNT/A cleaves SNAP-23, BoNT/B, BoNT/D, BoNT/F, BoNT/G, and BoNT/X cleave VAMP-3. BoNT/X, which contains the lowest consensus identity with other BoNTs is similar to BoNT/B/F/G, in

that it cleaves VAMPs-1,2,3 but in addition BoNT/X is the only neurotoxin that cleaves VAMP-4,5 and Ykt6 (Zhang et al., 2017).

SNARE Protein	Botulinum Neurotoxin Serotype											Target?	
	A1	B1	C/CD	D/DC	E1	F1	FA	G	X	Wo	En	Exocytosis	Constitutive Secretion
VAMP-1		$Q^{78}F$		$K^{61}L$		$Q^{60}K$	$L^{56}E$	$A^{83}A$	$R^{68}A$ (R)	$W^{92}W$ (R)	$A^{69}D$ (R)		
VAMP-2		$Q^{76}F$		$K^{59}L$		$Q^{58}K$	$L^{54}E$	$A^{81}A$	$R^{66}A$ (R)	$W^{89}W$ (R)	$A^{67}D$ (R)		
VAMP-3		$Q^{63}F$		$K^{46}L$		$Q^{45}K$	$L^{41}E$	$A^{68}A$	$R^{53}A$ (R)	WW	$A^{54}D$ (R)	Yes	Yes
VAMP-4		NC		NC		NC	NC	NC	$K^{87}S$ (R)	NC	NC		
VAMP-5		NC		KL		NC	NC	NC	$R^{40}S$ (R)	NC	NC		
YKT-6		NC		KL		NC	NC	NC	$K^{173}S$ (R)	NC	NC		Yes?
VAMP-7		NC		NC		NC	NC	NC	NC	NC	NC		
VAMP-8		NC		NC		NC	NC	NC	NC	WW	NC	Yes?	
SNAP-23	$T^{202}R$ (M)		NC		$K^{185}I$ (M)						$K^{58}D$ (R)	Yes?	
SNAP-25	$Q^{197}R$		$R^{198}A$		$K^{180}I$						$K^{63}D$ (R)		
SNAP-29	NC		NC		NC								
SNAP-47	NC		NC		NC								
STX-1A			$K^{253}A$										
STX-1B			$K^{252}A$										
STX-2			$K^{253}A$ (M) $K^{254}A$ (R) $K^{252}A$ (H)										
STX-3			$K^{253}A$									Yes	
STX-4			NC										
STX-5			NC										
STX-6			NC										
STX-7			KA									Yes?	
STX-8			NC										
STX-10			NC										
STX-11			KA										
STX-12			KA										
STX-15			NC										
STX-16			KA										
STX-17			KA										
STX-18			NC										
STX-19			NC										

Table 1.3: Different SNARE proteins targeted by various serotypes of BoNTs. The yellow shading indicates where the peptide bonds in human, rat, and mouse isoforms of SNAREs have been experimentally proven to be cleaved by the indicated BoNT. The letter in brackets indicates which species the cleave site was experimentally proven. H is human, M is mouse and R is rat. The conserved or non-conserved peptide bonds which were proven to be non-cleavable in experimental steps are displayed by NC in pink colour. The green shading indicates suspected cleavage sites that have not been experimentally proven. The last two columns indicated the predicted/speculative impact that cleavage of the indicated SNARE would have on regulated exocytosis and degranulation in MCs and constitutive secretion of de novo mediators. This table was compiled using information from Pirazzini et al (2017), Zhang et al (2018), and Zhang et al (2017), predicted affects in exocytosis by I Huston/Seward lab.

Mutagenesis of BoNT LCs and engineering of receptor binding domains have been used to alter the substrate specificity and extend the cells that may be targeted. For example, introduction of mutations into BoNT/A and /E have successfully redirected the proteases to cleave SNAP-23 (Chen and Barbieri, 2009), (Sikorra et al., 2020) and BoNT/F to VAMP-7 (Blum et al., 2021). Replacing the receptor binding domain of BoNT/D with IL-1β has been shown to successfully redirect the toxin to macrophages and inhibit IL-6 secretion (Tang et al., 2019). Similar approaches should prove effective in developing BoNTs to selectively inhibit mediator secretion from MCs.

1.3.3 Therapeutic uses of BoNTs

In the last 15 years, BoNTs has become an increasingly effective treatment in different conditions such as strabismus and many movement disorders. Although clinical reports suggest many exciting possibilities for additional applications, but many of these uses have remained anecdotal. However, BoNTs is an attractive option in some chronic cases due to its effectiveness, relative safety and its reversible action. In some conditions, it can be used as an optional way to surgical procedure (Munchau and Bhatia, 2000).

In most dermatological conditions such as atopic dermatitis, psoriasis and rosacea, the pruriceptive itching is commonly seen as a result of stimulation of nerve fibres located in the epidermis. pruriceptive itch might be experimentally induced by different exogenous and endogenous stimuli. Consequently, these stimuli lead to degranulate MC and release histamine which causes itch by binding to and stimulating C fibres. Other mediators released from MCs such as prostaglandin, serotonin could enhance the effects of histamine caused itch sensation (Ramachandran et al., 2018b). BoNT/A and B have been commonly used in clinical research for explaining the mechanisms by which they might block pain transduction in different conditions (Chen, 2012).

Clinical applications for BoNTs are found to use in different disorders caused by muscle over contractility and neuromuscular conditions including dystonia and spasticity, pain management including chronic migraines, urological disorders such as urinary incontinence, ophthalmology including strabismus and blepharospasm, and cosmetic applications as correct the facial wrinkles and lines and treat the alopecia (Chen, 2012). BoNTs has been used in treated of conditions like tics and tremors, today, medical clinics use BoNT/A most often for conditions such as spasticity, hemifacial spasm (Munchau and Bhatia, 2000).

Recent research discovering that BoNT/A can restore skin cells and improve global skin cases implies that BoNTs effect extend beyond their specific action on SNARE proteins in neuronal endings. Moreover, BoNTs have shown in different studies to have

protective effects on wound healing and skin flaps, hypertrophic scars and anti-inflammatory and anticancer effects also observed. To reduce the risk of iatrogenic effects, topical BoNTs application is a potential treatment way for elderly patients (Rasetti-Escargueil and Palea, 2024). The research demonstrated improved gait in cases diagnosed with cerebral palsy with progressive dynamic equinovarus or equinovalgus foot deformities. Treating children with cerebral palsy in their early stage, specifically during the developmental stage of walking skills, improves prognosis and can often help to avoid surgical intervention for bony torsion. For those with multiple sclerosis, BoNTs can reduce thigh adductor contractions, thereby improving sitting, positioning and urethral catheterisation (Munchau and Bhatia, 2000).

BoNTs are classically known to inhibit the release of neurotransmitter by blocking exocytosis. It has also been shown that BoNTs can block neuronal hyperexcitability driven by ionic currents, indicating that BoNTs act on more than just SNARE protein cleavage. The injection of BoNTs leads to decrease of neurogenic inflammation in different diseases such as neuropathic neuralgia and phantom pain. However, translating of experimental study from healthy volunteers experiencing acute pain to the context of sustained pathological pain is challenging as chronic pain is characteristically more sever. Moreover, the possibility the central action of BoNT/A cannot be excluded, given the long-term pain relief noticed after a single dose injection. More research is needed to explain how BoNT/A affects the neuropathic pain. Future works to improve BoNT safety should include the development of toxin subtypes with selective nociceptive fibres targeting and the use of cutaneous delivery techniques (Rasetti-Escargueil and Palea, 2024). In most dangerous cases of laryngeal dystonia, treatment with BoNT/A effectively restored normal or near normal voice in cases with adductor type (strained or strangled voice) and with patients having abductor type observed considerable improvement (breathy or whispery voice) (Munchau and Bhatia, 2000). The injections of BoNT/A can be used either via indirect laryngoscopy or percutaneously with electromyographic. Patients may have a mild adverse symptom such as hypophonia, hoarseness and mild aspiration of fluids. The use of BoNTs has also effective in treating hemifacial spasm and before start treatment, brain MRI is necessary to exclude structural lesions in the cerebello-pontine region. The injections

are effective in most of cases with improvement and the effect longer approximately five months compared to patients diagnosed with dystonia. For example, in cases of involuntary eye closure, treatment is individualized by injection only orbicularis oculi, the muscle whose contractions are most affecting in these patients. A common side effect is excessive weakening of the facial muscles. While BoNTs has been used to treat a wide range of conditions and its licensed applications in the UK are approved and currently prescribed in the clinic (Munchau and Bhatia, 2000).

Research question:

To what extent do BoNT-LCs inhibit the secretion of pre-formed granule, and *de novo* synthesized inflammatory mediators from activated MCs, and what are the specific target SNARE proteins and receptor-trafficking pathways driving these effects?

Hypothesis:

The secretion of inflammatory mediators from activated MCs may be inhibited by BoNT-LC directly by preventing SNARE-dependent fusion of vesicles with the plasma membrane and by indirectly by inhibiting the trafficking of activating receptors to the plasma membrane.

Thesis aims:

This study aims to evaluate the effects of BoNTs LC on the secretion of granule mediators and *de novo* synthesised mediators from activated MCs and to identify the putative target SNARE proteins(s) responsible for any inhibitory effects.

Chapter 2: Materials and Methods

2.1 Primary cell cultures

2.1.1 RBL-2H3

RBL-2H3 mast cells line (ATCC) was thawed from -80˚C under warm tap water for 2-3 minutes. The RBL-2H3 cells were grown in complete Modified Eagle's Medium (MEM) without Sodium Pyruvate (Gibco Life Technologies, Netherlands, Cat. No. 21090-022), Supplemented with 10% heat-inactivated Foetal Bovine Serum (FBS), and 1% GlutaMAX^{TM} (Gibco), and 100U mL^{-1} penicillin&100 µg mL^{-1} streptomycin (Gibco). Cells were kept in a humidified incubator at 37 °C in a 5% CO^2. Media was changed every two to three days and using Trypsin agent (detachment agent) (Gibco) for five minutes, and the cell density was kept at 0.5-1X10^6 viable cells/ml.

2.1.2 MC9

The MC/9 (CRL-3616) mast cell line was obtained from ATCC® and was cultured following their guidelines. MC/9 cells were grown in Dulbecco's Modified Eagle's Medium (DMEM) (Gibco, 11995-065), containing 2 mM L-glutamine, 4.5 g/L glucose and 110 mg/L sodium pyruvate, supplemented with additional 2 mM L-glutamine (Gibco®, 25030-081), 50 µM 2-mercaptoethanol (Gibco®, 31350-010), 10% fetal bovine serum(FBS) (Gibco, 10500-064),10% Rat T-STIM (Corning®, DLW354115) and Penicillin-Streptomycin (Pen/Strep; 100 µg/L) (Gibco™, 10378-016). The cells were kept in T75 flask (Thermo Fisher, 156800) in a humidified incubator at 37 °C in a 5% CO^2. Media was changed every three days, and the cell density was maintained at 0.5-1X10^6 viable cells/ml.

2.1.3 Isolation and Culturing of Bone Marrow Mast Derived Cells (BMMCs)

Mast cells that derived from mouse bone marrow serve as a positive model to examine the function of mucosal type of mast cells (Gruenbaum et al., 1981). These cells were isolated from wild type mice C57Bl6 aged 8-12 weeks.

2.1.3.1 Preparation and Isolation of mice BMMCs

BMMCs were generated from mouse femurs and tibias under sterile conditions. Bone marrow cells were isolated by flushing the bones with ice-cold calcium- and magnesium-free phosphate-buffered saline (PBS 1X, Gibco 2695366), followed by centrifugation (340 xg, 10 min, 4°C). Erythrocytes were lysed using ammonium chloride-based lysis buffer(Ery-lyse- buffer: 0.83% ammonium chloride, 4.15g/500ml; 0.168% sodium carbonate, 0.84g/500ml; 1mM EDTA -1 ml of 0.5 M stock in 500 ml, pH 7.3, filtered sterile) for 10 min at room temperature, and the reaction was terminated by the addition of complete Dulbecco's Modified Eagle Medium (DMEM). Following a second centrifugation step, cells were resuspended in complete DMEM (Table 2.1), filtered through a sterile 100µm nylon mesh cell strainer, and seeded into 75 cm^2 tissue culture flasks at a density of 0.5–1 × 10^6 cells/ml. Cultures were supplemented with recombinant mouse interleukin-3 (IL-3; 5 ng/mL) and recombinant mouse stem cell factor (rmSCF; 10 ng/mL) (Table 2.2) and maintained at 37°C in a humidified atmosphere containing 7.5% CO_2 for 4 weeks to allow differentiation into BMMCs. Cell maturation was confirmed by flow cytometric analysis (FACS) of MC surface markers. BD Microlance 3 : (27G X ½) (0.4 X 13mm) LOT 240319, BD Plastipak 10ml LOT 1506001, Fisherbrand: Sterile Cell Strainer 100um Nylon Mesh Cat. No, 22363549.

Full DMEM reagent	Amount	Concentration	Company
DMEM with D-Glucose, L-Glutamine and Sodium Pyruvate	45 ml	1X	gibco 2994601
Heat Inactivated Fetal Bovine Serum	5 ml	10%	Gibco V3007790RP
L-Glutamine with Penicillin/Streptomycin 100X	500 µl	100 µ/ml	Corning 30009072
MEM Vitamin 100X	500 µl	1%	Gibco 2797763
2-mercaptoethanol	50 µl	50 uM	Gibco 2771904
Sodium Pyruvate 100mM	500 µl	1%	Gibco 2537192
Non-essential amino acid X100	500 µl	1%	Gibco 11140-035

Table 2.1: Contents of BMMCs culture media

Growth Factors Reagent	Amount	Concentration	Company
Recombinant Mouse IL-3(rm IL-3)	25 µl	5 ng/ml	R&D BR1123101
Recombinant Mouse SCF(rm SCF)	50 µl	10 ng/ml	R&D CW2221071

Table 2.2: Contents of BMMCs supplements

2.1.3.2 Maintenance of BMMCs

The media was changed every week by transferring the non-adherent cells to 50 ml Falcon tube and at centrifuge at 340 xg for 10 min at 4°C. After that, the supernatant was thrown out, and the cell pellet was resuspended with fresh, full media. Then, cells were counted and transferred to a new flask at a density $0.5x10^6$ -$1x10^6$ cells/ml for further culturing.

2.1.3.3 BMMCs counting

In each experiment, a specific number of cells was required, the cell counting method was performed using an Automated Cell Counter. 10 µl of Trypan Blue solution (Bio-Rad) was added to 10 µl of cell solution, then mixed well, and10 µl of this solution was pipetted into counting slide.

2.2 Mediators release assays

After BMMCs were cultured for 4 weeks, the cells were stimulated by either IgE-dependent or IgE-independent ways. Following stimulation, specific tests for each mediator group were used:

1. Pre-stored mediator secretion and degranulation: β-hexosaminidase.

2. Newly synthesised cytokines: IL-13, IL-6, and TNF-α measured by ELISA, TNF-α by flow cytometry.

2.2.1 BMMCs Stimulation

Two main pathways known to stimulate exocytosis in mast cells: the Antigen (Ag)-activated pathway and the non-antigen-activated pathway.

2.2.1.1 Ag-activated BMMCs stimulation

It is well known that mast cells are stimulated by antigen(Ag) through the aggregation of high-affinity IgE receptor(FcεRI). Therefore,$1X10^6$ cells/ ml from BMMCs were incubated in their full media with 100 ng/ml of monoclonal Anti-Dinitrophenyl antibody (DNP) produced in mouse (IgE) (D8406-100UG from Merk) at 7.5% CO^2 at 37 °C overnight. The next day, cells were collected into 15 ml Falcon tube, centrifuged at 340 xg for 5 min and washed 3 times with full media to remove excess IgE. The last wash, the cell pellet was resuspended with 90 µl/well from full media and added to the 96 wells plate according to our experiment plan. To stimulate BMMCs with DNP Ag, 10 µl of 100X DNP Ag were added to the labelled wells and 10 µl of media was added to the control wells. The final concentration of DNP was from 0,10,30,100,300 ng/ml. The plate was incubated for 30 min at 37°C.

2.2.2 Measurement of Mast cell degranulation using the β-hexosaminidase release assay

β-hexosaminidase is lysosomal-associated enzyme that is normally released into the cell solution after mast cell stimulation. The activity of this enzyme may be measured by using 4-Nitrophenyl N-acetyl-β-D-glucosaminidase as substrate. β-hexosaminidase changes 4-Nitrophenyl N-acetyl-β-D-glucosaminidase into 4-nitrophenol, which can be measured at 405 nm absorbance using spectroscopy (Wendeler and Sandhoff, 2009).

BMMCs (2×10^5 cells/well) were seeded into 96-well V-bottom plates and stimulated with the indicated agonists or culture medium (unstimulated control) for 30 min at 37°C. Following centrifugation (340 xg, 5 min, 4°C), 50 µl of the supernatant was transferred to a flat-bottom 96-well plate and incubated with an equal volume of substrate solution prepared in citrate buffer (PH 4.5) for 2 hours at 37°C. Cell pellets were lysed in 150 µl of 0.5% Triton X-100 for 10 min at room temperature, centrifuged, and 50 µl of the lysate supernatant was similarly incubated with substrate. Enzymatic reactions were terminated by the addition of 90 µl of 1 M Trizma buffer (PH 9.0), and absorbance was measured at 405 nm using an OPTIMA microplate reader. Background absorbance was determined using buffer-only wells and subtracted from all samples. All conditions were assayed in technical triplicate, and experiments were independently repeated at least three times.

The β-hexa% was calculated using this formula:

Degranulation % = ((Supernatant-Blank) / (Total-Blank)) X100

Results are presented as mean ± SEM. Significance was calculated using t-test.

Reagent	Amount	Conc.	Supplier
Citric acid	2.34g	121.2M	Sigma,C1909
Na Citrate	2.588g	88M	BDH 301284C
Autoclaved ddH_2O	100ml		

Adjust the pH to 7.5 and store at room temperature.

Table 2.3: Recipe of the β-hexa buffers (0.2M)

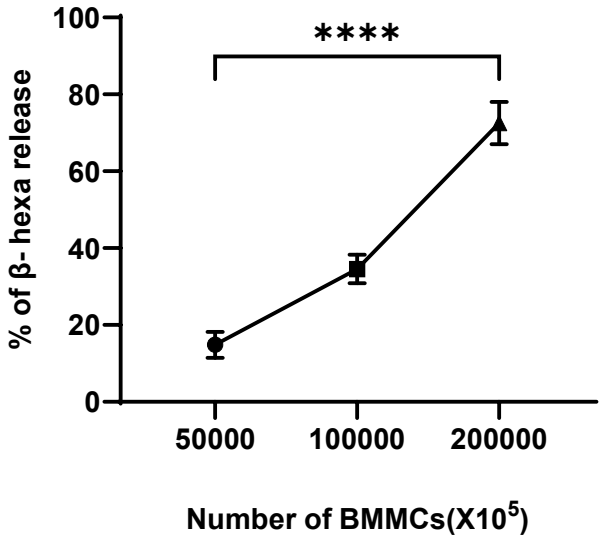

Figure 2.1: Comparison between the number of BMMCs and the % of B-hexa.

2.2.3 Measuring cytokines release by ELISA (IL-13)

IL-13 is key cytokine that control both homeostatic and inflammatory responses in MCs. To prepare the cell sample for this assay, BMMCs (2 × 10^5 cells/well) were stimulated with ionomycin (1 μM), DNP (100 ng/mL), or IL-33 (10 ng/mL) for 6 h at 37°C. Following stimulation, cell suspensions were centrifuged at 5000 xg for 2 min at 4°C, and cell-free supernatants were collected on ice and stored at −20°C until analysis. Cytokine concentrations were quantified using commercially available ELISA kits according to the manufacturer's instructions (Table 2.4). Briefly, samples and standards were added to pre-coated microplates, followed by incubation with the appropriate detection conjugate and substrate. Absorbance was measured at 450 nm with wavelength correction at 540 nm using an OPTIMA microplate reader. Cytokine concentrations were determined by interpolation from standard curves generated using serially diluted standards. Samples and standards were analysed in duplicate, and each experiment was performed independently at least twice. Data are presented as the mean ± SEM, and statistical significance was determined using one-way analysis of variance (ANOVA).

cytokine	Supplier	Cat.no.
IL-13	R&D	M1300CB-1

Table 2.4: IL-13 Cytokines ELISA kits

2.2.4 Measuring cytokines release by ELISA (IL-6)

BMMCs (2 × 10^5 cells/well) were stimulated with DNP (10, 100, or 300 ng/mL) or IL-33 (10 ng/mL) for 6 h at 37°C. Following stimulation, cell-free supernatants were collected by centrifugation (5,000 xg, 2 min, 4°C) and stored at −20°C until analysis. IL-6 concentrations were determined using a commercially available ELISA kit according to the manufacturer's instructions (Table 2.5). Absorbance was measured at 450 nm with wavelength correction at 540 nm using an OPTIMA microplate reader, and cytokine concentrations were calculated from standard curves generated using serially diluted IL-6 standards (500–7.8 pg/mL). Samples and standards were analysed in duplicate, and each experiment was independently repeated at least twice. Data are presented as the mean ± SEM, and statistical significance was determined using one-way analysis of variance (ANOVA).

cytokine	Supplier	Cat.no.
IL-6	R&D	M6000B-1

Table 2.5: IL-6 Cytokines ELISA kits

2.2.5 Measuring cytokines release by ELISA (TNF-α)

BMMCs (2 × 10^5 cells/well) were stimulated with DNP (100 ng/mL) or IL-33 (10 ng/mL) for 6 h at 37°C. Cell-free supernatants were collected by centrifugation (5,000 xg, 2 min, 4°C) and stored at −20°C until analysis. TNF-α concentrations were quantified using a commercially available ELISA kit according to the manufacturer's instructions (Table 2.6). Absorbance was measured at 450 nm with wavelength correction at 540 nm using an OPTIMA microplate reader, and cytokine concentrations were calculated from standard curves generated using serially diluted TNF-α standards (500–7.8 pg/mL). Samples and standards were analysed in duplicate, and each experiment was independently repeated at least twice. Data are presented as the mean ± SEM, and statistical significance was determined using one-way analysis of variance (ANOVA).

cytokine	Supplier	Cat.no.
TNF-α	R&D	MTA00B-1

Table 2.6: TNF-α Cytokines ELISA kits

2.3 Protein expression assays

2.3.1 Western Blot

Western blotting is a method for protein identification in cells. It comprises gel electrophoresis, a method for separating proteins according to their molecular sizes. Subsequently, proteins are transported to a membrane and treated with antibodies to facilitate protein identification. Finally, protein identification is visualised by chemiluminescent or fluorescent methodologies. All immunoblots included in my thesis run in mouse MCs to look at endogenous VAMP-3 and we have been done once.

2.3.1.1 Preparing cell lysis

BMMCs (2–4 × 10^6 cells) were harvested, washed twice with sterile PBS, and lysed in ice-cold RIPA buffer supplemented with protease inhibitors. Lysates were incubated for 20 min at 4°C with continuous mixing before centrifugation at 17,000 xg for 30 min at 4°C to remove insoluble debris. The clarified supernatants containing total cellular protein were transferred to fresh pre-chilled microcentrifuge tubes and either used immediately for downstream applications or stored at −80°C until analysis.

2.3.1.2 Bradford assay to determine protein concentration

The Protein Assay Dye Reagent Concentrate (PADRC) was diluted 1:5 in Milli-Q water. Subsequently, 2 µL of lysate was added to 1 mL of the diluted PADRC (final dilution 1:500) in a 1.5 mL Eppendorf tube, and the mixture was transferred to a cuvette for

measurement. A blank control was prepared in parallel using diluted PADRC without protein. The Bradford assay was used to measure absorbance levels, allowing determination of protein concentration. The lysate was diluted in RIPA buffer and 5x Laemmli to the planned final protein concentration (typically 1-2 ug/ul). Finally, each lysate tube was boiled at 95 ^{o}C for 5 min (At this step, lysates can be aliquoted and stored at -20 ^{o}C for next use).

2.3.1.3 Running Sodium dodecyl sulphate-polyacrylamide gel electrophoresis (SDS-PAGE)

A 17% SDS–PAGE gel was placed into the gel holder, which was then put into the electrophoresis tank with the short plate facing in. The tank was filled with 1× running buffer to the four-gel mark. A molecular weight ladder was loaded (typically 3 µL), and 60 µg of protein (after optimising) from each sample was loaded into the wells of the gel. Electrophoresis was performed at 100 V for approximately 1.5 hours (for small protein run only 80% of the way down the gel), because limiting the run to 80% of the gel should prevent VAMP-3 running off of the bottom of the gel as it is so small molecular weight. With less 15% gels small proteins (less than 20 KDa) may run off the bottom if the protein front is run to the bottom of the gel.

2.3.1.4 Transferring SDS-PAGE gel onto 0.2 µm PDVF

The transfer stack was prepared in a tray containing transfer buffer in the following order: the black side of the cassette, sponge, three sheets of filter paper, the gel, and a 0.2 µm PVDF membrane that had been pre-activated in methanol for 5 minutes, followed by three additional sheets of filter paper, a sponge, and the red side of the cassette as described in figure 2.2 below. The cassette was then sealed and locked in place. An ice block was placed in the transfer tank, which was subsequently filled with fresh transfer buffer, and the cassette was inserted into the tank. Protein transfer was performed for 30 minutes at 100 V. Note: use three sheets of filter paper instead of

two, as this enhances the contact between the gel and the membrane, which is ideal for transferring small proteins.

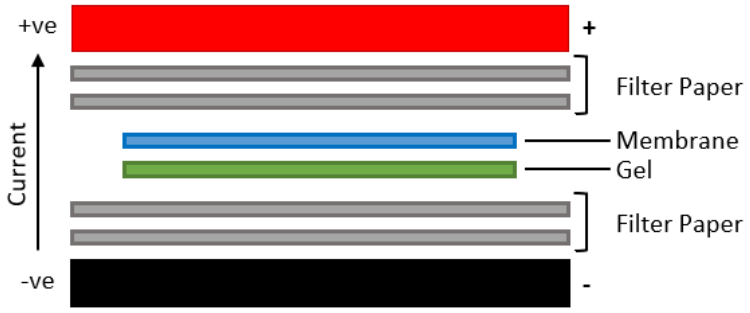

Figure 2.2: Schematic example of a prepared stack for a wet transfer.

2.3.1.5 Blocking 0.2 µm PDVF membrane

The blocking buffer was prepared and kept cold. Following completion of the transfer, the membrane was stained with Ponceau S, a reversible red dye used to confirm successful protein transfer and visualise protein bands. After several seconds, the membrane was removed from the Ponceau S solution and washed repeatedly with distilled water until the background staining was reduced. The membrane was then cut between 37 KDa and 25 KDa. Subsequently, the membrane was blocked in 50mL of blocking buffer (5% milk in TBS-T) in a square Petri dish on a rocker for 1 hour at room temperature.

2.3.1.6 Antibody staining

The membrane was incubated overnight at 4°C on a rotor with primary antibodies diluted in blocking buffer. The upper part of the membrane was probed with anti-GAPDH rabbit antibody (1:2000), while the lower part was incubated with anti-VAMP-3 rabbit antibody (1:200). The next day, the membrane was washed three times with TBS-T for 10 minutes per wash. The membrane was then incubated with a fluorescent secondary antibody (680 anti-rabbit) diluted 1:25,000 in TBS-T for 1 hour at room temperature, (Use only rabbit antibody, as the cells originate from mice). After incubation, the membrane was washed again three times with TBS-T for 10 minutes per wash. Finally, the membrane was removed using tweezers, placed on an imaging tray, and visualised using the Li-Cor imaging system.

This protocol was adapted from the Western Blot protocols developed by Dr Ryan JH West in 2017 and Prof Kurt De Vos in 2020

Materials and Reagents:

Equipment	**Reagent**
Rotor 4 ºC	Bradford solutions
Centrifuge 4 ºC	Sterile 1x PBS
Heat Block 95 ºC	17% SDS-PAGE Gel (Using a 17% gel because it has smaller pores than a lower percentage gel. So, it is more recommended to proteins which are less than 20kDa).
Bio-Rad Gel Tank	0.2 µm PDVF membrane (Its better for low molecular weight protein as VAMP-3)

Bio-Rad Transfer Tank with Ice Block	Filter paper
Rocker	
LI-COR	

Table 2.7: Equipment and reagent needed in western blot

Reagent	
1x TBS-T	0.1% Tween 20 in 1x TBS
5x Laemmli Buffer	300μM Tris-HCL pH 6.8 10% Sodium Dodecyl Sulphate (SDS) 25% β-Mercaptoethanol 0.01% Bromophenol Blue
Radioimmunoprecipitation Assay (RIPA) Buffer	10μM Tris pH 8.0 0.5μM Ethylene Glycol Tetra-acetic Acid (EGTA) 1μM Ethylenediaminetetraacetic (EDTA) 1% Triton X-100 0.1% Sodium Dodecyl Sulphate (SDS) 140μM Sodium Chloride (NaCl) Protease Inhibitors (1:50) Note: increase the amount due to mouse MCs full are of protease.
Running Buffer	25μM Tris base

	192µM glycine 0.1% Sodium Dodecyl Sulphate (SDS) Adjust pH to 8.3
Transfer Buffer	25µM Tris base 192µM glycine 20% Methanol Adjust pH to 8.3
Blocking Buffer	20% Milk in TBS-T

Table 2.8: Buffers in western blot

Antibodies	
Primary antibody: VAMP-3/Cellubrevin Polyclonal antibody	Cat. No.: 10702-1-AP Lot No.: 00054524 Proteintech
Secondary antibody Alexa Fluor® (680-AffiniPure Anti-Rabbit IgG	Ca. No.: 711-625-152 Jackson ImmunoResearch

Table 2.9: Antibodies in western blot

2.3.2 Flow cytometry test

The expression of BMMCs surface was examined using flow cytometry. $2X10^5$ BMMCs per sample were washed 2 times with cold PBS and centrifuged at 340 xg for 10 minutes. Then, the cells of each sample were resuspended with 100µl of cold FACS buffer its contents described in table 2.10 below. All following steps were performed on ice, and all antibodies that planned to use were diluted in FACS buffer. Cells were blocked with 50µl of Fc Blocker(CD16/32) at a 1:100 dilution and incubated on ice for 15 minutes. The cells were washed 2 times with FACS buffer and then incubated with the targeted concentration of antibodies for 30 minutes on ice. After that, the cells were washed with 900 µl of FACS buffer and centrifuged at 340 xg for 2 minutes then the cell pellet was resuspended with 200µl of FACS buffer for each sample. Fluorescence was measured with the SONY MA900 Cell Sorter machine at emission wavelengths of 488 nm for Alexa Fluor® 488, 665 nm for APC, and Alexa Fluor® 647. For the examination of live and dead cells, an unstained sample was gated based on side and forward scatter

Material	50 ml (Total volume)
PBS (Ca/Mg-)	47.150 µl
FBS (2%)	1000 µl
HEPES 1M	1250 µl
EDTA 0.5M	100 µl

Table 2.10: Contents of FACS buffer

Name	Dilution	Cat. No.	Company
Anti-MoCD16/CD32	1:100	14-0161-82	Invitrogen
Anti-Mo FcεR1alpha APC	1:100	17-5898-80	Invitrogen
Alexa Fluor® 488 anti-mouse CD117(c-Kit)	1:100	105815	Biolegend
Alexa Fluor® 647 anti-mouse CD107a(LAMP-1)	4:100	121610	Biolegend

Table 2.11: Contents of FACS antibodies

2.3.2.1 Flow cytometry for measuring Cytokine (TNF-α)

Intracellular TNF-α expression was assessed by flow cytometry. BMMCs (2×10^5 cells/sample) were stimulated with DNP or ionomycin/phorbol 12-myristate 13-acetate (PMA), while unstimulated cells served as negative controls. Following 2 hours of stimulation at 37°C in 5% CO_2, cells were incubated with Monensin and Brefeldin A for an additional 1 hour to inhibit cytokine secretion. Cells were subsequently blocked with Fc receptor blocking reagent, fixed and permeabilised using the Cyto-Fast Fix/Perm kit according to the manufacturer's protocol, and stained with Brilliant Violet 421-conjugated anti-TNF-α antibody. After washing, cells were resuspended in cell staining buffer and analysed using a SONY MA900 Cell Sorter. Flow cytometry data were analysed to quantify intracellular TNF-α expression.

Reagent	
Cyto-Fast Fix/Perm Solution	Cat. No.: 750000133 Lot No.: B426818 Biolegend
Cyto-Fast Perm/Wash Solution 10X	Cat. No.: 750000135 Lot No.: B428422 Biolegend
Cell Staining Buffer	Cat. No.: 420201 Lot No.: B353220 Biolegend
Brefeldin A Solution (1000X)	Cat. No.: 420601 Biolegend
Monensin Solution (1.000X)	Cat. No.: 420701 Biolegend
Brilliant Violet 421 anti-mouse TNF-α, Clone: MP6-XT22 (dilution 1:200)	Cat. No.: 506328 Biolegend
APC/Cyanine 7 anti-mouse TNF-α, Clone: MP6-XT22 (dilution 1:200)	Cat. No.: 506343 Biolegend

Table 2.12: Buffers and reagents used in flow experiments

2.4 Amaxa nucleofection in BMMCs

Transfection is a procedure of introducing exogenous nucleic acids into cells. It is a powerful technique for examining intracellular signalling pathways and gene function by altering protein production. Nucleofection is a novel and effective non-viral technique for transfecting primary cells. Compared with other non-viral assays, nucleofection demonstrated better transfection efficiency than methods like PEI and Lipofectamine, as well as higher cell viability compared to physical methods such as electroporation (Jacobsen et al., 2006).

An existing feature of the nucleofection method is that it can directly deliver negative exogenous materials to the nucleus using both the principles of chemical and physical transfection assays. The chemical concept involves binding the exogenous part to a nuclear-localisation signal protein to form a complex in a specific solution for the cell line. Whereas the physical technique involves using specific electrical shocks to create tiny pores in the cell membrane. These pores permit the complex of protein molecules to transfer to into the cell. Another advantage of nucleofection is that the exogenous part is introduced directly into the nucleus, thus allowing cell division to be independently. All these advantages make nucleofection a good option for non-dividing cells (Hagemann et al., 2006). Transfection of BMMCs is likely to be challenging due to their low growth rate. Therefore, nucleofection by the Nucleofector IIb technique(Amaxa, Lonza) Kit V was used in this study.

2.4.1 Final protocol of Amaxa nucleofection of BMMCs

Briefly, 2×10^6 BMMCs/reaction were washed PBS1x twice and centrifuged at 340 xg for 10 min. Then, the supernatant was discarded, cell pellets were resuspended with 82µl and 18µl of cell nucleofector solution and supplement (comes with kit), respectively. 4µg of DNA was added and well mixed. Then, the cell solution was transferred into the nucleocuvette (included with the kit) and inserted into the Amaxa

Nucleofector IIb using the optimising program (X-001). Immediately, 400µl of warm media without P/S was added to the cuvette and was gently transferred to a prepared 6-well plate (final volume 2.5 ml media/well). The plate was then incubated for 4 hours at 37 ºC and 5 CO^2 to allow cell recovery. After incubation for 4 hours, check the cells under the microscope. Then, 500µl of warm media without P/S was added to each well. Then, incubate the plate until the analysis was performed.

For mammalian expression the light chain domains of BoNT/B and BoNT/D were cloned into pEGFP-C3 (figure 2.3), a CMV based vector. The eGFP is at the N-terminus of the light chain. The full-length B construct is 672aa and the D construct is 686aa.

The control sample in all my experiments was pmaxeGFP from Lonza Amaxa Nucleofector kits (Nucleofector® 2b Kit V For Cell Lines, Cat. No.: VCA-1003 Lot No.: F-16307 Expiration date: 29-NOV-2026).

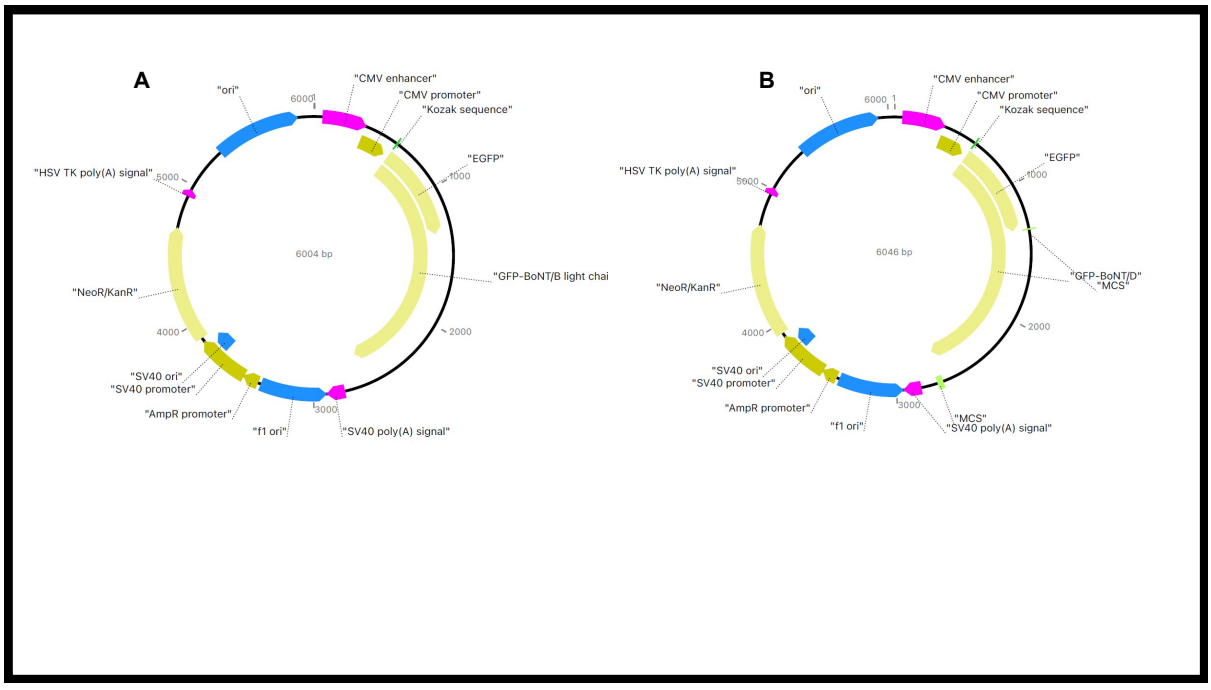

Figure 2.3: Plasmid maps of expression vectors encoding GFP-tagged BoNT LCs. Schematic representation of the expression constructs for (**A**) GFP-BoNT/B LC (6004 bp) and (B) GFP-BoNT/D LC (6046 bp). This information from Prof.Andrew Peden.

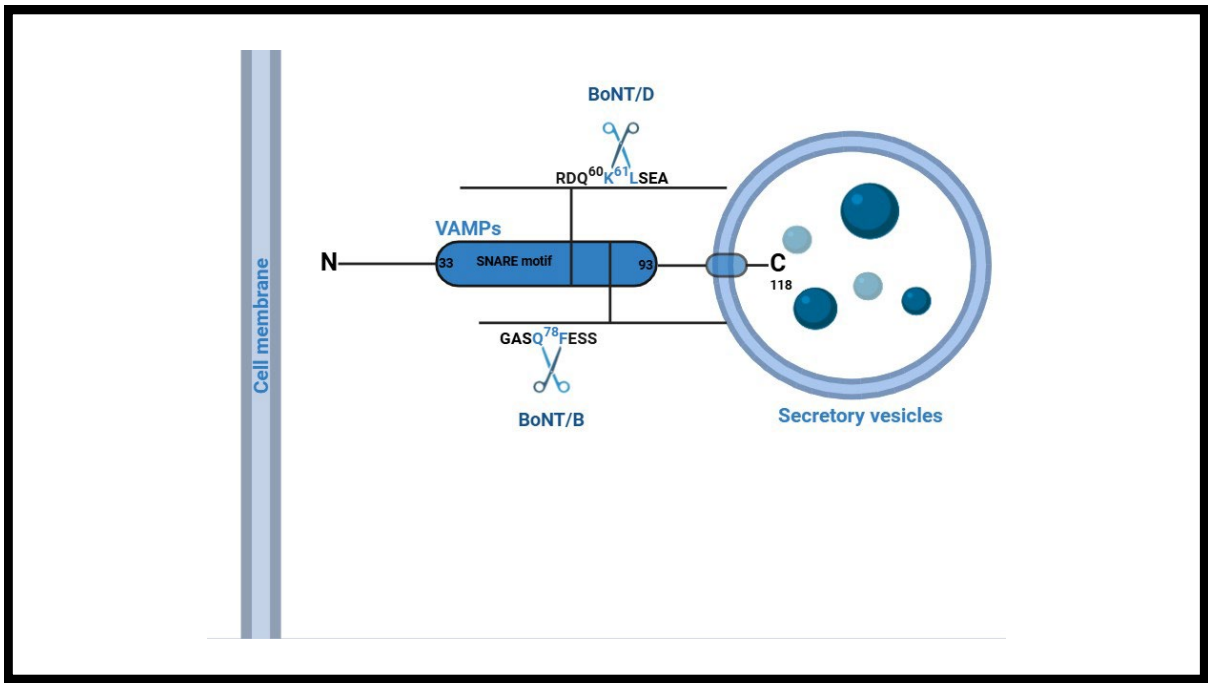

Figure 2.4: A schematic diagram describing the proteolytic cleavage sites of BoNT/B&D LC on specific SNARE motifs. Serotype-specific enzymatic cleavage sites are indicated on each protein, highlighting the precise peptide bonds targeted by the BoNTs. This enzymatic fragmentation structurally deactivates the SNARE core complex, ultimately preventing vesicular exocytosis in MCs. Adapted from (Pirazzini et al., 2017). And created with BioRender.com.

2.5 Statistical analysis

All data processing, statistical analyses, and graphical representations were carried out using GraphPad Prism (Version 10.5.0). The results are described in the figures as the mean ± standard error of the mean (SEM) from a minimum of 3 independent experiments, unless otherwise specified. For comparisons between two experimental variables, an unpaired t-test was used and for data including three or more variables, statistical comparisons were assessed using one-way repeated measures (ANOVA). A probability value of $P < 0.05$ was defined as the threshold for statistical significance.

Chapter 3: Characterisation of Mast cell lines

3.1 Introduction

MCs are immune cells found in almost all vascular tissues. When activated they secrete a wide range of biologically active mediators, either stored in cytoplasmic granules (e.g., histamine, heparin, and various proteases), or produced *de novo* (e.g., prostaglandins, leukotrienes, cytokines, chemokines, and growth factors) (Chen et al., 2005). The major cytokines that facilitate MC differentiation and maturation are SCF and IL-3. SCF is essential for the development, growth, and survival of MCs, whereas IL-3, although important for MC development, often supports the survival of early progenitor cells in synergy with SCF (Mitsui et al., 1993). Mature MCs are recognized by high surface expression of FcεRI and c-Kit, as well as their ability to exhibit functional responses following cross-linking and IgE-mediated activation (Kulka and Metcalfe, 2010). Due to their presence in low numbers within healthy tissues, mature MCs present challenges for isolating adequate quantities of primary cells for experimental research (Kulka and Metcalfe, 2010). An alternative approach to obtaining large numbers of mast cells for research is the in vitro differentiation of bone marrow stem cells, to produce bone marrow-derived mast cells, BMMCs (Bischoff, 2007), or use of immortal cell lines with mast cell like properties, e.g. RBL-2H3, MC9, LAD2 (Bischoff, 2007). MC line characterisation typically includes several key factors to confirm their identity, phenotype, and functional properties (Laidlaw et al., 2011). Common criteria and methods include:

(1) Morphology: Examination by light microscopy to assess size, shape, and granular content.

(2) Surface Marker Expression: Flow cytometry or immunofluorescence to detect high surface expression of markers such as FcεRI (high-affinity IgE receptor) and c-Kit (CD117), both hallmark receptors on mature MCs.
(3) Functional Responses: assessing degranulation or mediator secretion (e.g., β-hexosaminidase release for assessment of degranulation, cytokine synthesis and secretion) after IgE-mediated crosslinking.

(4) Ultrastructural Analysis: Electron microscopy to observe characteristic granule structures (Kirshenbaum et al., 2003).

SCF is a cytokine that plays a pivotal role in haematopoiesis through its binding with c-Kit receptors (Zhang and Lodish, 2008). While all hematopoietic progenitor cells initially express c-kit receptors, MCs represent a remarkable exception, as they maintain c-kit expression throughout their maturation stages, whereas other lineages downregulate c-kit expression upon differentiation (Zhang and Lodish, 2008). MCs are unique among mature hematopoietic cells as they expressed c-kit receptors (Okayama and Kawakami, 2006). SCF acts as a growth factor for MCs, in addition to that it has been reported to modulate IgE-mediated mast cell activation. Specifically, the accompanying administration of SCF and antigen synergistically enhances IgE-dependent mast cell activation (Hundley et al., 2004).

In this study, I used 3 MC lines: RBL-2H3, MC9 and BMMCs. The primary differences between RBL-2H3, MC9, and BMMCs were found receptor expression, and functional responses. These differences underscore the importance of careful selection of MC models based on experimental objectives and interpreting results within the context of the limitations and advantages of each cell type.

The aims of this chapter are to evaluate different MC models. At the end of these experiments, I chose to carry on with BMMCs. Also measuring of degranulation in three different MC lines using two different stimuli (IgE/Ag)DNP and ionomycin/PMA.

3.2 Results

3.2.1 Assessment of degranulation in RBL-2H3, MC9 and BMMCs by assay of secreted Beta-hexosaminidase

3.2.1.1 RBL-2H3 cells

The β-hexosaminidase release assay in MCs is based on the determination of the amount of enzyme activity released from cytoplasmic granules upon degranulation, allowing indirect measurement of exocytotic activity through colorimetric or fluorescent detection of the product (Tsvilovskyy et al., 2018). Initial experiments were performed to assess the functionality of the various MC models which may be used in my project. I started by assessing their potential to undergo degranulation in response to antigen stimulation.

RBL-2H3 cells are a cell line derived from rat basophilic leukaemia. Although they are more closely related to basophils, they are widely used as a model cell line for studying MC biology because of their similar properties and functions (Passante and Frankish, 2009). They form monolayers in culture, useful for imaging studies, though their elongated shape is more similar to fibroblast and their cytoplasmic granules are smaller compared with primary MCs. RBL-2H3 cells express high-affinity IgE receptors (FcεRI) and moderate degranulation upon stimulation, consequently they are widely used in research related to allergic reactions, inflammation, and immune processes (Choi et al., 2004, Passante and Frankish, 2009). We evaluated the properties of RBL-2H3 cells obtained from ATCC. As shown in figure 3.1A, they grew as adherent cells with a characteristic elongated shape.

A

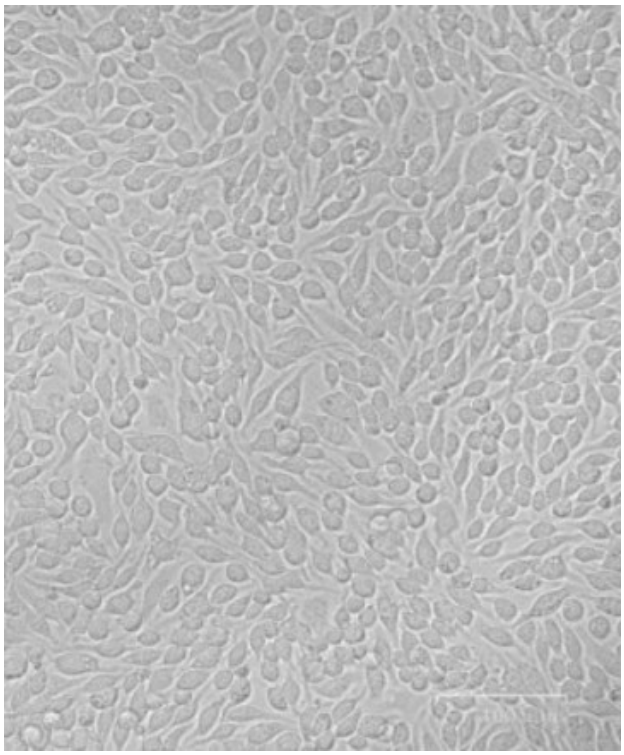

B

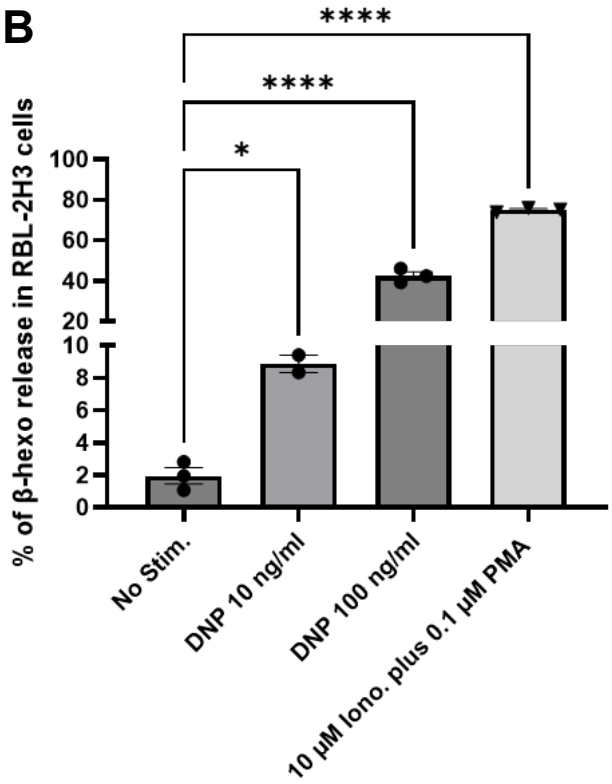
****
****
*
% of β-hexo release in RBL-2H3 cells
100
80
60
40
20
10
8
6
4
2
0
No Stim.
DNP 10 ng/ml
DNP 100 ng/ml
10 µM Iono. plus 0.1 µM PMA

Figure 3.1: RBL-2H3 Characterisation. A: Brightfield image of live cells (scale bar 100 μm). **B:** β-hexosaminidase secreted from RBL-2H3 expressed as a percentage of the total β-hexosaminidase measured following cell lysis. DNP-IgE sensitised cells were treated with either PBS (diluent, control), DNP (10 ng/ml & 100 ng/ml) and the calcium ionophore ionomycin (10 μM) and PKC activator PMA (0.1 μM) for 30 min. The data shown are mean ± SEM of 3 independent experiments compared to no stimulus group. * $p < 0.05$, **** indicates $\rho < 0.0001$. Data were analyzed using a one-way ANOVA test.

These cells are characterized by their ability to degranulate in response to IgE-mediated stimulation, making them a valuable cell line for analysing the signalling mechanisms underlying MC stimulation and allergic responses (Wagner et al., 2023). Following overnight sensitisation with DNP-IgE, 30 minutes stimulation with the antigen, degranulation was measured by assaying the activity of β-hexosaminidase in the supernatant (Kuehn et al., 2010). As shown in figure 3.1B, stimulation with antigen produced concentration-dependent degranulation. By contrast, control cells treated with the diluent (PBS) showed minimal degranulation due to spontaneous release. Receptor independent stimulation with ionomycin plus PMA also triggered robust degranulation, consistent with previous reports (Narenjkar et al., 1999),(Aketani et al., 2001), (Passante et al., 2009). Together these results confirmed the ability of RBL-2H3 cells to undergo degranulation, their expression of functional FcεRI and validated our protocol for measuring degranulation using the β-hexosaminidase assay.

3.2.1.2 MC9 cells

The MC9 cell line is a mouse MC line derived from fetal liver at 13 days gestation; it's dependent on IL-3 for proliferation and survival and reported to express FcεRI and c-kit (Nabel et al., 1981), They have been reported to represent mucosal MC cells that can be used to investigate cytokine secretion, signalling pathways and intracellular signalling. In response to specific stimuli, MC9 cells have been reported to be capable of secreting key cytokines such as IL-6 and TNF-α; notably RBL-2H3 cells have been reported to not produce strong cytokine responses (Wagner et al., 2023). This makes them potentially a valuable in vitro model for studying MC functions and their roles in both physiological and pathological reactions. Unlike RBL-2H3 cells, MC9 cells are non-adherent figure 3.2A; their ability to undergo agonist dependent degranulation in response to FcεRI cross-linking is however, unclear with some investigators reporting robust expression (Musch and Siegel, 1986), (Sudo et al., 1996) and others not (Wagner et al. 2023).

As shown in figure 3.2B, when I assayed MC9 cells for their ability to undergo degranulation, in agreement with Wagner et al. 2023, I found very weak responses to DNP in DNP-IgE sensitised cells. In contrast, the same cells showed robust degranulation in response to 1 μM ionomycin and 0.1 μM PMA (figure 3.2). By contrast, control MC9 cells treated with the diluent (PBS) showed minimal degranulation due to spontaneous release. This shows that the cells are capable of degranulation and suggests that the weak responses to antigen stimulation result from low expression of the receptor. I therefore proceeded to evaluate the expression levels of FcεRI in MC9 cells by flow cytometry (as described in material and methods chapter 2). As shown in figure 3.3 and figure 3.4, expression of FcεRI in MC9 cells was detected, however the levels were relatively low when compared with BMMCs (see section 1.2.3).

A

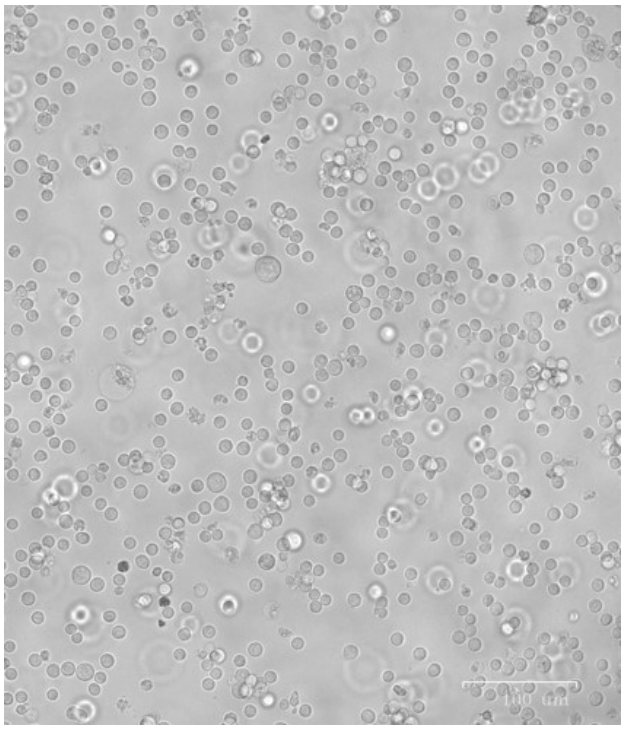

B

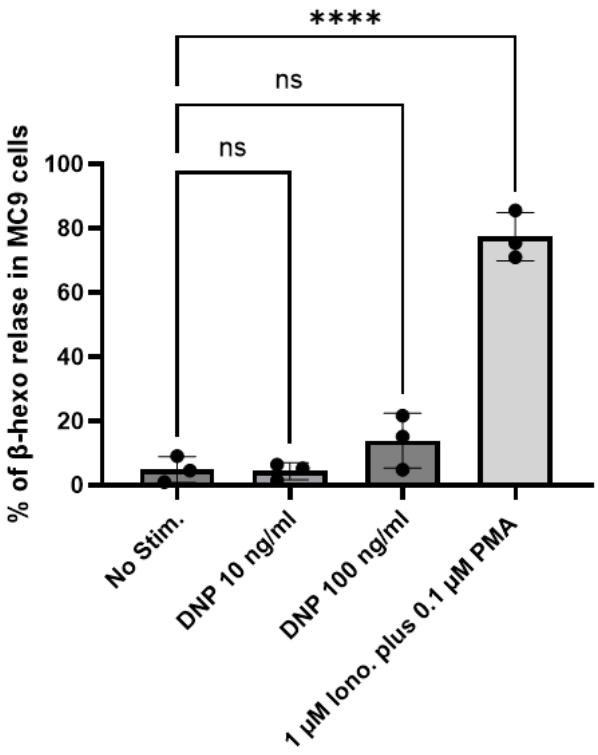
****
ns
ns
% of β-hexo relase in MC9 cells
100
80
60
40
20
0
No Stim.
DNP 10 ng/ml
DNP 100 ng/ml
1 µM Iono. plus 0.1 µM PMA

Figure 3.2: Characterisation of MC9 cells. A: Brightfield image of live MC9 cells (scale bar 100 um), **B:** β-hexosaminidase secreted from DNP-IgE sensitised MC9 cells expressed as a percentage of the total β-hexosaminidase measured following cell lysis. DNP-IgE sensitised cells were treated with either PBS (diluent, control), DNP (10 and 100 ng/ml) and ionomycin 0.1 μM and PMA 0.1 μM for 30 minutes. Data shown are mean ± SEM of 3 independent experiments and each did in triplicate. $***$ indicates $\rho < 0.0001$ compared to no stimulus group. Data were analyzed using a one-way ANOVA test.

A

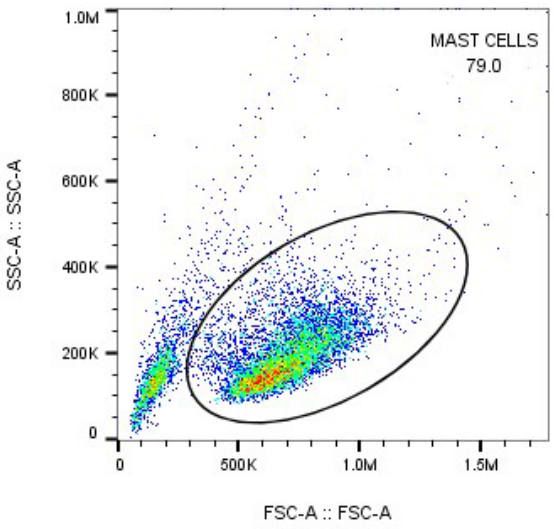

B

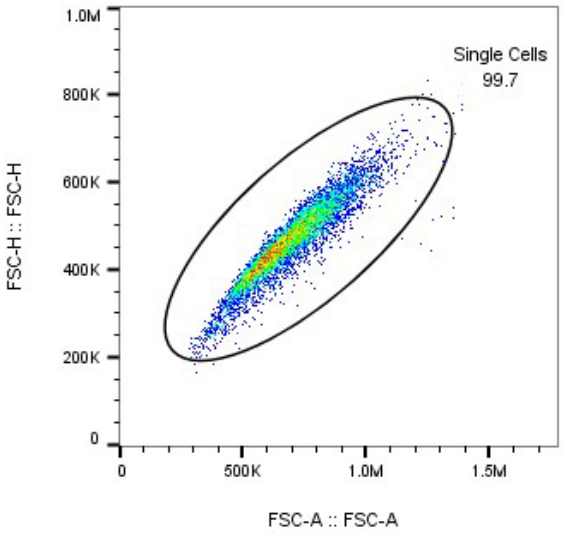

C

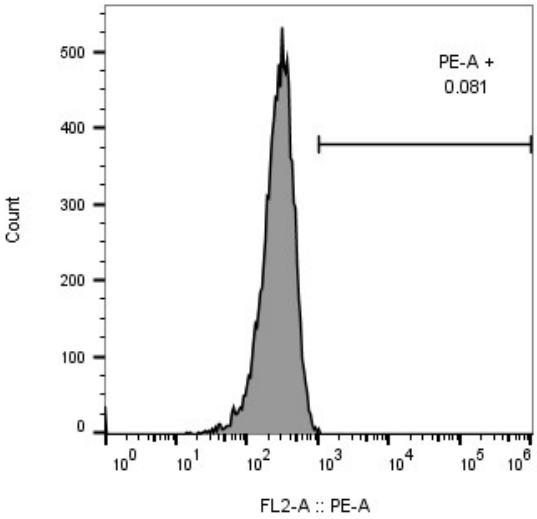

D

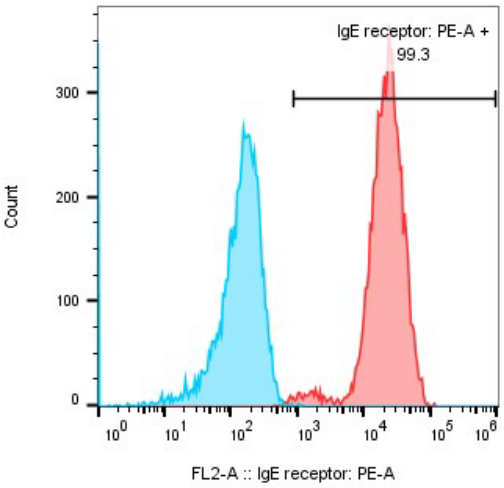

Single Cells: **Mean** : *IgE receptor: PE-A*: 158

Single Cells: **Mean** : *IgE receptor: PE-A*: 23662

Figure 3.3: IgE receptor in MC9. Flow cytometry testing of cell surface expression of FcεRI in MC9 cells ($200X10^5$ MC9 per condition). **A:** Gating the MC9 cells. **B:** Gating the single cells. **C:** Gating the anti-FcεRI (PE) in the unstained sample. **D:** Overlapping of the stained sample (red) with the unstained sample (blue) for the expression of anti-FcεRI (PE).

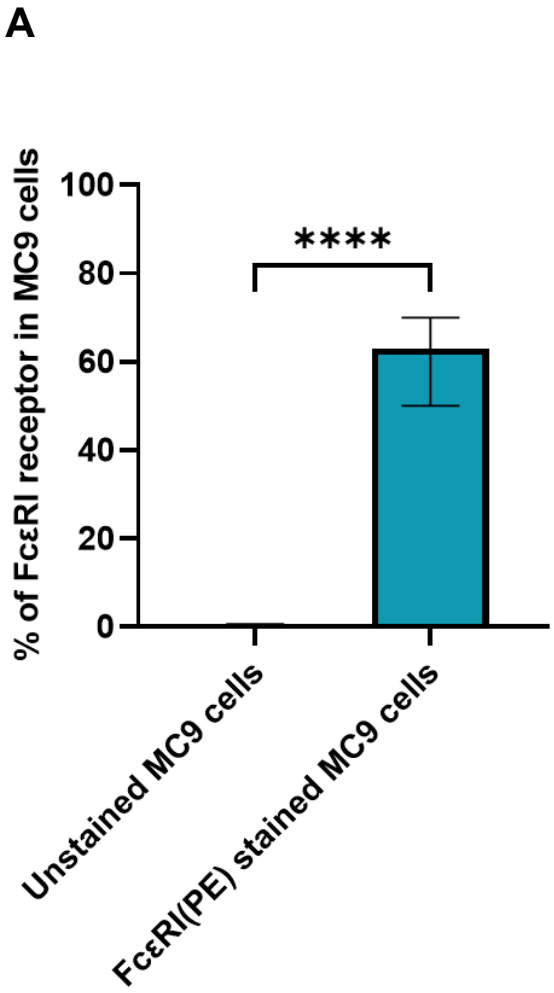

Figure 3.4: Statistical summary for IgE(PE) receptor in MC9. Representative conditions of 5 independent experiments. **** indicates $\rho < 0.0001$ compared to FcεRI(PE) in MC9 cells with unstained sample. Data were analyzed using an unpaired t-test test.

I next evaluated the surface expression of CD107a (Lamp1a) as a potential marker of degranulation in MCs (Grutzkau et al., 2004), (Elst et al., 2021), (Mendez-Enriquez et al., 2022). Flow cytometric analysis of surface CD107a has previously been shown to be a reliable marker of degranulation in living human MCs. This assay is ideally suited to cells like MC9 and BMMCs (see below), cells that grow in suspension because they can be easily loaded into the flow cytometer, without the need for enzymatic treatments to dislodge them from tissue culture surfaces. Moreover, flow cytometry offers the advantage that measurements of multiple fluorophores can be made on single cells. For these pilot experiments, I stimulated cells with ionomycin 0.1 μM and PMA 0.1 μM for 30 minutes; these match the stimulation conditions shown previously to work with the β-hexosaminidase assay (figure 3.2B). As shown in Figure 3.5D stimulation of MC9 cells with the calcium ionophore 0.1 μM and PMA 0.1 μM produced a robust increase in surface expression of CD107a in >90% of cells and a significant increase in MFI, thereby validating this assay as an additional means for evaluating degranulation in living MCs.

A

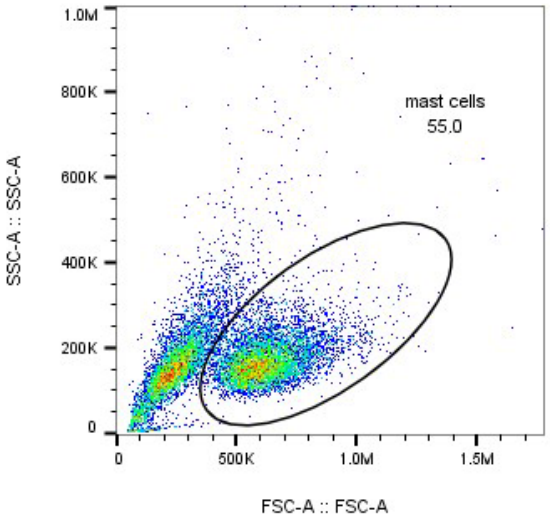

B

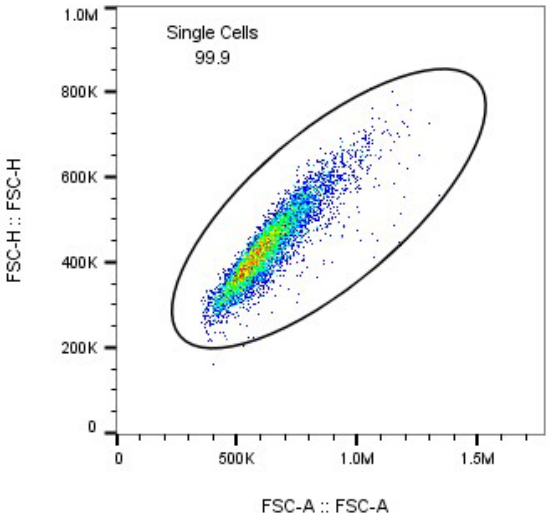

C

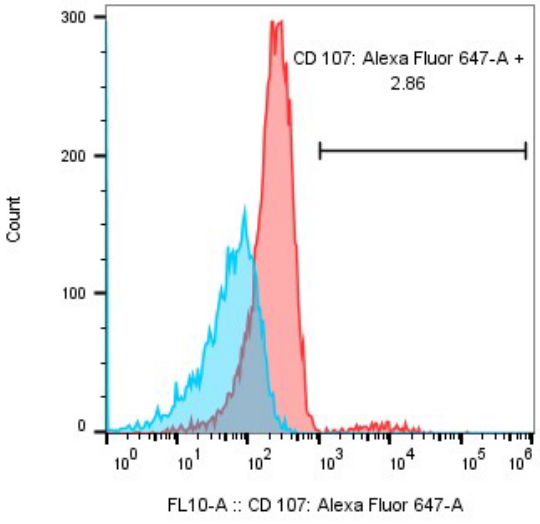

Single Cells: **Mean** : *CD 107: Alexa Fluor 647-A*:

Single Cells: **Mean** : *CD 107: Alexa Fluor 647-A*:

D

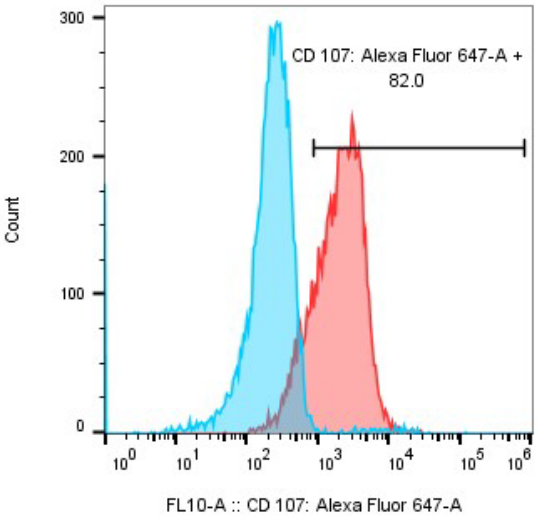

Single Cells: **Mean** : *CD 107: Alexa Fluor 647-A*: 636

Single Cells: **Mean** : *CD 107: Alexa Fluor 647-A*: 2551

Figure 3.5: Surface expression of CD107a is increased on the surface of MC9 cells following stimulation with ionomycin 0.1μM and PMA 0.1μM. A: Gating of MC9 cells. **B:** Gating the single cells. **C:** Representative histogram showing surface labelling with AlexaFluor647anti-mouse CD107a antibody in stained (blue) and stained &stimulated cells (red). **D:** Representative histogram showing surface labelling with AlexaFluor647anti-mouse CD107a antibody in unstimulated (blue) and cells stimulated with ionomycin 0.1 μM and PMA 0.1 μM for 30 min (red); the gate used to quantify cells with increased surface expression over control (unstimulated) is shown as an overlaid black bar.

A

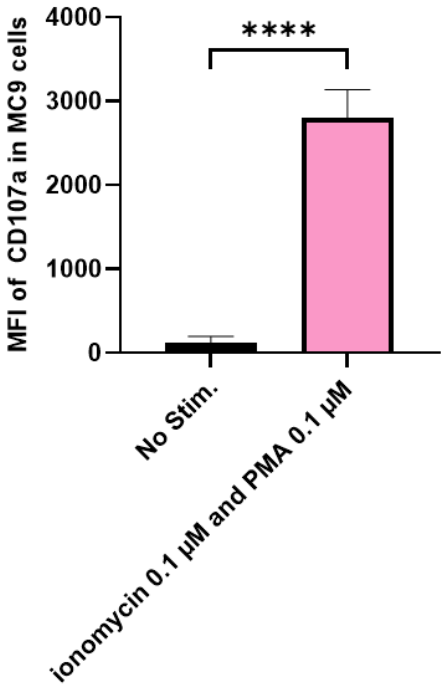

Figure 3.6: MFI of CD107a in MC9. A: Bar graph summarising the mean MFI ± SEM of 5 independent experiments . **** indicates $\rho < 0.0001$ compared to no stimulus group. Data were analyzed using an unpaired t-test test.

3.2.1.3 BMMCs

BMMCs are the most widely used and best characterised of the rodent derived MC models (Jensen et al., 2006). Their robust expression of FcεRI and robust secretory responses, including cytokines (IL-6 and TNF-α) upon antigen-stimulation (Moellerherm et al., 2017) make them a preferred model for studies focussed on allergic regulation of secretion. A disadvantage of BMMCs compared with the immortal cell lines (RBL-2H3 and MC9) is however that they are relatively expensive to maintain, requiring specific growth factors (IL-3 and SCF) for their survival and differentiation (Kirshenbaum et al., 1992), and it takes 3-4 weeks for them to reach maturity, after which point their growth rate slows (figure 3.7B).

A

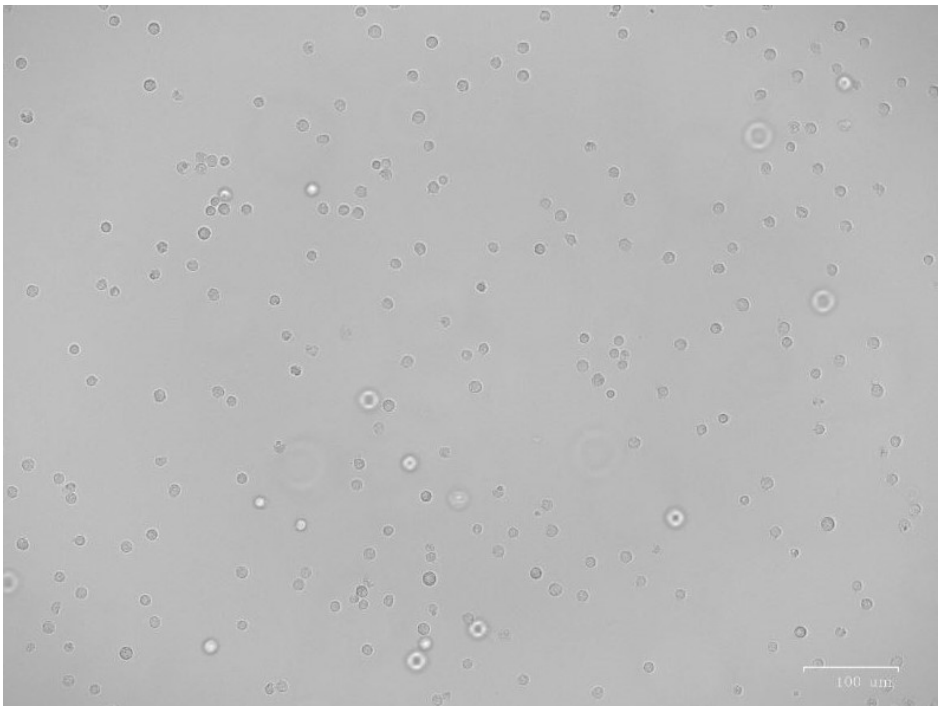
100 um

B

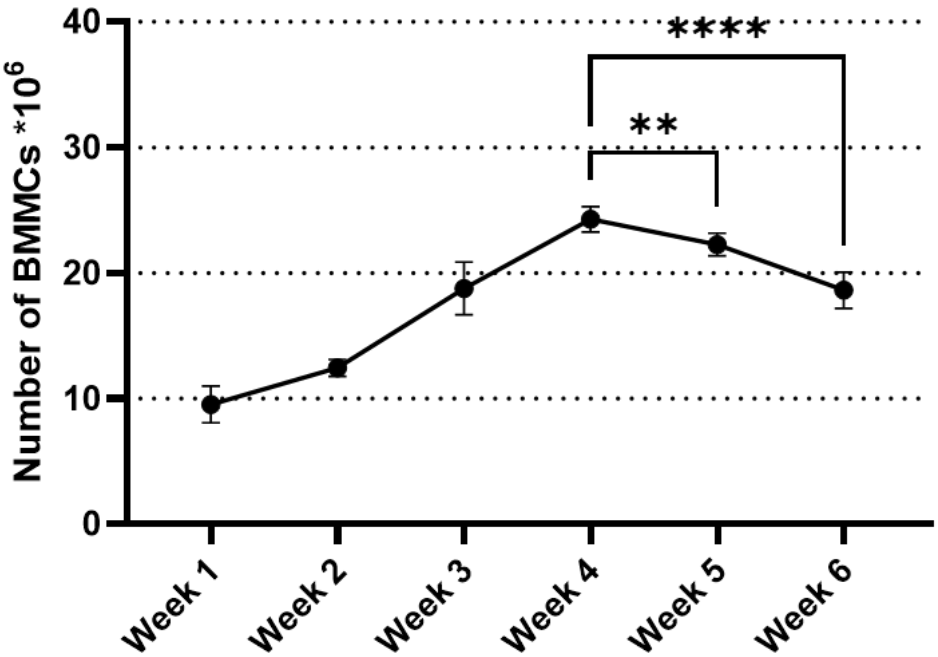
Number of BMMCs *10^6
40
30
20
10
0
****
**
Week 1
Week 2
Week 3
Week 4
Week 5
Week 6

Figure 3.7: Characterisation of BMMCs growing and growth rate of BMMCs during 6 weeks of culture. A: Brightfield image of live BMMCs (scale bar 100 μm). **B:** BMMCs were counted every week when growing in complete DMEM media with supplements (SCF and IL-3) (N=11). Statistical significance was determine using One way ANOVA, $** \rho < 0.01$,$**** \rho < 0.0001$.

A

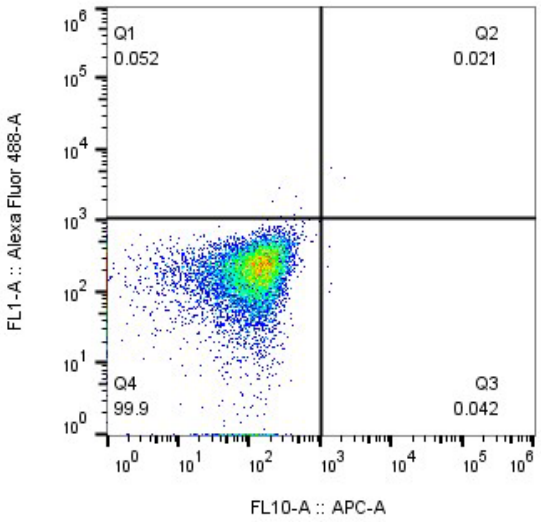
Q1
0.052
Q2
0.021
Q4
99.9
Q3
0.042
FL1-A :: Alexa Fluor 488-A
FL10-A :: APC-A

B

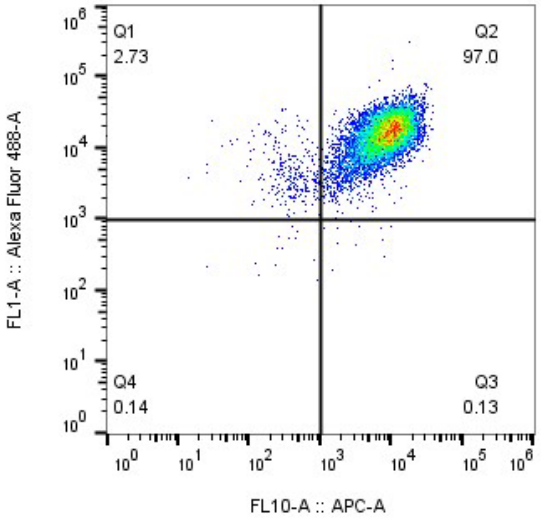
Q1
2.73
Q2
97.0
Q4
0.14
Q3
0.13
FL1-A :: Alexa Fluor 488-A
FL10-A :: APC-A

C

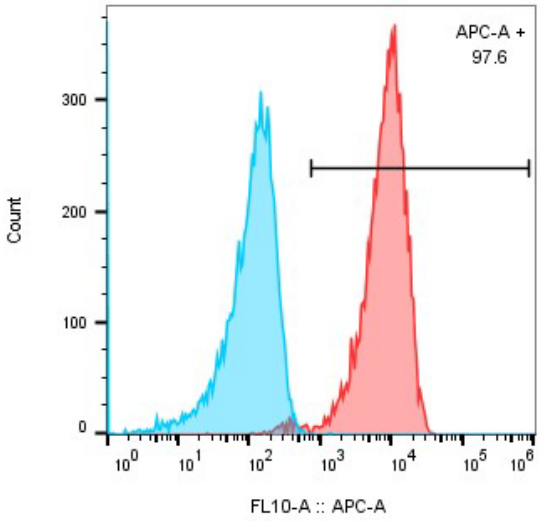
APC-A +
97.6
Count
FL10-A :: APC-A

D

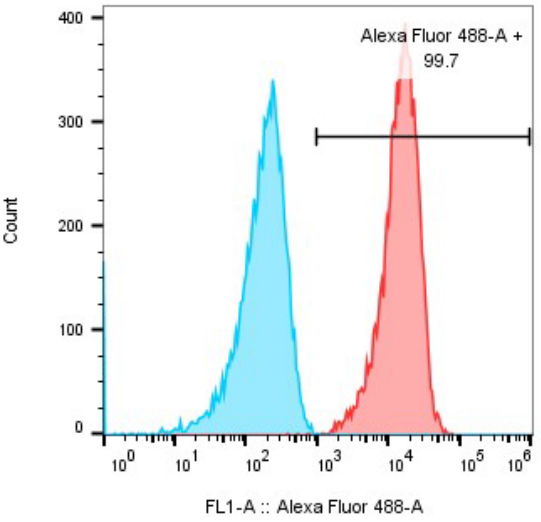
Alexa Fluor 488-A +
99.7
Count
FL1-A :: Alexa Fluor 488-A

Figure 3.8: Maturation of BMMCs. The maturation of BMMCs is confirmed by co-expression of FcεRI(APC) and c-Kit (Alexa Flour 488) receptors testing by flow cytometry. **A:** Flow cytometry testing in an unstained sample of BMMCs. **B:** Flow cytometry testing in a stained sample of BMMCs with both antibodies (anti-FcεRI(APC) and c-Kit(Alexa Fluor 488). **C:** Histogram represents the overlapping of the unstained sample (blue) with the stained sample (red) for the expression of anti-FcεRI(APC). **D:** Histogram represents the overlapping of the unstained sample (blue) with the stained sample (red) for the expression of anti-c-kit(Alexa Flour 488).

The maturation of all BMMC cultures used in the research reported in this thesis, was investigated by evaluating the surface expression of FcεRI and c-Kit, the two defining surface markers of mature MCs (Metcalfe et al., 1997). BMMCs were cultured for at least 4 weeks in presence of both SCF and IL-3 (described in chapter materials and methods), labelled with anti-FcεRI and c-Kit antibodies and analyzed by flow cytometry prior to being used for further experiments (described in chapter materials and methods). After 4 weeks, the BMMCs were collected and stained with anti-FcεRI(APC) and c-Kit(Alexa Flour 488), then forward and side scatters were detected; a gate was set by a polygon and used to include single cells; additional gates for analysis of fluorescent-labelled antibodies were set as illustrated in figure 3.8. From the flow testing, BMMCs cultures showed the same high expression level of FcεRI(APC) and c-Kit(Alexa Fluor 488) (97% and 99% respectively). The average of their maturity it was 96% (75%-99%) in Ten mice tested by flow cytometry technique as shown below in figure 3.9.

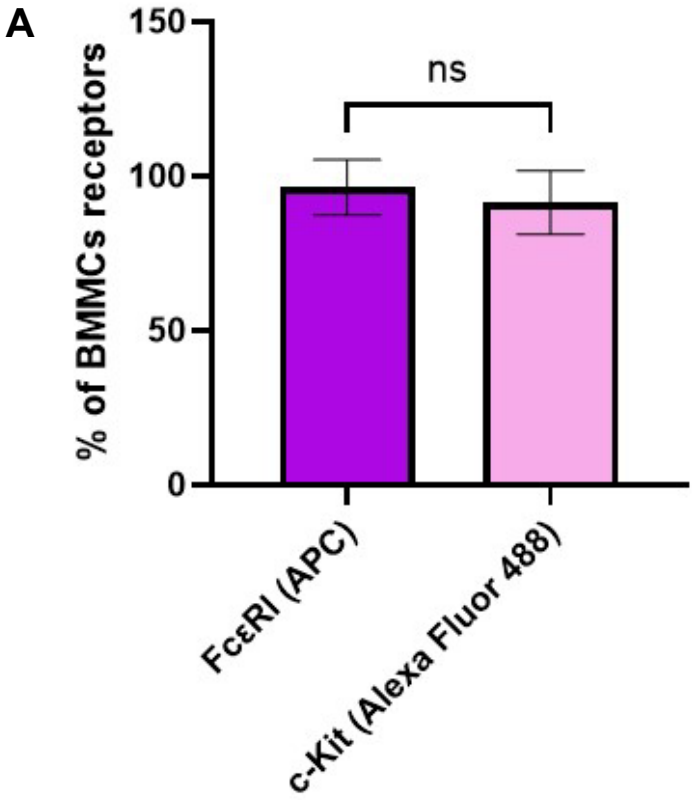
A
150
100
50
0
% of BMMCs receptors
ns
FcεRI (APC)
c-Kit (Alexa Fluor 488)

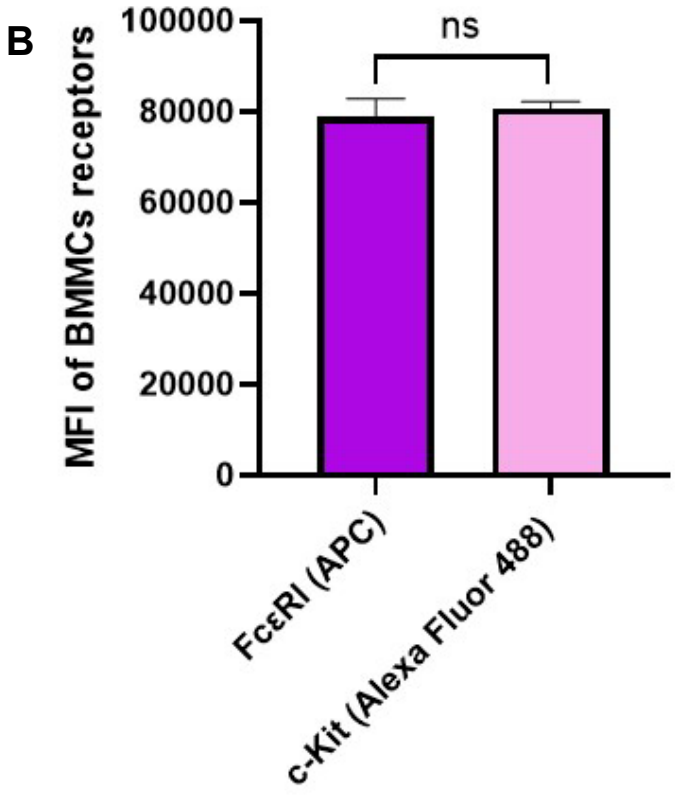
B
100000
80000
60000
40000
20000
0
MFI of BMMCs receptors
ns
FcεRI (APC)
c-Kit (Alexa Fluor 488)

Figure 3.9: Percentage of FcεRI (APC) and c-Kit (Alexa Fluor 488) receptors in BMMCs after 6 weeks of culture. Representative bar chart for the percentage of both FcεRI (APC) and c-Kit (Alexa Fluor 488) in BMMCs. **B:** Representative bar chart for MFI of both FcεRI and c-Kit in BMMCs. Representative conditions of 10 independent experiments. Statistical significance was determine using an unpaired t-test.

The antigen-sensitivity of BMMCs was investigated by measuring degranulation in DNP-IgE sensitised cells. Comparison of responses stimulated in cells sensitised with varying concentrations of the antibody, confirmed that degranulation by the antigen DNP was dependent on prior sensitisation (figure 3.10A); while in the same cells, ionomycin 1 μM and PMA 0.1 μM stimulated degranulation is independent of IgE sensitisation. By contrast, control BMMCs treated with the diluent (PBS) showed minimal degranulation due to spontaneous release. The amount of degranulation measured in response to DNP-stimulation was concentration-dependent (figure 3.10B) reaching a maximum at 100 ng/ml, consistent with a receptor-mediated response. In side-by-side comparisons, ionomycin 1 μM and PMA 0.1 μM consistently stimulated more degranulation than DNP 100ng/ml as shown in figure 3.10C, in sensitised BMMCs, providing a convenient, receptor-independent means of evaluating the function of the regulated secretory pathway in BMMCs.

A

B

C

Figure 3.10: Activation of FcεRI stimulates the degranulation of BMMCs. A: Degranulation of BMMCs, measured by secreted β-hexosaminidase, in response to a 30-minute stimulation with buffer (control, black bars), DNP 100 ng/ml (light pink bars) or ionomycin 1μM and PMA 0.1 μM (dark pink bars), in cells sensitised overnight with the indicated concentrations of mouse anti-DNP IgE. **B:** Concentration-response curve for DNP stimulation of degranulation of BMMC, sensitised overnight with 500 ng/ml anti-DNP IgE (data are mean ± SEM N=3). **C:** Data shown are mean ± SEM, N=3. **** indicates $\rho < 0.0001$ compared to no stimulus group. Data were analyzed using a one-way ANOVA test.

Finally, we also assayed degranulation of single BMMCs using flow cytometry and analysing the surface expression of CD107a as shown in figure 3.11. The gate was adjusted for anti-CD107a Alexa Fluor 647 and overlaid according to unstained sample. Sensitisation of anti-DNP-IgE (500 ng/ml) stimulated BMMCs with either DNP (30,100,300 ng/ml) or ionomycin 1 μM and PMA 0.1 μM was observed to increase both the percentage of cells gated positive for surface expression of CD107a (Figure 3.12A) and the mean fluorescent intensity of the cells (figure 3.12B). Concomitant staining of the cells with DAPI (which can only enter permeable/dead cells) confirmed that >99% cells gated positive for CD107a were negative for DAPI, confirming the antibody was labelling the surface of live cells (figure 3.12C).

A

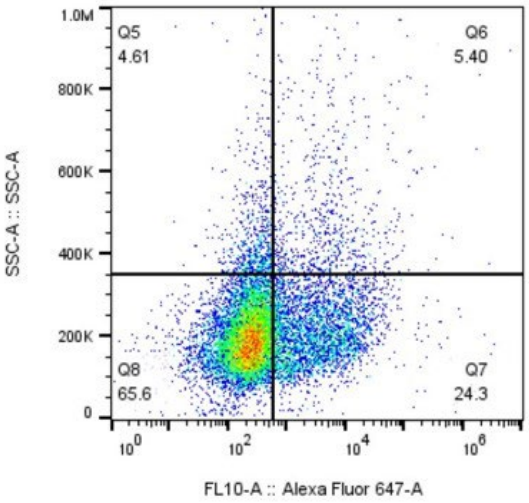

B

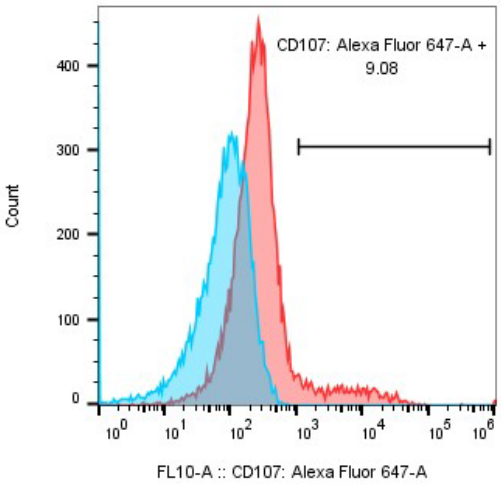

Single Cells: **Mean** : *CD107: Alexa Fluor 647-A*: 92.3

Single Cells: **Mean** : *CD107: Alexa Fluor 647-A*: 1860

C

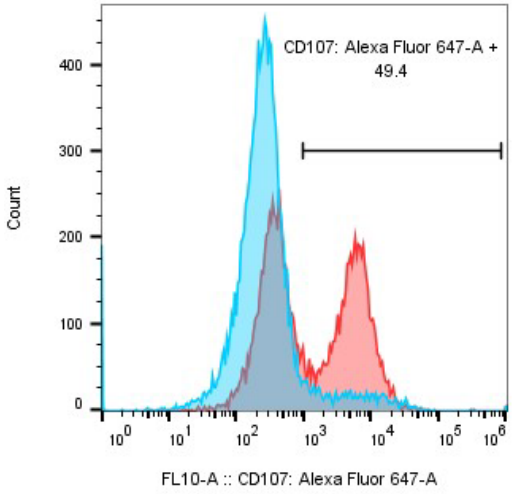

Single Cells: **Mean** : *CD107: Alexa Fluor 647-A*: 1860

Single Cells: **Mean** : *CD107 : Alexa Fluor 647-A*: 4332

D

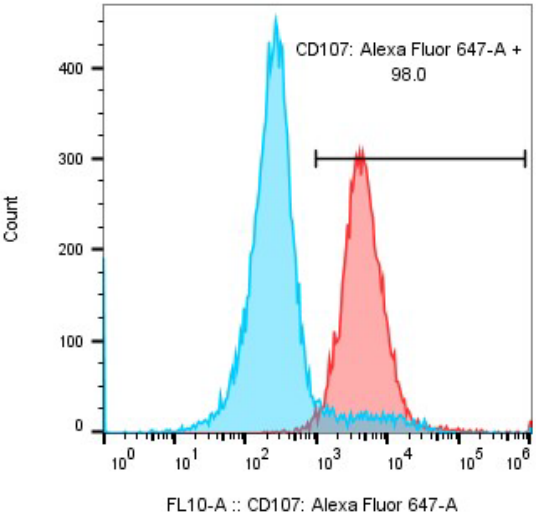

Single Cells: **Mean** : *CD107: Alexa Fluor 647-A*: 1860

Single Cells: **Mean** : *CD107: Alexa Fluor 647-A*: 9292

Figure 3.11: Flow cytometry analysis of CD107a expression in BMMCs. A: Representative example of gating CD107 detected by anti-CD107-Alexa Fluor 647 in BMMCs stained, non-stimulated sample. **B:** Representative example of CD107 expression detected by anti-CD107-Alexa Fluor 647 in BMMCs in the no-stimulated, unstained sample(blue) overlaid with the no-stimulated, stained sample(red). **C:** Representative example of CD107 expression detected by anti-CD107-Alexa Fluor 647 in BMMCs was stimulated with DNP100 ng/ml. **D:** Representative example of CD107 expression detected by anti-CD107-Alexa Fluor 647 in BMMCs was stimulated with ionomycin1μM and PMA 0.1μM.

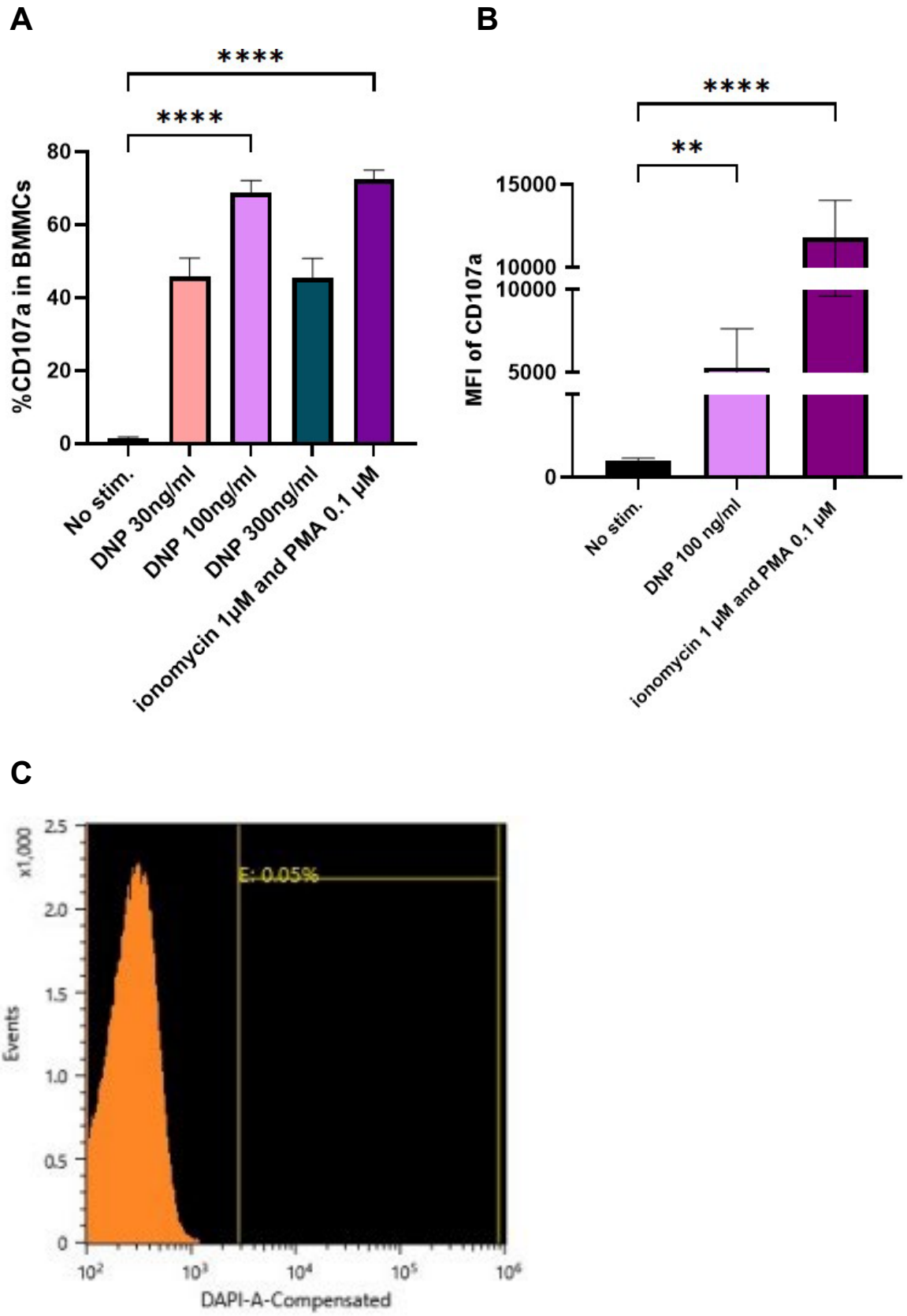
A
****
****
%CD107a in BMMCs
80
60
40
20
0
No stim.
DNP 30ng/ml
DNP 100ng/ml
DNP 300ng/ml
ionomycin 1μM and PMA 0.1 μM
B
****
**
MFI of CD107a
15000
10000
10000
5000
0
No stim.
DNP 100 ng/ml
ionomycin 1 μM and PMA 0.1 μM
C
x1,000
2.5
2.0
1.5
1.0
0.5
0
Events
E: 0.05%
10²
10³
10⁴
10⁵
10⁶
DAPI-A-Compensated

Figure 3.12: Statistics for CD107a in BMMCs. A: Concentration-dose response bar chart for DNP stimulation of BMMCs, sensitised overnight with 500 ng/ml anti-DNP IgE (data are mean $\pm$ SEM n=4) and ionomycin 1 μM and PMA 0.1 μM**. B:** MFI of CD107 in stimulated BMMCs in cells stimulated with 100 ng/ml DNP and ionomycin 1 μM and PMA 0.1 μM. Stimulation of BMMCs with ionomycin 1 μM and PMA 0.1 μM (band with dark purple) degranulate higher than those stimulated with 100 ng/ml DNP(band with light purple). The cells were sensitised with IgE overnight, then stimulated with Ag for 30 minutes and degranulation measured. Data shown are mean $\pm$ SEM of 4 independent experiments. $**$ indicates $\rho < 0.01$ $****$ indicates $\rho <$ 0.0001 compared to the no stimulus group. Data were analyzed using a one-way ANOVA test. **C:** Staining of the cells with DAPI(negative for DAPI after gating),confirming the antibody was labelling the surface of live cells only.

3.3 Discussion

Prior to establishing an in-vitro model for studying to control MCs, it was essential to find the optimal protocol for the generation of mature and functional MCs. MCs develop phenotypical and pharmacological characteristics in response to local micro-environmental factors. These factors include, but are not limited to, different cytokines and inflammatory mediators (Moon et al., 2010). These factors, either alone or in combination regulate gene expression in MCs and contribute to phenotypic alterations and tissue-specific heterogeneity. MC heterogeneity determines and controls mediator production in response to different stimuli. Furthermore, MCs heterogeneity is detected not only across species but also between different organs and even within distinct parts of the same organ (Metcalfe et al., 1997). This complexity poses a challenge to isolating large numbers of mature MCs with identical characteristics directly from tissue. As an alternative approach, in-vitro cultures from MC progenitors, such as BMMCs, have been developed to generate a large number of homogenous MCs (Moon et al., 2010). BMMCs may be reliably differentiated in-vitro, their only limitation is that their viability declines after 9+ weeks in culture (Choi and Abraham, 2015).

At the start of my project, we compared three different in-vitro MC lines (RBL-2H3, MC9, and BMMCs) cultures, focussing in particular on their functional maturity, as defined by their expression of FcεRI and ability to undergo robust and reliable antigen-stimulated degranulation. As a positive control, cells were also stimulated with ionomycin and PMA, which bypasses receptor-mediated signaling to directly increase cytosolic calcium and activate PKC and stimulate degranulation (Hong-Geller and Cerione, 2000).

To evaluate this, the degranulation responses of RBL-2H3, MC9 and BMMCs were measured at different stimuli. Ionomycin plus PMA stimulated both RBL-2H3 and BMMCs to degranulate, reaching maximum of response approximately 60-70% at

concentration of ionomycin 10 μM and PMA 0.1 μM and ionomycin 1 μM and PMA 0.1 μM respectively, after 30 minutes, whereas in MC9 cell shows the same % of degranulation but at ionomycin 1 μM and PMA 0.1 μM after 30 minutes. In contrast, BMMCs and RBL-2H3 cells degranulated robust in response to IgE/Ag stimulation with a maximum release of approximately 40-60% following exposure to 100 ng/ml DNP for 30 minutes. Compared with BMMCs, RBL-2H3 cells exhibited much lower degranulation in response to IgE/Ag stimulation for 30 minutes with approximately 40% when the cells stimulated with 100 ng/ml DNP. However, MC9 cells did not degranulate to IgE/Ag at any concentration (10,100 ng/ml) after 30 min of stimulation.

Our finding corresponds with study indicate that MC9 cells exhibit minimal degranulation when stimulated by IgE/Ag (DNP) (Wagner et al., 2023). Whereas RBL-2H3 and BMMCs are considered more reliable examples for studying MCs degranulation due to their rapid response to both IgE/Ag and ionomycin and PMA (Wagner et al., 2023).

Chapter 4: Investigation of the effects of BoNT proteases on antigen-induced degranulation in MCs

4.1 Introduction

MCs serve as key effector cells in inflammatory responses by releasing mediators through degranulation, synthesis of lipid mediators and synthesis and secretion of cytokines and chemokines (discussed in introduction chapter). MC degranulation is mediated by the activation of cell-surface receptors such as FcεRI, P2RX7, and MRGPRX2. Degranulation is triggered primarily by the binding of antigen-specific IgE to the high-affinity FcεRI receptors; however, recent studies have identified additional receptors capable of mediating IgE-independent degranulation in MCs (Yang et al., 2023). Unlike FcεRI, receptors that mediate IgE-independent degranulation are not expressed in all MC populations; rather, their expression is typically restricted to specific subsets (Yang et al., 2023). The expression patterns of these receptors exhibit tissue-specific variation, enabling the classification of MC types based on receptor profiles within particular tissue microenvironments (Yang et al., 2023). It is therefore important to consider, that being able to inhibit MC secretion via a mechanism that is independent of the activation mechanism is receptor and signalling pathways, would be advantageous for developing a novel therapeutic to treat MC diseases.

MC degranulation and secretion of newly synthesised cytokines and chemokines is reliant on the function of SNARE proteins regulating vesicle fusion. Native and engineered BoNTs targeting MC SNAREs therefore offer an attractive potential biological means of inhibiting MC mediated inflammatory responses. Native BoNT/A, and E cleave SNAP-25 (Chen and Barbieri, 2006), (Pirazzini et al., 2017), whereas VAMPs-1,2,3 are cleaved by BoNT/B, D, F, and G; additionally, syntaxin 1 is cleaved by BoNT/C (Pirazzini et al., 2017).

To evaluate the effect of BoNTs on MC mediators secretion, I transfected BMMCs with fluorescently tagged BoNT light chains (described in introduction) which encoded the active protease domains of BoNT/B and BoNT/D. Degranulation in BMMC was stimulated either by DNP in DNP-IgE sensitised cells or with ionomycin and PMA, as

described previously (see Chapter 3). The effects of expression of the BoNT/LC on degranulation were quantified by measurement of secreted β-hexosaminidase and flow cytometry analysis of surface CD107a in live cells. The aim of this chapter is to investigate of the effects of BoNT proteases on antigen-induced degranulation in MCs as well as measure of IgE receptors and degranulation in transfected BMMCs.

4.1 Results

4.1.1 Nucleofection of BMMCs does not inhibit FcεRI expression or function

MC transfection, in both humans and mice, is known to be technically challenging due to their resistance to conventional gene delivery systems; however, progress has been made using specific reagents and optimized protocols (Hazzan et al., 2017).

The susceptibility of MCs to transfection depends on factors such as cell source (primary versus cell line), cell age, and the reagent used. Optimization of each protocol is essential (Duguay et al., 2018). High-efficiency transfection is often associated with cytotoxicity; therefore, careful titration of both DNA and transfection reagents is required to achieve optimal results (Duguay et al., 2018). Assessing functional and phenotypic profiles post-transfection is also critical to confirm the maintenance of MC identity and responsiveness (Hazzan et al., 2017)..

Transfection may or may not affect the expression, function, and signaling of the high-affinity IgE receptor (FcεRI) in MCs (Xia et al., 2011). These effects may be direct—through the introduction or silencing of components of the receptor complex—or indirect, through altered intracellular signaling and receptor stability (Xia et al., 2011). The primary function of FcεRI is to bind IgE with high affinity, thereby initiating downstream signaling pathways that regulate allergic responses and immune defense by enabling IgE-mediated cytokine release and degranulation (Xia et al., 2011). Transfection of MCs is a valuable approach for studying IgE receptor regulated functions, and experimental outcomes following transfection can be assessed by quantifying functional responses such as degranulation, cytokine release, and changes in cellular proliferation (Ali et al., 2019).

In general, eGFP transfection serves as neutral labelling way (Positive control),permitting both functional and imaging analyses in cells without changing receptor expression or interfering with function, as long as standard nucleic acid

concentrations and carefully optimised transfection protocols are used to minimize the cell toxicity and maintain cell viability (Alam et al., 2023).

Previous studies in our lab established that nucleofection using the AMAXA system was very effective in introducing siRNA into BMMCs (Magadmi et al., 2019). For all transfections reported in this thesis, I used Kit V and program X-001. Analysis of cell viability 24 hours post transfection with pmaxeGFP showed approximately 50% loss of cell viability ($1X10^6$ to $5.3X10^5$ average 10 experiments), the remaining live cells showed good expression of eGFP (figure 4.1B,C). The transfection efficiency, as evidenced from flow cytometry analysis of eGFP fluorescence in live BMMCs, was high with a mean of 70 ± 7% (SEM, N=6) BMMCs gated as positive. Similar experiments performed on BMMCs from five different mice showed that the mean percentage of FcεRI-positive cells was 88%, ranging from 72% to 96%. Previous studies by (Dahlin et al., 2015),(Swindle, 2020),(Chen et al., 2005) have reported that using the same differentiation protocol results in more than 90% FcεRI-positive cells. Our findings are therefore consistent with those reported in the literature. Moreover, analysis FcεRI expression in eGFP expressing cells as shown in figure 4.1D,E compared with paired untransfected cells, showed no significant differences either in the percentage of cells expressing the receptor nor in the MFI, a measure of cell surface expression levels (figure 4.1F).

Figure 4.1: Transfection of BMMCs with GFP does not impact their expression of FcεRI. A: Brightfield image of live BMMCs transfected 24 hours previously with Lonza pmax eGFP (2 µg/ml per $2x10^6$ cells) using AMAXA nucleofection Kit V, program X-001. **B:** Fluorescent image of the same cells shown in (**A)** using 488 nm excitation, revealing the expression of eGFP. **C:** Flow cytometry analysis of eGFP fluorescence in single BMMC. Quadrangle gate shows separation of eGFP negative (low fluorescence) population from eGFP positive (high fluorescence) population. Numbers in each quarter represent the % events detected. Control, untransfected cells from the same BMMC preparation was used to set the gate. **D:** Flow cytometry analysis of APC-anti-FcεRI fluorescence in eGFP positive BMMCs. Quadrangle gate shows separation of negative (low fluorescence) population from positive (high fluorescence) population. Numbers in each quarter represent the % events detected. An unstained sample of untransfected cells was used to set the gate. **E:** Histogram showing flow cytometry analysis of anti-FcεRI-APC fluorescence in eGFP-positive BMMCs. Pale blue histogram shows the background fluorescence from no added antibody control cells; purple histogram shows fluorescence from cells stained with antibody. The bar above the histogram shows the gate used to quantify FcεRI positive cells. Numbers at the top are the percentage of events in the antibody-stained sample gated as positive (top right) and negative (top left). **F:** Summary data comparing the percentage of cells staining positive for FcεRI (left graph) and the mean fluorescent intensity (MFI) for APC-anti-FcεRI (right graph) in control, untransfected and transfected, eGFP expressing cells (N=4). Data shown is mean ± sem. Mann-Whitney test used to determine statistical significance.

Next, I investigated any potential toxicity effects of transfection by comparing degranulation responses in untransfected and eGFP transfected BMMCs. Flow cytometry analysis was used to measure cell surface expression of Alexa Fluor 647 CD107a in live cells following either antigen-stimulation or ionomycin and PMA. The gating strategy used to select cells expressing eGFP is shown in figure 4.2A, these cells were then further analysed for surface expression of CD107a in the absence of added stimulus or following 30 min stimulation with either DNP (100 ng/ml, figure 4.2B or ionomycin 1 μM and PMA 0.1 μM (figure 4.2C). As can be seen in the histograms of the CD107a fluorescence, in the presence of stimulus there is a clear shift to the right (compare overlaid unstimulated histogram in blue, with stimulated in red) consistent with an increase in surface expression following stimulation of the cells. As observed previously, ionomycin and PMA produced a larger increase in both the percentage of cells showing an increase in CD107a and the MFI of cells when compared with DNP. The two peaks observed in the histogram for the DNP stimulated cells show that not all cells respond equally to DNP, as also observed in untransfected cells (Chapter 3). Mean data from replicate experiments show that both stimuli produced robust responses in eGFP-transfected BMMCs (figure 4.2D,E) and that these responses were not different from results obtained from untransfected cells run in parallel experiments (figure 4.2F). Taken together with the results shown in figure 4.1, I concluded that the protocol I used to transfect BMMCs did not impact their function in so far as responses to antigen and receptor expression, and that expression of eGFP could be used to identify transfected cells. In parallel experiments, cells from the same culture were transfected with eGFP and subjected to the same conditions.

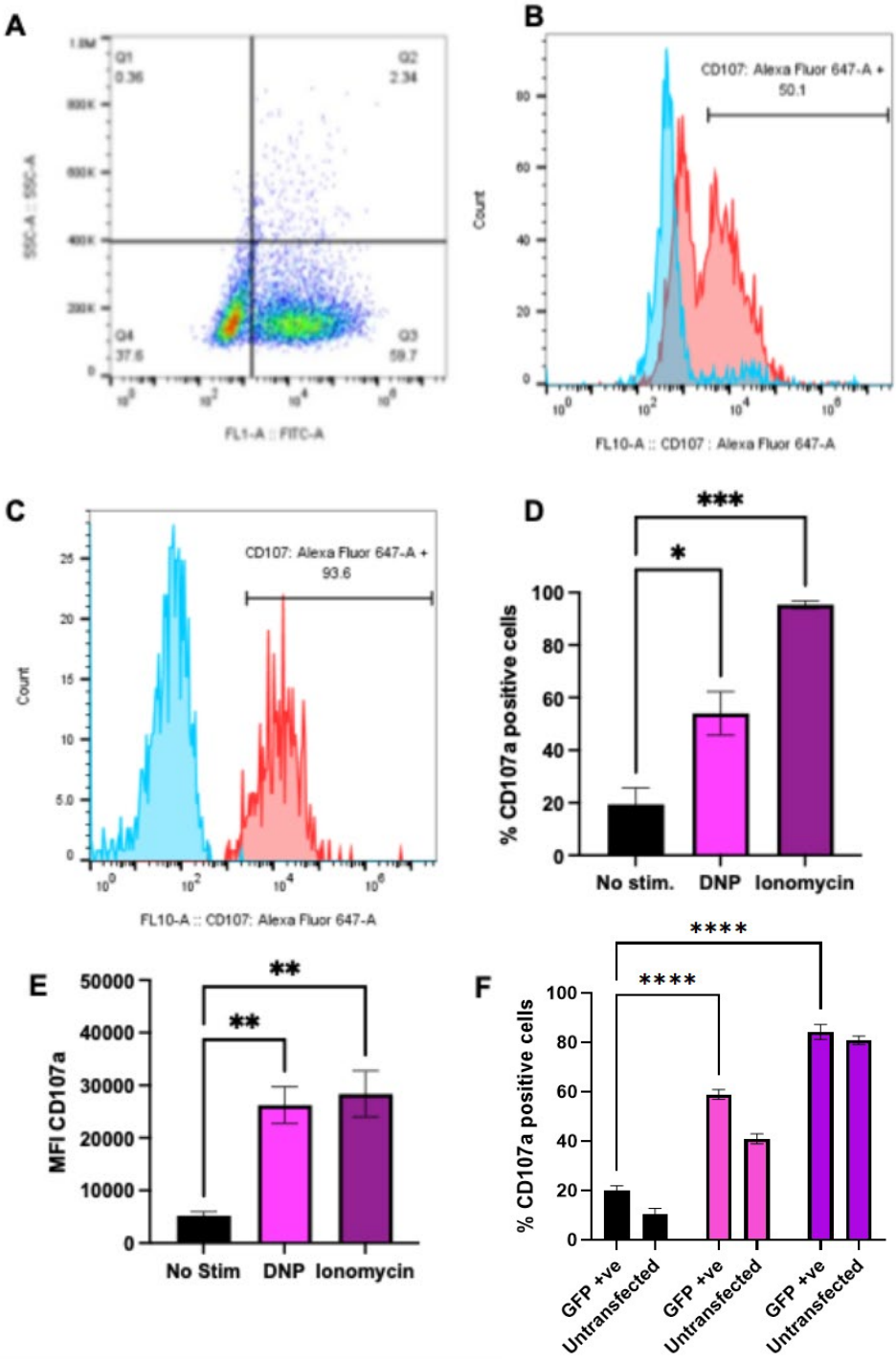
A
Q1
0.36
Q2
2.34
Q4
37.6
Q3
59.7
FL1-A :: FITC-A
B
CD107: Alexa Fluor 647-A +
50.1
Count
FL10-A :: CD107 : Alexa Fluor 647-A
C
CD107: Alexa Fluor 647-A +
93.6
Count
FL10-A :: CD107: Alexa Fluor 647-A
D
% CD107a positive cells
No stim.
DNP
Ionomycin
E
MFI CD107a
No Stim
DNP
Ionomycin
F
% CD107a positive cells
GFP +ve
Untransfected
GFP +ve
Untransfected
GFP +ve
Untransfected

Figure 4.2: eGFP transfected BMMCs degranulate in response to antigen stimulation. **A**: Representative example of the gating strategy used to select the population of eGFP expressing cells in a sample of BMMCs transfected with pmaxeGFP. Numbers in each quadrant correspond to the % cells, in this sample 59.7% of cells were gated at positive for eGFP expression. **B:** Overlaid representative histogram showing flow cytometry analysis of Alexa-647 anti-CD107a fluorescence measured in the eGFP-positive BMMCs , from a no stimulus control sample (pale blue) and following 30 minutes stimulation with 100 ng/ml DNP (red). The gate used to quantify responding cells is shown above. **C:** Data showing overlaid histograms comparing Alexa-647 anti-CD107a fluorescence measured in no stimulus control sample (pale blue) and ionomycin 1 μM and PMA 0.1 μM stimulated cells (red). The gate used to quantify responding cells is shown above. **D:** Summary data of % responding (CD107a positive) of eGFP-expressing cells measured under each condition, in eGFP expressing cells, N=3, data were analyzed using a one-way ANOVA test. **E:** Summary data of MFI (CD107a positive) of eGFP-expressing cells measured under each condition, N=3. CD107 expression against different stimuli. Data were analyzed using a one-way ANOVA test. **F**: Summary data comparing the percentage of cells in untransfected and eGFP-expressing BMMCs gated positive for CD107a under different conditions. Black bars represent the no stimulus control, pink bars cells stimulated with 100 ng/ml DNP, dark pink bars cells stimulated with ionomycin1 μM and PMA 0.1 μM stimulated cells. BMMCs were sensitised 24 hours previously with anti-DNP-IgE. * $p < 0.05$, ** $p < 0.01$, *** $p < 0.001$.

4.1.2 Expression of eGFP-BoNT.LC/B does not inhibit FcεRI expression or degranulation of BMMCs

BoNTs intoxicate cells by binding to cell surface receptors through their heavy chains as in introduction chapter (Mishima et al., 2022). My research project was focussed on evaluating the effects of BoNTs B and D, both of which target VAMP-1,2,3, with VAMP-3 having previously been identified in MCs (introduction chapter). However, MCs do not express the neuronal receptors involved in toxin uptake, therefore in my experiments I introduced the proteolytic light chain of the toxins into BMMCs using AMAXA transfection. Transfecting the light chain domains of BoNTs (BoNT/LC) to bypass receptor mediated entry has previously been shown to be very effective (Aguado et al., 1997), (Yamamoto et al., 2012); moreover N' terminal tagging of the BoNT/LCs with eGFP provides a useful method to monitor expression, without compromising function (Asnawi, 2021). The eGFP-BoNT.LC/B used in my research, were designed and previously tested for functionality in the laboratory of our collaborator Prof Andrew Peden (University of Sheffield), and eGFP-BoNT.LC/D was used by Wirda Ansnawi (PhD student in lab Andrew, University of Sheffield). While there is strong evidence that VAMP-7 and VAMP-8 regulate degranulation in MCs, the role of VAMP-3 is less clear, with one study reporting that knockdown of VAMP-3 in RBL-2H3 cells impairs granule maturation, decreases surface levels of FcεRI and impairs plasma membrane homeostasis (Mishima et al. 2022).

Here I report my results investigating the effects of expression of eGFP-BoNT.LC/B on BMMCs. Using an approach similar to that described above for eGFP transfection, flow cytometry analysis of eGFP fluorescence in transfected living BMMCs was used to identify cells expressing eGFP-BoNT.LC/B. At the same time and in the same cells, labelling with anti-FcεRI APC was used to analyse FcεRI expression. Background fluorescence used to set the gates was determined by omitting the antibody from a sample of the same cells. As shown in figure 4.3 and similar to the results obtained with eGFP transfections (figure 4.1), transfection efficiency was high with eGFP-BoNT.LC/B and as judged by analysis of anti-FcεRI APC staining, high levels of

receptor was detected (figure 4.5); I found no evidence for downregulation of FcεRI by expression of eGFP-BoNT.LC/B within the time-course of my experiments as I measured after 72 hours post-transfection. Analysis of anti-FcεRI APC staining in eGFP-BoNT.LC/B expressing cells, gated by their fluorescence in the 488-excitation channel, showed that high levels or receptor were detected on the cell surface; comparison with samples transfected in parallel with control plasmid (pmaxeGFP) showed no significant differences in either the percentage of BMMCs expressing FcεRI or the MFI of staining with the antibody (figure 4.4A,B).

A

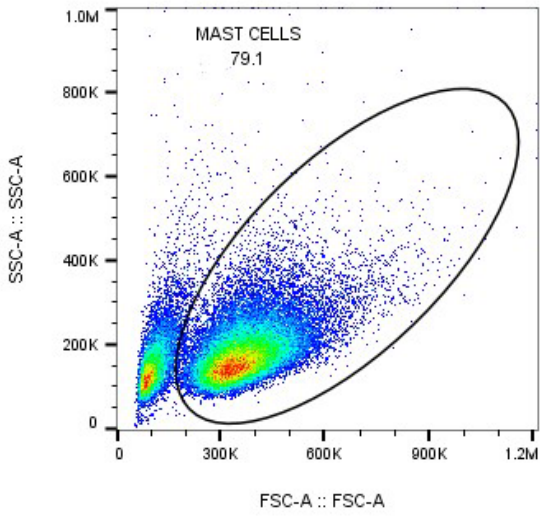

B

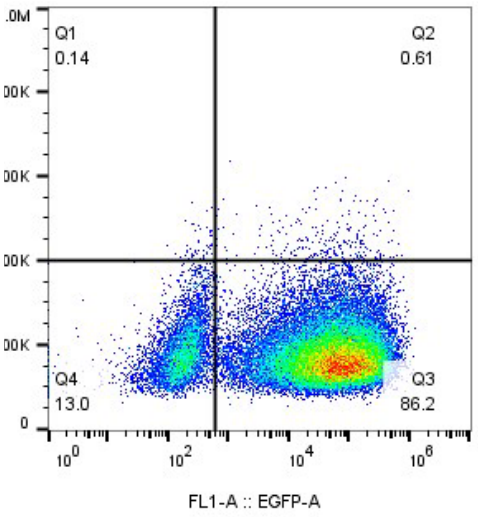

C

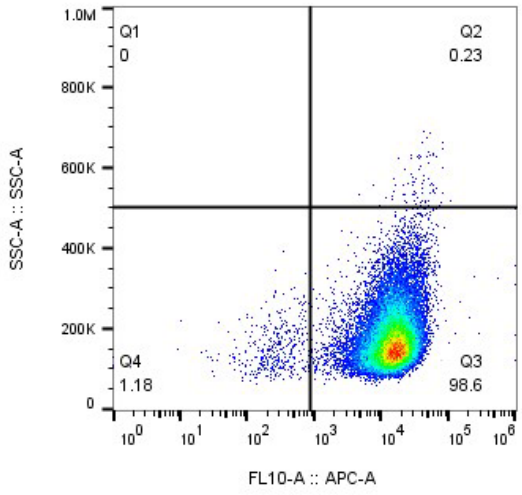

D

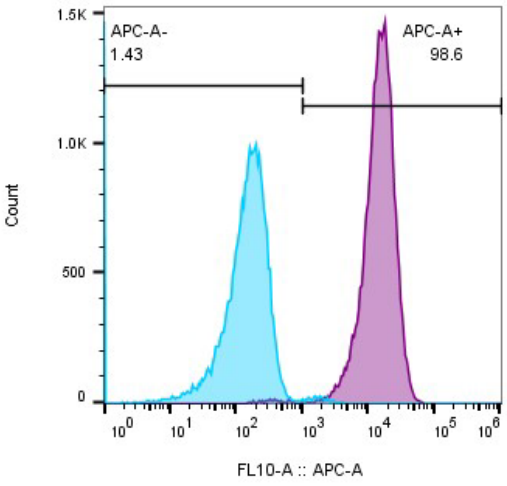

APC-A+: **Mean** : *APC-A*: 4360
APC-A+: **Mean** : *APC-A*: 16021

Figure 4.3: Flow cytometry analysis of FcεRI expression in eGFP-BoNT.LC/B transfected BMMCs. A: Representative example of gating strategy used to identify BMMCs in a sample of transfected cells. Living cells are selected with the elliptical gate, the number in the top right represents the percentage of events within the gate. **B:** Living BMMCs are subsequently analysed for eGFP fluorescence, the quadrangle gate separating the positive eGFP-BoNT.LC/B transfected BMMCs from the untransfected cells exhibiting minimal fluorescence. **C:** Gating of the positive eGFP-BoNT.LC/B expressing cells for analysis of APC anti-FcεRI. **D:** Overlaid histogram showing the analysis of anti-FcεRI APC fluorescence detected in the eGFP-BoNT.LC/B sample shown in **(C) (**purple graph**)** compared with the cells from the same sample which were not expose to antibody, i.e. 'unstained cells' (blue graph). The gate was set using an unstained cell sample. Numbers at the top of the graph represent the percentage of events on either side of the gate for the 'stained sample'. Values below the graph represent the MFI for events in the 'stained sample'.

Figure 4.4 Expression of eGFP-BoNT.LC/B does not inhibit FcεRI expression in BMMCs. Summary data in which the expression of FcεRI was assessed by flow cytometry analysis of staining with APC anti-FcεR in cells gated as positive for expression by their green fluorescence. **A:** shows analysis of the percentage of cells gated as positive for staining by the antibody. **B:** shows the MFI for these cells. Data shown is mean + SEM. For each experiment, as a control, comparisons were made with cells transfected in parallel with pmax-eGFP. Mann-Whitney test used to determine statistical significance, ns: $p > 0.05$.

Next, I assessed the impact of expression of eGFP-BoNT.LC/B on degranulation. I used the CD107a live cell surface labelling assay; this allowed me to perform single cell measurements on BMMCs identified as expressing the protease through eGFP fluorescence. I decided not to use the beta-hexosaminidase assay for two reasons, it requires high cell numbers which would be very costly in reagents, but also, as this assay measures degranulation from a cell population the results do not distinguish between transfected and untransfected cells thereby complicating interpretation of the results.

24 hours after BMMCs were transfected with eGFP-BoNT.LC/B, they were sensitised overnight with 500 ng/ml DNP-IgE. Degranulation was stimulated either by exposure to 100 ng/ml DNP or ionomycin 1 μM and PMA 0.1 μM for 30 minutes at 37°. Control, unstimulated cells were treated with PBS. After the stimulation period, cells were transferred onto ice, stained with anti-CD107a (or control-no antibody) and taken for flow cytometry analysis. Four samples were run in each experiment, one sample from the unstimulated cells treated with vehicle (PBS) to which no antibody was added (this was used to set the CD107a gate), one anti-CD107a stained sample from the unstimulated cells, one anti-CD107a stained sample of cells stimulated for 30 minutes with DNP and one sample stimulated for 30 minutes with ionomycin and PMA. In each case a minimum of 10,000 cells were analyzed. I first gated for cells expressing eGFP-BoNT.LC/B by their green fluorescence intensity (figure 4.6A) and then analysed the surface expression of CD107a in these cells (figure 4.5B). Surface expression of CD107a in BMMCs gating positive for expression eGFP-BoNT.LC/B showed the characteristic increase following stimulation with either the antigen DNP or ionomycin and PMA (figure 4.6C,D). As observed previously, DNP was less effective at stimulating degranulation compared with ionomycin and PMA, showing the characteristic two peaks in the histogram representing low and high responding cells. From the summary data, it is clear that the expression of eGFP-BoNT.LC/B did not significantly inhibit degranulation to either stimulus. Moreover, there were no significant differences between the percentage of BMMCs responding to DNP or ionomycin and PMA between eGFP-BoNT.LC/B expressing cells (figure 4.6) and eGFP expressing cells (figure 4.2), respectively, nor were there any significant differences in the MFI.

A

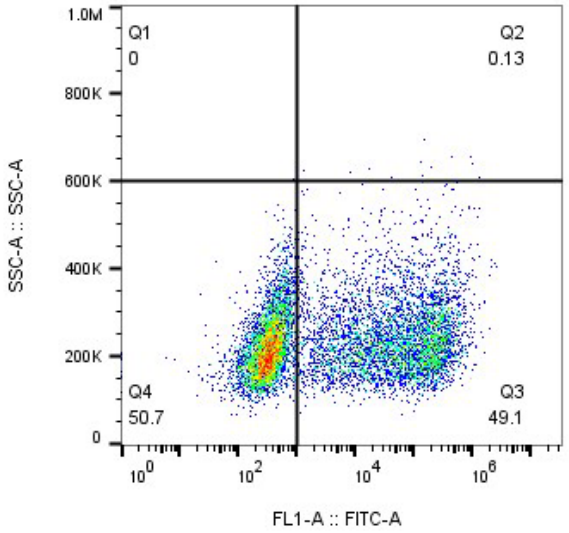
1.0M
800K
600K
400K
200K
0
SSC-A :: SSC-A
Q1
0
Q2
0.13
Q4
50.7
Q3
49.1
10^0
10^2
10^4
10^6
FL1-A :: FITC-A

B

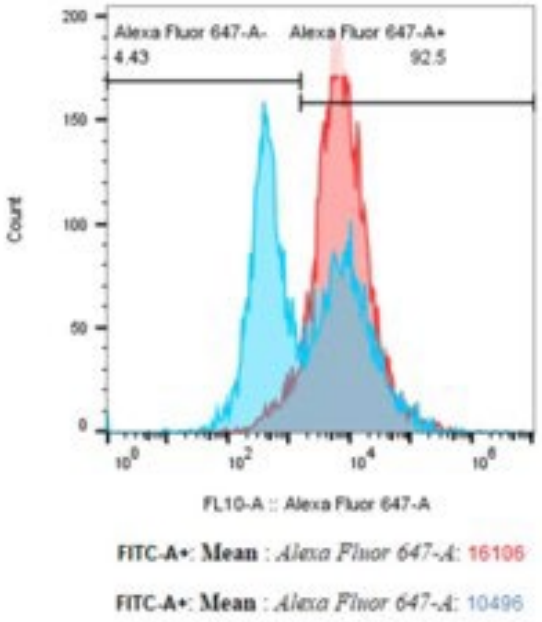
200
150
100
50
0
Count
Alexa Fluor 647-A-
4.43
Alexa Fluor 647-A+
92.5
10^0
10^2
10^4
10^6
FL10-A :: Alexa Fluor 647-A
FITC-A+: Mean : Alexa Fluor 647-A: 16106
FITC-A+: Mean : Alexa Fluor 647-A: 10496

C

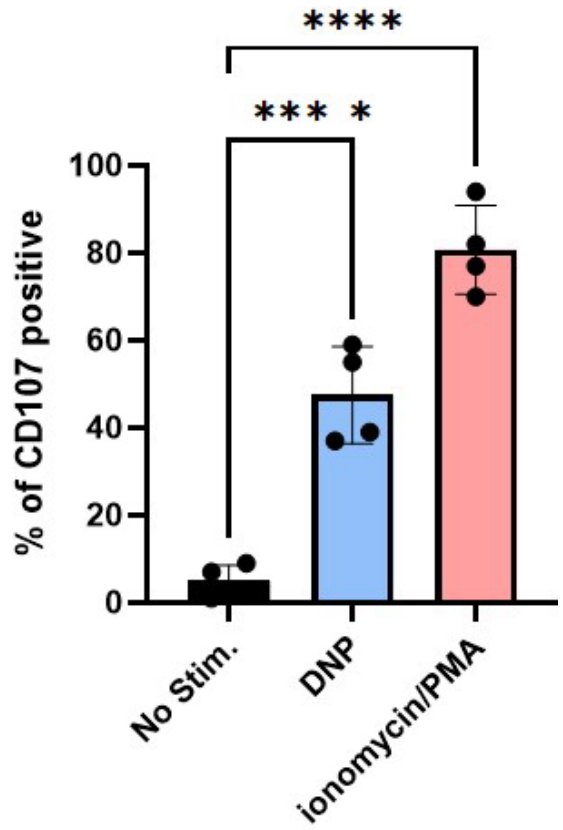
****
*** *
100
80
60
40
20
0
% of CD107 positive
No Stim.
DNP
ionomycin/PMA

D

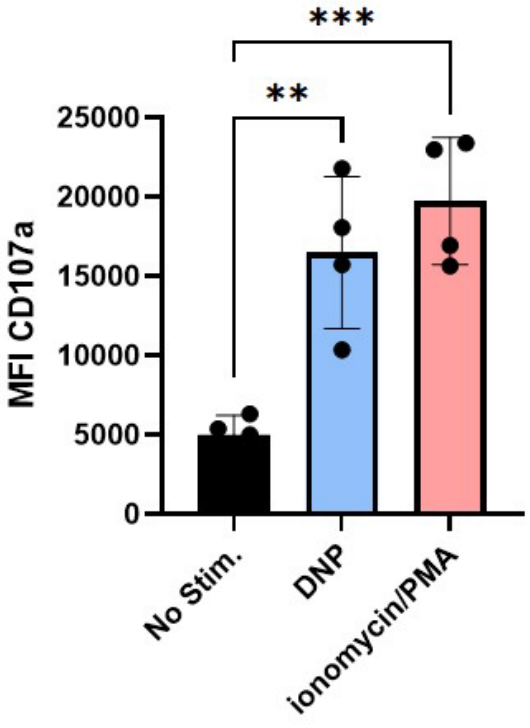
***
**
25000
20000
15000
10000
5000
0
MFI CD107a
No Stim.
DNP
ionomycin/PMA

Figure 4.5: Flow cytometry analysis of CD107a in eGFP-BoNT.LC/B-transfected BMMCs. A: Representative example of gating used to select eGFP-BoNT.LC/B expressing cells using their fluorescence in the eGFP (FITC emission filter set) channel. Numbers in each quadrant represent the percentage of cells detected from the total analysed. **B:** Overlaid histograms showing anti-CD107a staining measured in eGFP-BoNT.LC/B positive cells stimulated with ionomycin 1 μM and PMA 0.1 μM (red) or DNP 100ng/ml (blue). Two peaks are detected in the DNP stimulated sample, representing low and high responders. **C**: Summary data showing the percentage of cells staining positive for CD107a within the eGFP-BoNT.LC/B expressing cells. **D**: Summary data for MFI of CD107a staining within the eGFP-BoNT.LC/B expressing cells. Data shown are mean ± SEM (N=4). Ordinary one-way ANOVA test used to determine statistical significance, ** $p < 0.005$, ***, $p < 0.001$ ****$p < 0.0001$.

4.1.3 Expression of eGFP-BoNT.LC/D does not inhibit FcεRI expression or degranulation of BMMCs

Although the affinities of eGFP-BoNT.LC/B and eGFP-BoNT.LC/D for VAMP-3 are very similar, their catalytic efficiency is significantly different. In-vitro assays of VAMP-3 cleavage, show that BoNT.LC/D has 34-fold increased catalytic efficiency compared with eGFP-BoNT.LC/B (Yamamoto et al. 2012). With this in mind, I next examined the effects of transfection of eGFP-BoNT.LC/D on FcεRI expression and degranulation in BMMCs. Using the same experimental strategy as described in BoNT/B, flow cytometry and eGFP fluorescence was used to analyse the effects of toxin LC expression on receptor expression in living, single cells. As shown in figure 4.7, expression of the toxin failed to alter the percentage of BMMCs expressing FcεRI at the plasma membrane (figure 4.7C). Interestingly, there was a small decrease in the MFI when compared to eGFP control transfected cells (figure 4.7D). Whether this has a functional impact on the cells was examined by quantifying degranulation.

Figure 4.6: Flow cytometry analysis of FcεRI expression in eGFP-BoNT.LC/D transfected BMMCs. A: Live transfected BMMCs were analysed for eGFP fluorescence by flow cytometry; the quadrangle gate separates the positive eGFP-BoNT.LC/D expressing cells, from non-expressing cells in the same sample. **B:** Overlaid histogram showing the analysis of APC-anti-FcεRI fluorescence in eGFP-BoNT.LC/D positive cells (purple graph**)** compared with cells from the same sample which were not exposed to antibody, i.e. 'unstained cells' (blue graph). The gate was set using the unstained cell sample. Number at the top of the graph represents the percentage of events on either side of the gate for the 'stained' sample. Values below the graph represent the MFI for events in the 'stained' sample. **C:** Summary data showing the percentage of cells gated as positive for staining by APC-anti-FcεRI, and **D:** MFI for these cells. Data shown is mean ± SEM. For comparisons, data from cells transfected with pmax-eGFP is shown. Mann-Whitney test used to determine statistical significance, ns: $p > 0.05$., * $p < 0.05$.

Then, I proceeded to examine the effects of expression of eGFP-BoNT.LC/D on antigen- and ionomycin and PMA stimulated degranulation using the CD107a assay. The same experimental protocol used (section 4.1.2) to assess eGFP-BoNT.LC/D effect on BMMCs. Similar to the results obtained with eGFP-BoNT.LC/B, expression of eGFP-BoNT.LC/D did not prevent degranulation in response to either stimuli (figure 4.8).

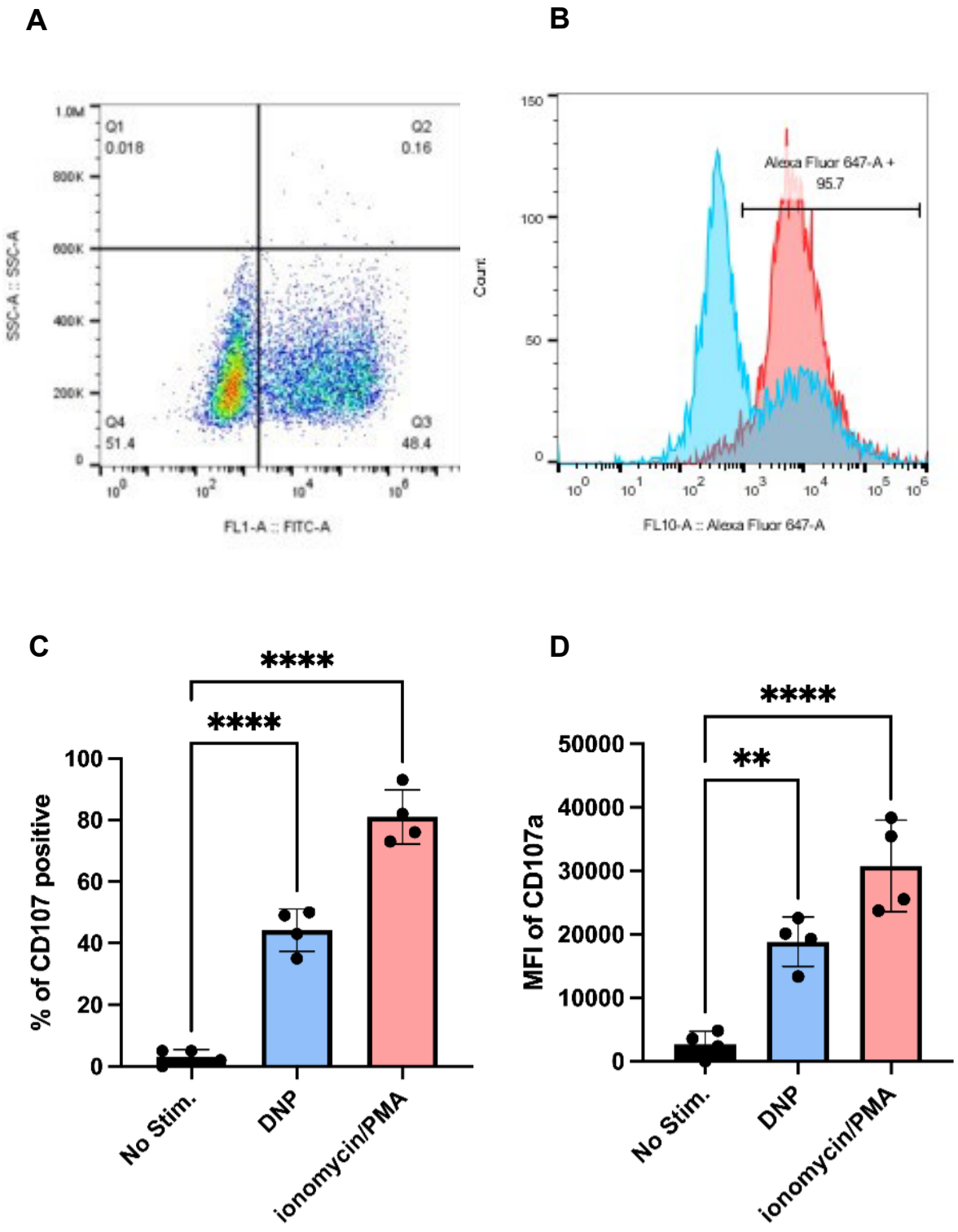
A
B
Q1
0.018
Q2
0.16
Q4
51.4
Q3
48.4
SSC-A :: SSC-A
FL1-A :: FITC-A
Alexa Fluor 647-A +
95.7
Count
FL10-A :: Alexa Fluor 647-A
C
D
****
****
% of CD107 positive
**
MFI of CD107a
No Stim.
DNP
ionomycin/PMA

Figure 4.7: Flow cytometry analysis of CD107a in eGFP-BoNT.LC/D-transfected BMMCs. A: Representative example of gating used to select eGFP-BoNT.LC/D expressing cells using their fluorescence in the eGFP (FITC emission filter set) channel. Numbers in each quadrant represent the percentage of cells detected from the total analysed. **B:** Overlaid histograms showing anti-CD107a staining measured in eGFP-BoNT.LC/D positive cells stimulated with ionomycin 1 μM and PMA 0.1 μM (red) or DNP 100ng/ml (blue). Two peaks are detected in the DNP stimulated sample, representing low and high responders. **C**: Summary data showing the percentage of cells staining positive for CD107a within the eGFP-BoNT.LC/D expressing cells. **D**: Summary data for MFI of CD107a staining within the eGFP-BoNT.LC/D expressing cells. Data shown are mean ± SEM (N=4). Ordinary one-way ANOVA test used to determine statistical significance, ** $p < 0.005$, ****$p < 0.0005$.

4.1.4 VAMP-3 expression in BMMCs

Although it is well established that eGFP-BoNT.LC/B and eGFP-BoNT.LC/D cleave VAMP-3, and independent experiments both in our lab and that of Prof Andrew Peden had validated the functionality of our chimeras in cell lines, it was important to also show they are active in BMMCs under the conditions in which I performed my functional assays. Figure 4.9 shows the results of western blots for VAMP-3 performed with lysates prepared from untransfected, pmaxeGFP, eGFP-BoNT.LC/B and eGFP-BoNT.LC/D transfected cells, from two independent experiments. Expression of VAMP-3 (predicted mw 11.5 KDa) is clearly detected in the untransfected and eGFP transfected samples but is barely detectable in cells transfected with the toxin LCs. The disappearance of the band is consistent with proteolysis of the protein by the toxin LCs and subsequent degradation of cleaved VAMP-3. Semi-quantitative densitometry shows that BoNT.LC/D reduces the normalised VAMP3/GAPDH ratio from ~1.27 (untreated control) to ~0.31, corresponding to a cleavage efficiency of ~76%. In contrast, BoNT.LC/B caused no significant reduction in the ratio (~6% cleavage), confirming VAMP3 is a substrate for BoNT.LC/D but not BoNT.LC/B under these conditions.

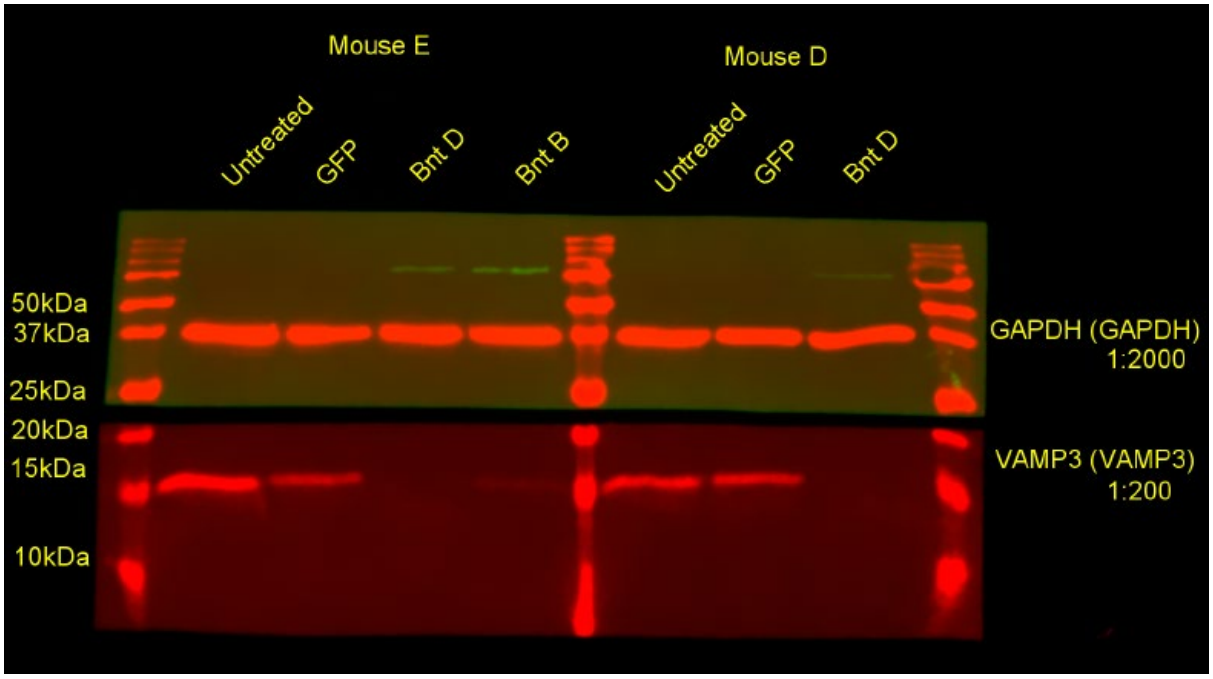

Figure 4.8: Proteolysis and degradation of VAMP-3 in eGFP-BoNT.LC/B and eGFP-BoNT.LC/D transfected BMMCs. Immunoblot showing VAMP-3 expression in lysates prepared from BMMCs prepared from two mice. Untransfected cells (labelled untreated) and cells were transfected with either pmaxeGFP, eGFP-BoNT.LC/B or eGFP-BoNT.LC/D, as indicated above the blot. Expression confirmed by fluorescent microscopy after 48 hours, at which time samples were prepared. GAPDH was used as a loading control. A faint band, indicating residual VAMP-3, can be seen in the eGFP-BoNT.LC/B transfected cells from mouse E. This likely arises from untransfected cells present in this sample, although incomplete cleavage and degradation of VAMP3 in transfected cells cannot be ruled out. The western Blotting and image provided by Ms Tamara Allcock, University of Sheffield.

4.2 Discussion

In this chapter I will examine the effect of eGFP-BoNTs.LC (B and D) on the degranulation in BMMCs. Recent studies have examined whether BoNT LC change antigen-induced degranulation in MCs, which are a key part in allergic and inflammatory reactions (Ramachandran et al., 2018a). Because IgE-dependent degranulation in BMMCs is mediated primarily by a VAMP-8,SNAP-23,syntaxin-4 exocytic proteins (Puri and Roche, 2008), also BoNT/B and D efficiently and specifically cleave different VAMP proteins (VAMPs-1,2,3) which are of less importance to this granular group, so, when apply BoNT/B and D does not significantly reduce surface expression of CD107a in antigen-stimulated murine BMMCs (Puri and Roche, 2008). My findings of this investigation confirm that BoNT serotype B and D does not inhibit the release of pre-formed mediators from stimulated MCs. These findings contrast with the studies by Choi (2019), Ramachandran (2018) who are noted that BoNT/A and B inhibit degranulation in stimulated MCs and reduce rosacea like inflammation and pruritus, as their work on skin and neuronal endings. A potential explanation for the discrepancy is that different BoNT serotypes have distinct target proteins and cellular mechanisms, when apply pre-treatment with BoNT/B and D does not significantly reduce surface expression of CD107a in antigen-stimulated murine BMMCs.

In murine BMMCs, the BoNTs LCs internalization and endosomal translocation have seemed to be slower and less efficient, and the LCs may accumulate in endosomal parts that interact poorly with secretory vesicles (Kumar and Singh, 2025). Meanwhile, the IgE- mediated degranulation is rapid, FcεRI cross-linking induces signaling and granule fusion within minutes, so a large fraction of these granules fuse and externalize CD107a before BoNTs can markedly cleave any accessible VAMPs pool (Razin et al., 1983).

The MCs exhibit complex secretory vesicles rather than containing a homogenous population of granules in their cytoplasm and they differ in biochemical content,

functional roles, and structural manners. These granule subsets are controlled by different complexes of SNARE proteins. The diversity in the use of SNARE proteins among granule types describe the basis that highlight the selectivity of fusion mechanisms and the vesicular trafficking, enabling the MCs to precisely regulate their secretory responses under the influence of different physiological and pathological stimuli (Beil et al., 2000). The key SNAREs responsible for exocytosis of pre-formed mediators (β-hexosaminidase, histamine, heparin, and proteases) in stimulate MCs are Syntaxin-4 and SNAP-23 on plasma membrane combined specifically with VAMP-8 on secretory vesicles (Yang et al., 2018).

In activated murine BMMCs, the dominant v-SNARE responsible for rapid degranulation is VAMP-8, which cooperates with SNAP-23 and Syntaxin-4 at the plasma membrane. VAMP-8 on preformed granules is rapidly prepared into tight four-helix SNARE structure with SNAP-23 and Syntaxin-4. This structure hides the cleavage site (the cleavage site is a specific amino acid sequence on the v-SNARE protein) within the complex and interfere with proteases part to accesses (Palma et al., 2021). Therefore, VAMP-8 is not targeting substrate for BoNT/B and D under physiological circumstances, primarily due to sequence differences around the cleavage sites (Piromchai et al., 2021).

From the mechanistic view, several studies (neurotoxicology, allergy and dermatology) (1992,1993,1995,2018) describe the mechanisms action of BoNT/ B and D on MCs and the information provided mentioned that these two serotypes BoNTs (B and D) are directly targeted the VAMPs- 1,2,3 in the secretory machinery in MCs (Chen et al., 2008).

From experimental aspect, the CD107a (LAMP-1) is a lysosomal/secretory granule membrane protein that becomes exposed on the cell surface when MC granules fuse with plasma membrane. Upon IgE crosslinking, secretory granules undergo plasma membrane fusion and CD107a moves from the inner granule membrane to the external part within the plasma membrane. In the antigen stimulation (~30 minutes) result in strong and flow-detectable CD107a surface staining which is closely associated with β-hexosaminidase/histamine release in BMMCs. IgE- induced granule fusion depends on the SNARE proteins, mainly VAMP-8 (Lorentz et al., 2012), which

is markedly resistance to BoNT/B and D, subsequently, unchanged CD107a % of positive cells and MFI in BMMCs transfected with BoNT/B and D.

Therefore, the main v-SNARE actually responsible for the granule fusion that exposes CD107a is not a substrate for BoNT/B and D, subsequently IgE-dependent exocytosis persists despite exposure to the toxins, that is consistent with my result in this study. However, my study differs from Lorentz's work in several significant aspects. Lorentz, provides a mechanistic and largely literature-based investigation of SNARE usage in MCs, focusing on genetic and antibody-based disruption of VAMP-8 and its associated proteins, while my study focusses directly on measure IgE-induced degranulation to specific BoNT serotype B and D in murine BMMCs.

The VAMP-8 continues to combine with SNAP-23 and Syntaxin. This functional SNARE complex significantly mediated the fusion of the granule membrane with the plasma membrane (Behrendorff et al., 2011). This fusion process reveals the CD107a as a marker on the BMMCs surface, leading to no significant reduction in the flow cytometry expression of CD107a data compared to untransfected BMMCs, validating the important role of the VAMP8-dependent pathway (Chen et al., 2008). Therefore, detecting CD107a using flow cytometry on the surface of stimulated BMMCs serves as a direct way for degranulation. Murine BMMCs use a SNARE protein different from neurons for regulated exocytosis: the dominant plasma membrane t-SNARE is SNAP-23 (not SNAP-25) and the fusion of preformed mediator granules depend primarily on VAMP-7/8, with VAMP-8 begin genetically to be essential for β-hexosaminidase and histamine release and granule-granule/plasma membrane fusion (Lorentz et al., 2012). There are four clear reasons why is it basically expected that BoNT/B and D do not affect CD107a in murine BMMCs: SNARE proteins specificity (VAMP-8 versus VAMP-1,2,3) (Yang et al., 2018). All these factors, make the BoNT/B and D do not change CD107 in stimulated murine BMMCs.

Transfection with eGFP constructs is commonly used to label cells, investigate cellular processes. Recent reports shows that eGFP transfection through electroporation or lipofectamine methods does not inherently change the expression levels of the IgE (FcεRI) receptor on MCs membrane (Alam et al., 2023). Flow cytometry analyses consistently show preserved surface expression of FcεRI and robust IgE-binding appearance after eGFP transfection. Functionally, eGFP transfection itself does not

affect antigen-induced degranulation in BMMCs, this is identical to my results (Alam et al., 2023). Moreover, this study shown how the apolipoprotein C3 to enhance the internalization of cationic lipid nanoparticles into BMMCs without directly activation them, highlighting how MCs can be selectively targeted at the intracellular level. This provides an interesting parallel to my findings, where IgE-dependent degranulation persists despite exposure to BoNT serotype B and D. Suggesting that MCs can remain functionally responsive even when exposed to allergen. Collectively, BMMCs keep their ability for regulated exocytosis, either in the presence of apolipoprotein C3-coated nanoparticles or following treatment with BoNT/B and BoNT/D, describing that key parts of the degranulation machinery such as the dominant v-SNARE responsible for granule fusion, remain intact (Alam et al., 2023).

Sander et al 2008. was observed that VAMP-8 co-localizes with Syntaxin-4 following MC activation and also introducing neutralising antibodies against VAMP-7 markedly decreased histamine and other pre-stored mediators as well as identified an additional role of VAMP-8 for MC degranulation. On the other hand, cleavage VAMP-2 or 3 by Tetanus or anti-VAMP-2 and anti-VAMP-3 antibodies did not alter pre-stored mediators release such as histamine. This observations are consistent with the concept that VAMP-8, rather than VAMP-2 or VAMP-3 is the dominant v-SNARE causing rapid granule fusion in BMMCs, consequently remains functionally intact under these conditions. By discovering that MC exocytosis persists despite targeted interference with VAMP-2 and VAMP-3, my study supports the idea that MC secretory machinery is organised in a highly specialised way in which some v-SNAREs can be targeted without eliminating degranulation.

BoNTs specifically the enzymatic effect of the LCs, are known for their potent ability to inhibit exocytosis process in neurons (Ramachandran et al., 2018a). MCs are effector cells essential to initiate hypersensitivity and host defense, mediating their roles primarily through degranulation in response to antigen cross-linking of surface IgE (Pellett et al., 2015). The molecular mechanism underlying MCs exocytosis includes SNARE proteins such as (SNAP-23, VAMPs-3,7, and 8) which are similar to but different from neuronal SNARE proteins targeted by BoNT(B&D) LC (Introduction chapter) (Pellett et al., 2015).

Chapter 5: Investigation of BoNTs LC on antigen-induced cytokine secretion in MCs

5.1 Introduction

The secretory activity depends heavily on SNARE dependent exocytosis and these exocytic mechanisms has prompted growing interest in the role of BoNTs, whose proteolytic effect targeting of SNARE proteins could have implications for the controlling MC mediator release (Lorentz et al., 2012).

BoNTs toxins exert their biological activity through a highly specific and well-characterised mechanism involving receptor-mediated endocytosis, endosomal translocation of the LC, and subsequent proteolytic cleavage of SNARE proteins essential for vesicular fusion (Pirazzini et al., 2017).

Historically, research on BoNTs has focused predominantly on their paralytic effects resulting from inhibition of neurotransmitter release at cholinergic synapses. However, accumulating evidence now extends their functional relevance to non-neuronal secretory cells, including epithelial cells, immune cells, and notably MCs (Poulain et al., 2020). This shift has prompted interest in repurposing BoNTs as targeted modulators of inflammation, hypersensitivity, and chronic immune activation (Poulain et al., 2020).

Investigating the effects of BoNT LCs on antigen-induced cytokine secretion in MCs is an important research direction, as it seeks to expand the therapeutic applications of BoNTs beyond muscle paralysis to the control of chronic inflammatory and hypersensitivity reactions (Fonfria et al., 2018b). The main finding is that the efficacy of different BoNT LC serotypes is entirely dependent on the specific SNARE proteins utilised by the vesicles that transport each cytokine (Gaudenzio et al., 2016).

BoNT LCs, whether expressed intracellularly or delivered via receptor-mediated uptake, can cleave VAMP-3, a SNARE which has been implicate in regulating cytokine-containing vesicle trafficking (Lorentz et al., 2012). FcεRI engagement triggers a cascade of intracellular events involving calcium influx, activation of PKC, MAPK signalling, mitochondrial ROS modulation, and cytoskeletal remodelling—processes required for both immediate and delayed secretory responses (Gilfillan and Tkaczyk, 2006). Importantly, the transcription and post-Golgi sorting of cytokines,

induced following antigen stimulation, utilise trafficking routes distinct from classical granules (Lorentz et al., 2012). Newly synthesised cytokines such as TNF-α, IL-6, and CCL2 are directed into specialised secretory vesicles, recycling endosomes, or post-Golgi tubular carriers, before migrating to the plasma membrane for regulated exocytosis. The fusion of these vesicles is mediated by the SNARE proteins VAMP-3/8, STX-3/4/6, and SNAP-23 (Kawasaki et al., 2000) (Gaudenzio et al., 2016).

The secretion of antigen-stimulated cytokines in MCs differs mechanistically from rapid degranulation; therefore, BoNT LCs are likely to affect this process differently and with greater specificity (Lorentz et al., 2012). Existing findings, together with current knowledge of SNARE protein utilisation in cytokine trafficking, indicate that the effects of BoNT LCs are cargo- and compartment-specific and interfere only partially with the machinery that mediates granule exocytosis (Lorentz et al., 2012). Antigen stimulation via FcεRI triggers two parallel outcomes: the rapid release of pre-formed mediators and the slower secretion of newly synthesised cytokines (e.g., TNF-α, IL-6, and chemokines). These cytokines are transported through endosomal/TGN-derived compartments that employ SNARE protein sets distinct from, but partially overlapping with, those used for classical granule exocytosis (Lorentz et al., 2012).

In both human and murine MCs, TNF-α and various chemokines are trafficked via VAMP-3/8, with syntaxin-3/4 and endosomal SNAREs (e.g., STX6) contributing to cytokine release rather than histamine granule exocytosis (Lorentz et al., 2012). If a BoNT LC cleaves one or more of the VAMP isoforms used by these carriers, the efficiency of vesicle fusion is reduced, and consequently fewer cytokines reach the extracellular space, even though transcription and translation remain intact (Lorentz et al., 2012).

Several factors suggest that BoNT LCs only partially inhibit antigen-induced cytokine release. First, different VAMP isoforms may support the fusion of cytokine-containing vesicles; therefore, loss of one isoform still allows others to compensate (Lorentz et al., 2012). Second, compartmentalisation results in IL-6, TNF-α, and various chemokines being localised within carriers that are partially defined by the SNARE proteins they employ. Consequently, a specific LC may affect some cytokines more than others (Woska and Gillespie, 2012). For example, in MCs, TNF-α traffics through VAMP-3 dependent recycling/endosomal compartments, whereas VAMP-8 regulates

the secretion of certain chemokines such as CCL8 (Lorentz et al., 2012). Additionally, most BoNT LCs require time to cleave their substrates; thus, early waves of pre-formed TNF-α or cytokine secretion may be less sensitive to inhibition compared with later waves that depend on continued vesicle trafficking (Pellett et al., 2018).

The selective interactions between BoNT LCs and specific SNARE isoforms have important therapeutic implications. Because different cytokines rely on distinct vesicular trafficking pathways, BoNT LCs can inhibit the secretion of certain pro-inflammatory mediators while leaving other MC functions largely unaffected (Chen and Barbieri, 2011). This is in contrast to conventional anti-inflammatory or immunosuppressive drugs, which typically act broadly and suppress multiple signalling pathways simultaneously. It has also been demonstrated that BoNT/B specifically cleaves the VAMP-3 isoform, thereby inhibiting the delayed, VAMP-3 dependent release of inflammatory cytokines such as TNF-α and IL-6 in MCs (Galli et al., 2005). In particular, MC–derived cytokines such as TNF-α, IL-6, IL-13, and various chemokines play an essential roles in driving chronic allergic inflammation, and hypersensitivity reactions. By targeting the SNARE proteins required for the trafficking of these cytokines—without completely blocking granule exocytosis or other protective MC responses—BoNT LCs offer a more precise means of modulating MC activity (Pirazzini et al., 2017). The aim of this chapter is to investigation of BoNTs LC on antigen-induced cytokine secretion in MCs.

5.2 Results

5.2.1 Flow cytometry analysis of BoNT LCs effects on TNF-α synthesis and secretion

TNF-α is a pivotal pro-inflammatory cytokine synthesised by MCs, essential to the initiation and enhancement of immune and inflammatory responses (Gordon and Galli, 1990). TNF also known as cachectin, was initially identified by Carswell et al. as a serum factor in BCG-infected mice that promotes tumour necrosis (Mukai et al., 2018).

In contrast, to numerous immune cells that synthesise TNF-α *de novo* following activation, MCs distinctly store pre-formed TNF-α in their cytoplasmic granules, enabling its rapid release upon stimulation (Gordon and Galli, 1990). This immediate secretion enables MC-derived TNF-α to function as an early mediator of inflammation, facilitating endothelial activation, leucocyte recruitment, and the modulation of both innate and adaptive immune responses (Gordon and Galli, 1990).

MCs can produce TNF-α *de novo* in addition to their pre-formed group following prolonged stimulation, further prolonging inflammatory signalling (Theoharides et al., 2007). Given that both pre-formed and newly synthesised TNF-α depend on vesicular trafficking and exocytotic pathways, disruption of the molecular mechanisms regulating granule effusion is expected to influence TNF-α secretion directly (Theoharides et al., 2007).

Dysregulated MC TNF-α release has been linked to a number of diseases such as allergic inflammation, autoimmune diseases, and chronic inflammatory disorders, highlighting its importance as both a physiological regulator and therapeutic targets (Theoharides et al., 2007).

In this chapter, BoNTs LC, which specifically cleave SNARE proteins essential for vesicle-plasma membrane fusion serve as a powerful tool for analysing the role of regulated exocytosis in MC cytokine release (Chen and Barbieri, 2006). Consequently, analysing the impact of BoNTs LC on TNF-α secretion offers mechanistic

understanding of how the disruption of SNARE-dependent pathways influences MC-mediated inflammatory signalling, extending observations from degranulation assays to cytokine-mediated responses (Chen and Barbieri, 2006).

To measure the level of TNF-α in activated MCs with different stimulus and in absence and present of BoNTs LC, I firstly, cultured BMMCs from 8-12 weeks old mice for 4 weeks, after that transfected with eGFP-tagged plasmids, waited 24 hours to confirm expression and then sensitised the BMMC cells (overnight) with DNP-IgE before proceeding to stimulate the cells with either antigen DNP 100 ng/ml or ionomycin 1μM and PMA 0.1μM for 2 hours (see method section), and then I either quantified intracellular TNF-α by Flow cytometry and or secreted by ELISA. For the flow cytometry experiments, as a positive control, some samples with treated with brefeldin A (BFA; 3 μg/ml) and Monensin (2μM) to inhibit intracellular transport of the cytokine and thereby block its secretion; treatment with the transport inhibitors was delayed for 1 hour into the stimulation so as not to interfere with receptor signaling.

5.2.2 Untransfected BMMCs

Initial experiments to establish the protocol for assessing TNF-α secretion by flow cytometry analysis were performed with untransfected BMMCs. As shown in figure 5.1, in the absence of any stimulus, intracellular staining for TNF-α was minimal with only 3% of cells gating positive and a very modest MFI of 654. Following stimulation with either DNP or ionomycin and PMA (figure 5.2A, C) a very clear increase in both the percentage of cells gating positive for TNF-α and the MFI can be seen. Addition of BFA and Monensin further increases the MFI of staining with anti-TNF-α, consistent with intracellular trapping of the cytokine in the cells (figure 5.2B, D). Summary of data from 4 independent experiments (figure 5.3) show that BMMCs synthesize TNF-α *de novo* in response to both antigen and ionomycin and PMA and that flow cytometry analysis may be used to quantify intracellular trapping of the cytokine. Examination of the effects of BFA and Monensin show further that there is a significant increase in the MFI for TNF-α as expected with both stimulus conditions. For the no stimulus conditions there was a modest increase in MFI of 9.4 $\pm$ 5.7 % in the presence of BFA and Monensin compared with a 38.2 $\pm$ 2.7 % for DNP-stimulated cells and 38.5 $\pm$ 2.9 % for ionomycin and PMA stimulated cells. I reasoned that the differences observed in the stimulated groups between the two treatment groups, arise from ongoing secretion of the cytokine in the absence of BFA and Monensin, resulting in a lower MFI. Therefore, I can consider differences in MFI as an indirect measure of secretion. Comparison of the percentage of cells staining positive shows a significant increase for cells stimulated with ionomycin and PMA but not with DNP (figure 5.4). This again is expected, as ionomycin and PMA produce a maximum stimulation of cells compared with DNP, as seen in our previous assays of degranulation. In the presence of BFA and Monensin, however, cells producing very moderate amounts of TNF-α that fall below the detection limits of our analysis, would become detectable and gate positive when the cytokine is trapped intracellularly.

A

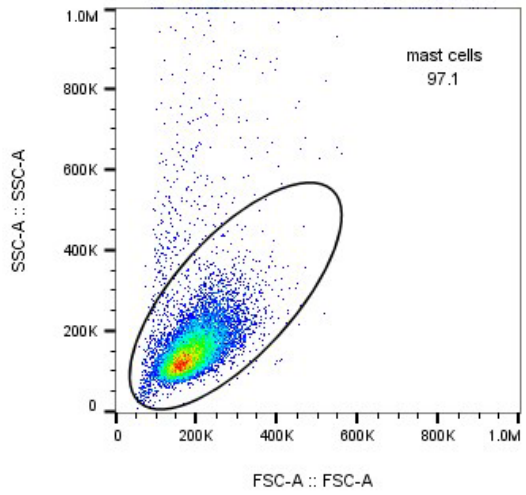

B

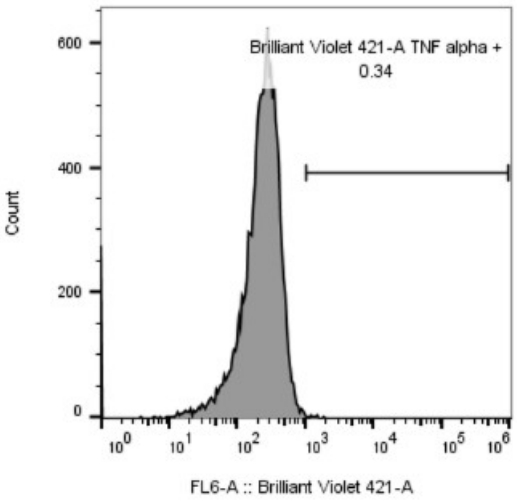

C

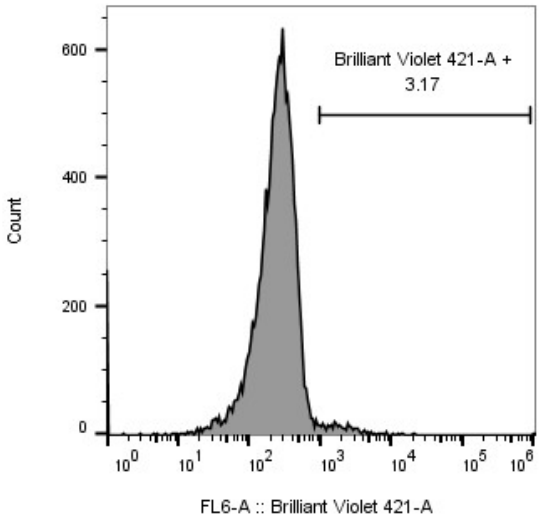

D

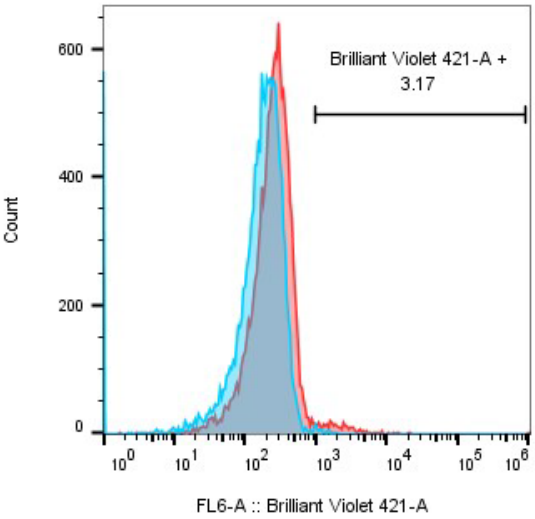

Single Cells: **Mean** : *Brilliant Violet 421-A*: 203

Single Cells: **Mean** : *Brilliant Violet 421-A*: 654

Figure 5.1: Flow cytometry analysis of TNF-α expression in no stimulus untransfected BMMCs. A: Representative example of a gating strategy used to identify single cells. **B:** Representative example of no stimulus and unstained with anti-TNF-α antibody in untransfected BMMCs. **C:** Representative example of TNF-α detected by anti- TNF-α Alexa Fluor 421 in untransfected BMMCs. **D:** Representative example of overlapping between unstained with anti- TNF-α in the no stimulus sample in untransfected BMMCs.

A

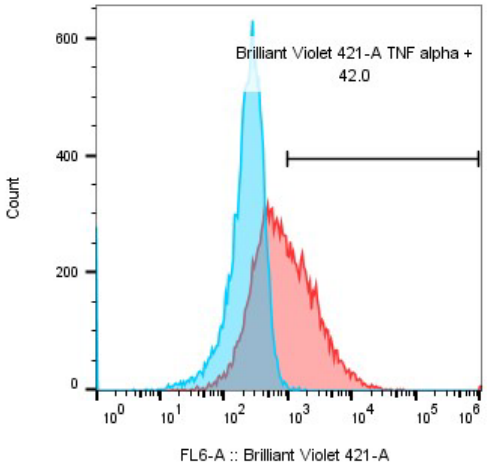
Brilliant Violet 421-A TNF alpha +
42.0
Count
FL6-A :: Brilliant Violet 421-A

B

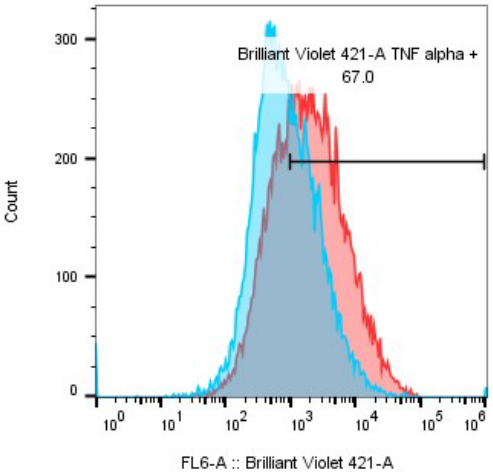
Brilliant Violet 421-A TNF alpha +
67.0
Count
FL6-A :: Brilliant Violet 421-A

C

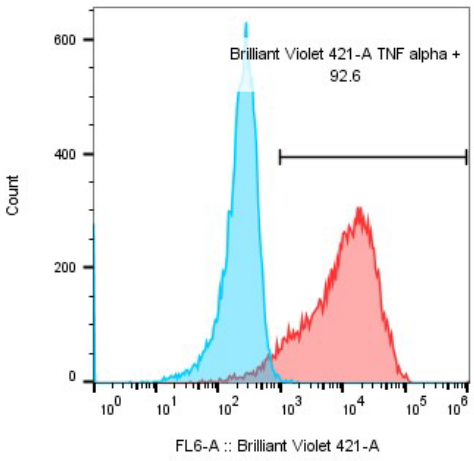
Brilliant Violet 421-A TNF alpha +
92.6
Count
FL6-A :: Brilliant Violet 421-A

D

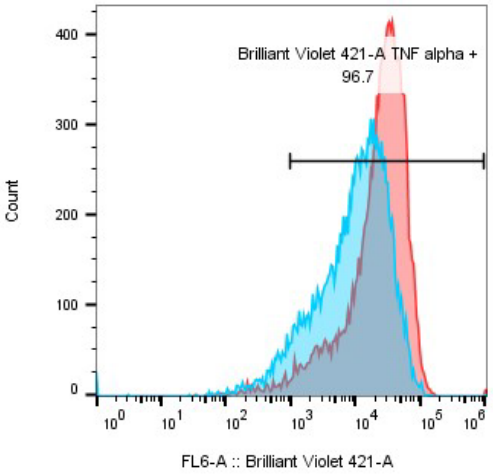
Brilliant Violet 421-A TNF alpha +
96.7
Count
FL6-A :: Brilliant Violet 421-A

Figure 5.2: Flow cytometry analysis of TNF-α expression in stimulated untransfected BMMCs. A: Representative example of TNF-α detected by anti- TNF-α Alexa Fluor 421 in untransfected BMMCs in response to DNP 100ng/ml. **B:** Representative example of TNF-α detected by anti- TNF-α Alexa Fluor 421 in untransfected BMMCs in response to DNP 100ng/ml in the presence of BFA and Monensin. **C:** Representative example of TNF-α detected by anti- TNF-α Alexa Fluor 421 in untransfected BMMCs in response to ionomycin 1μM and PMA 0.1μM. **D:** Representative example of TNF-α detected by anti- TNF-α Alexa Fluor 421 in untransfected BMMCs in response to ionomycin 1μM and PMA 0.1μM in the presence of BFA and Monensin.

A

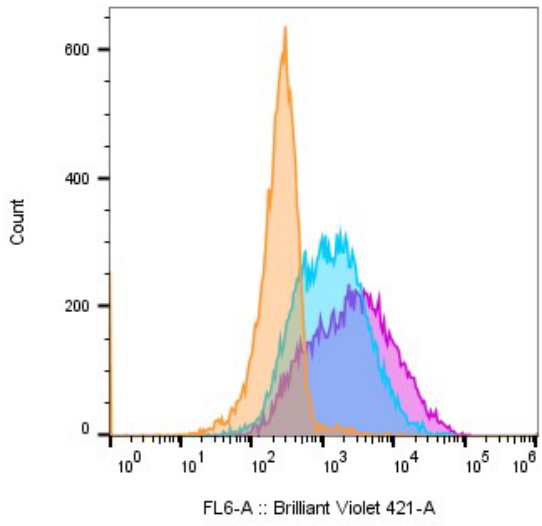

Single Cells: Mean : *Brilliant Violet 421-A*: 555

Single Cells: Mean : *Brilliant Violet 421-A*: 2665

Single Cells: Mean : *Brilliant Violet 421-A*: 5799

B

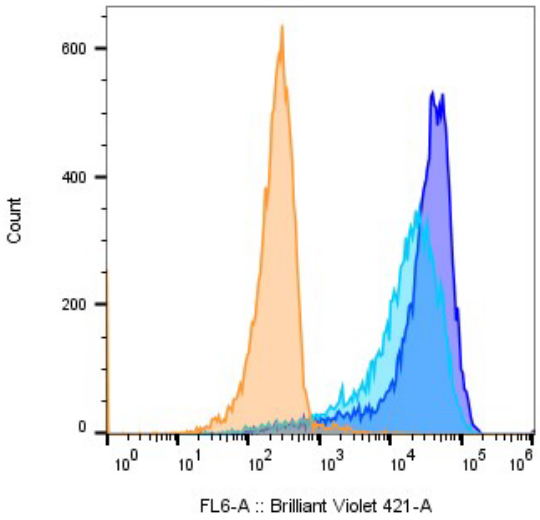

Single Cells: Mean : *Brilliant Violet 421-A*: 555

Single Cells: Mean : *Brilliant Violet 421-A*: 22787

Single Cells: Mean : *Brilliant Violet 421-A*: 37890

C

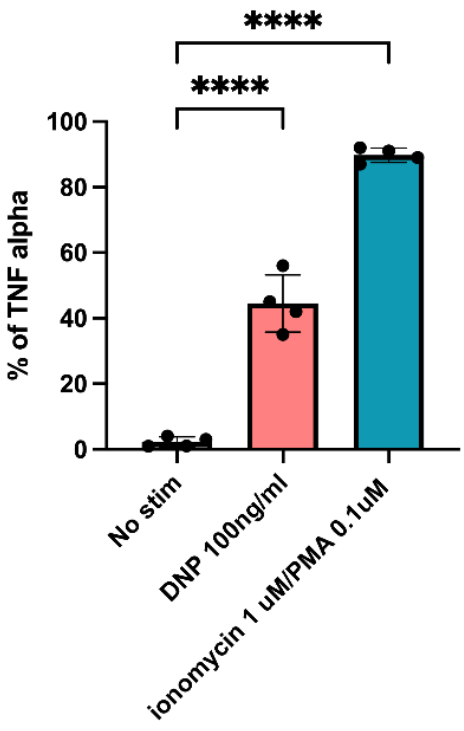

D

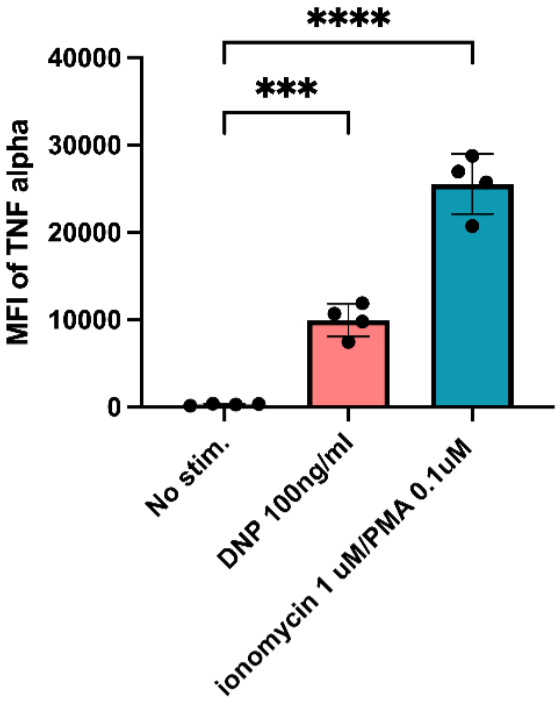

Figure 5.3: Flow cytometry analysis of TNF-α expression in untransfected BMMCs. A: Representative example of the overlapping of anti- TNF-α between DNP stimulus without BFA & Monensin and the sample with in untransfected BMMCs. **B:** Representative example of the overlapping of anti- TNF-α between ionomycin and PMA stimulus without BFA & Monensin and the sample with in untransfected BMMCs. **C:** Representative bar chart showing the analysis of % TNF-α expression against different stimuli, N=4. ,$****$ indicates $\rho < 0.0001$ Data were analyzed using a one-way ANOVA test. **D:** Representative bar chart showing MFI(Mean Fluorescent Intensity) of TNF-α expression in response to different stimuli in untransfected BMMCs, N=4. $**$ $*$ indicates $\rho < 0.001$, $****$ indicates $\rho < 0.0001$. Data were analyzed using a one-way ANOVA test.

A

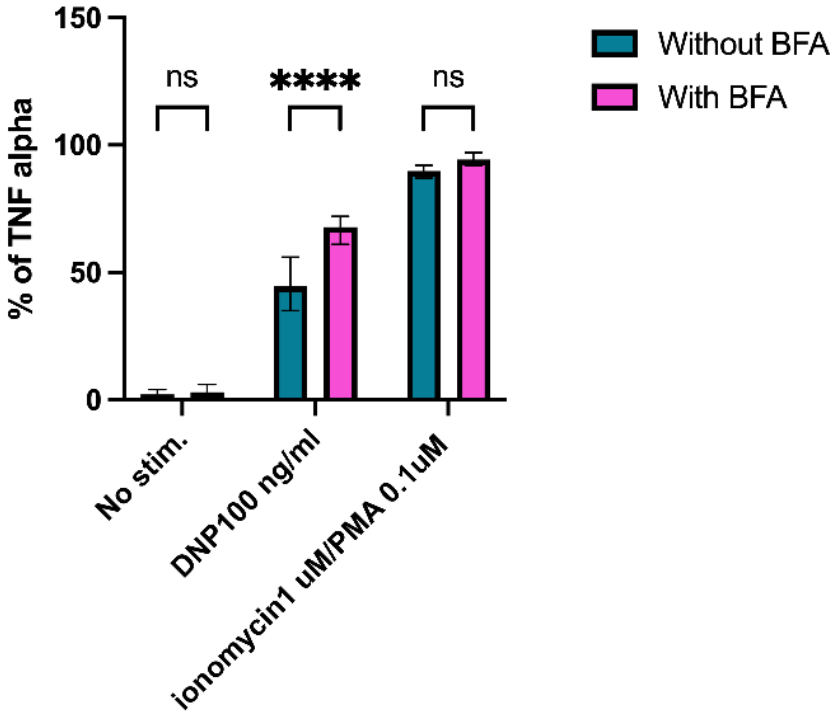
150
100
50
0
% of TNF alpha
ns
****
ns
Without BFA
With BFA
No stim.
DNP100 ng/ml
ionomycin1 uM/PMA 0.1uM

B

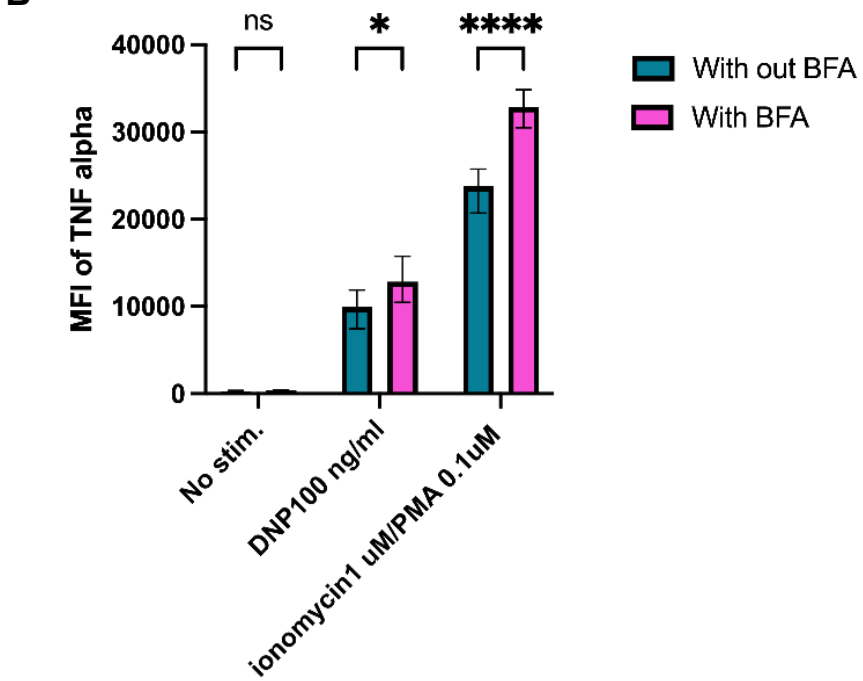
40000
30000
20000
10000
0
MFI of TNF alpha
ns
*
****
With out BFA
With BFA
No stim.
DNP100 ng/ml
ionomycin1 uM/PMA 0.1uM

Figure 5.4: BFA and Monensin cause accumulation of TNF-α in stimulated untransfected BMMCs. A: Representative example of %TNF-α detected by anti-TNF-α Alexa Fluor 421 in untransfected BMMCs in response to different stimuli, comparing the expression of TNF-α in +/- BFA and Monensin (N=4). $****$ indicates $\rho < 0.0001$. Data were analyzed using a one-way ANOVA test. **B:** Representative example of MFI detected by anti-TNF-α Alexa Fluor 421 in untransfected BMMCs in response to different stimuli, comparing the expression of TNF-α in +/- BFA and Monensin (N=4). $*$ indicates $\rho < 0.05$, $****$ indicates $\rho < 0.0001$. Data were analyzed using a one-way ANOVA test.

5.2.3 eGFP-transfected BMMCs

Having established a protocol for assessing TNF-α synthesis and secretion in BMMCs using flow cytometry, I next investigated the effects of transfection on stimulus induced cytokine production and secretion by transfecting BMMCs with eGFP. Cells were transfected with pmaxeGFP using the AMAXA protocol described in Chapter 4, left 24 hours to recover and express the eGFP, then sensitised overnight with DNP-IgE (500 ng/ml) before proceeding with the stimulation protocol described in the preceding section. When analysing TNF-α by flow cytometry in these experiments, I first identified the transfected cells by gating for green fluorescence (figure 5.5B), I then gated these cells for TNF-α (figure 5.6) before proceeding to analyse the effects of stimulation (figure 5.7). Flow cytometry analysis of 3 independent experiments (figure 5.8), shows that transfection and expression of eGFP did not inhibit the cells responses to the stimuli nor their ability to synthesize TNF-α, as well as increased %TNF-α in eGFP-transfected BMMCs indicates that eGFP did not successfully reduce TNF-α secretion even when used two different stimulus as appear in figure 5.8 A. Moreover, the increased MFI observed in the presence of BFA and Monensin, are consistent with ongoing secretion of the cytokine in the untreated samples (figure 5.9).

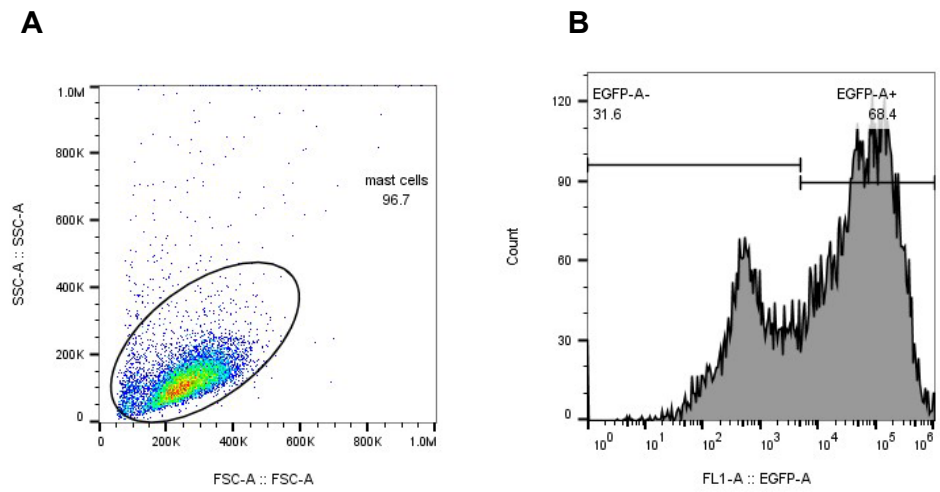

Figure 5.5: Flow cytometry analysis of TNF-α expression in eGFP-transfected BMMCs. A: Representative example of a gating strategy used to identify single cells. **B:** Representative example of GFP-positive cells.

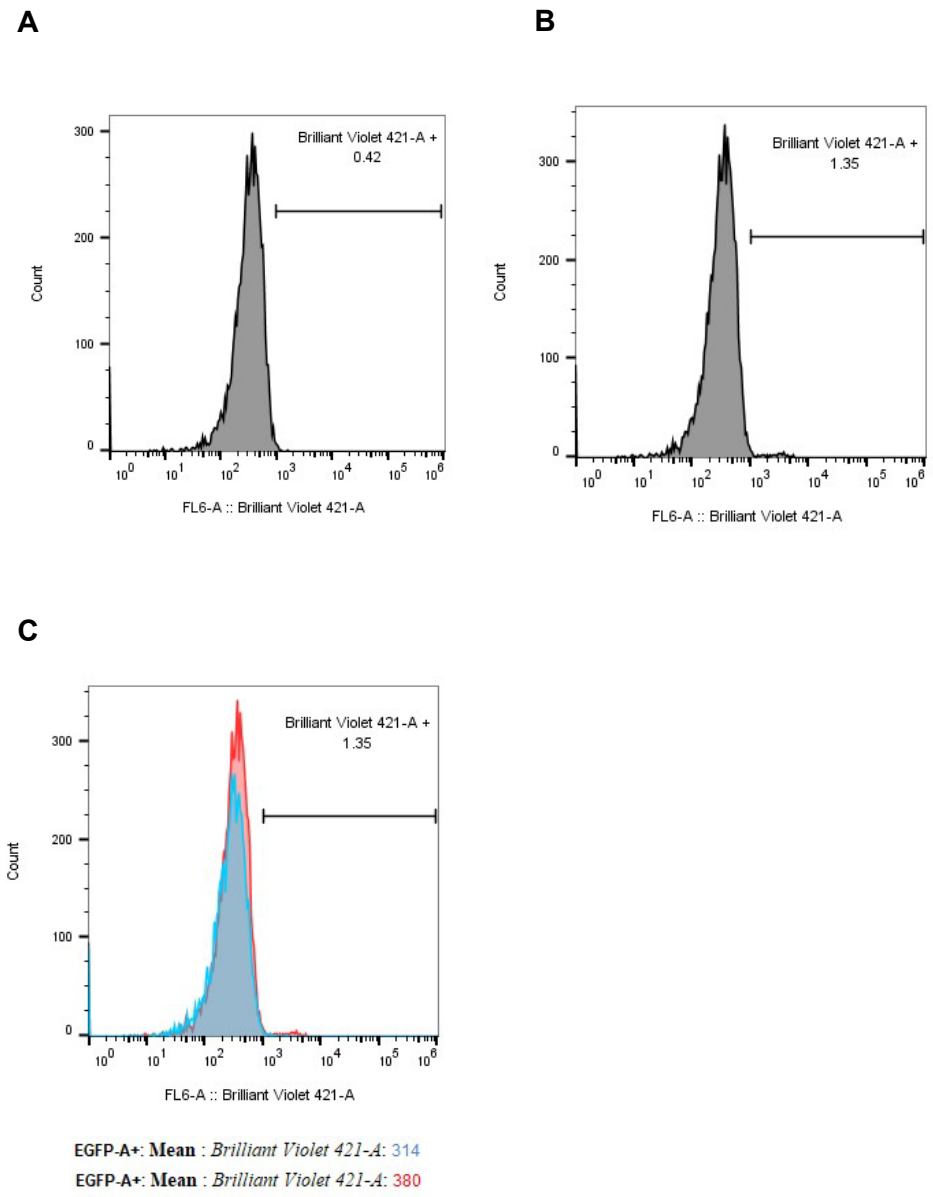

Figure 5.6: Flow cytometry analysis of TNF-α expression in no stimulus eGFP-transfected BMMCs. A: Representative example of no stimulus and unstained with anti-TNF-α antibody in eGFP-transfected BMMCs. **B:** Representative example of TNF-α detected by anti-TNF-α Alexa Fluor 421 in eGFP-transfected BMMCs. **C:** Representative example of overlapping between unstained with anti-TNF-α in the no stimulus sample in eGFP-transfected BMMCs.

A

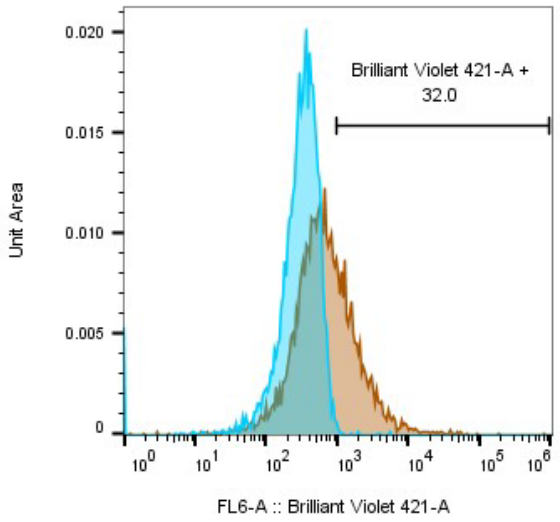

EGFP-A+: **Mean** : *Brilliant Violet 421-A*: 361

EGFP-A+: **Mean** : *Brilliant Violet 421-A*: 1343

B

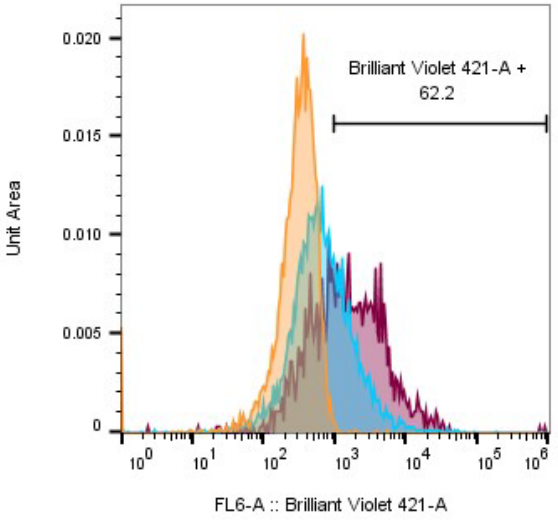

EGFP-A+: **Mean** : *Brilliant Violet 421-A*: 361

EGFP-A+: **Mean** : *Brilliant Violet 421-A*: 1343

EGFP-A+: **Mean** : *Brilliant Violet 421-A*: 3618

C

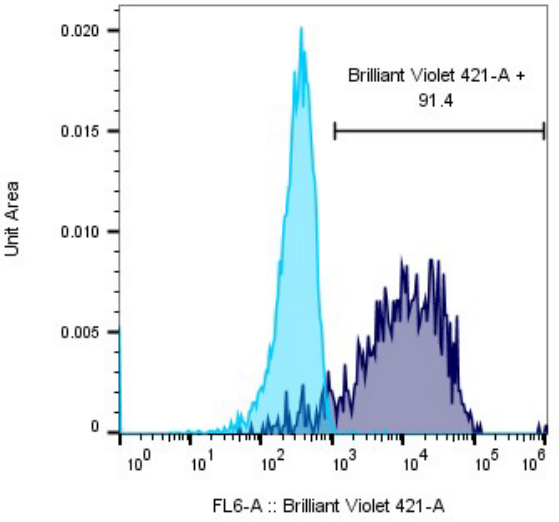

EGFP-A+: **Mean** : *Brilliant Violet 421-A*: 361

EGFP-A+: **Mean** : *Brilliant Violet 421-A*: 17150

D

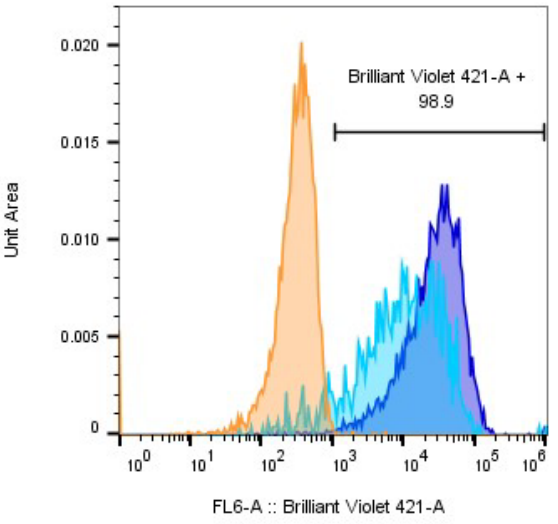

EGFP-A+: **Mean** : *Brilliant Violet 421-A*: 361

EGFP-A+: **Mean** : *Brilliant Violet 421-A*: 17150

EGFP-A+: **Mean** : *Brilliant Violet 421-A*: 35016

Figure 5.7: Flow cytometry analysis of TNF-α expression in stimulated eGFP-transfected BMMCs. A: Representative example of TNF-α detected by anti- TNF-α Alexa Fluor 421 in eGFP-transfected BMMCs in response to DNP 100ng/ml. **B:** Representative example of TNF-α detected by anti-TNF-α Alexa Fluor 421 in eGFP-transfected BMMCs in response to DNP 100ng/ml in the presence of BFA and Monensin. **C:** Representative example of TNF-α detected by anti-TNF-α Alexa Fluor 421 in untransfected BMMCs in response to ionomycin 1μM and PMA 0.1μM. **D:** Representative example of TNF-α detected by anti-TNF-α Alexa Fluor 421 in eGFP-transfected BMMCs in response to ionomycin 1μM and PMA 0.1μM in the presence of BFA and Monensin.

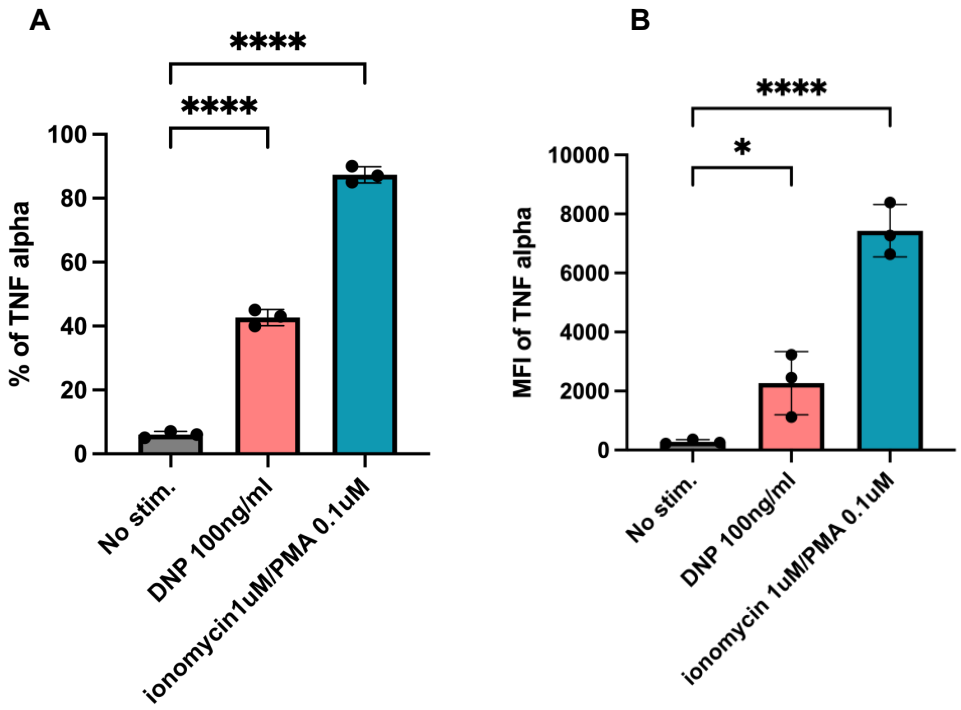

Figure 5.8: Statistical analysis of TNF-α expression in eGFP-transfected BMMCs. A: Representative bar chart showing the analysis of % TNF-α expression against different stimuli in eGFP-transfected BMMCs. N=3. $****$ indicates $\rho < 0.0001$. Data were analyzed using a one-way ANOVA test. **B:** Representative bar chart showing MFI of TNF-α expression in response to different stimuli in eGFP-transfected BMMCs. N=3. $*$ indicates $\rho < 0.05$, $****$ indicates $\rho < 0.0001$. Data were analyzed using a one-way ANOVA test.

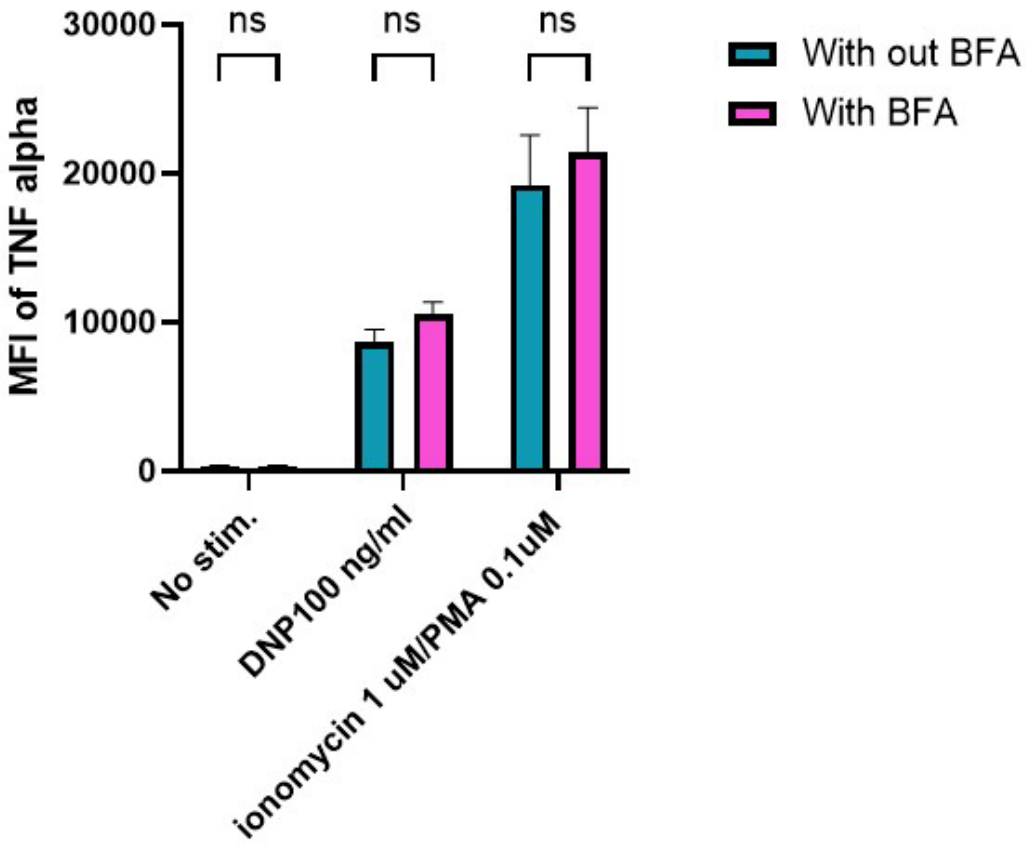

Figure 5.9: Statistical analysis for MFI of TNF-α expression in eGFP-transfected BMMCs in the presence and absence of BFA and Monensin. Representative bar chart showing the analysis MFI of TNF-α expression in eGFP-transfected BMMCs against different stimuli, N=3.

5.2.4 eGFP-BoNT.LC/B-transfected BMMCs

Having established that transfection assay does not negatively impact BMMCs ability to synthesize *de novo* cytokines in response to antigen stimulation, I proceeded to examine the effects of expression of eGFP-BoNT.LC/B on TNF-α. As described previously, I gated for cells exhibiting green fluorescence as a marker of successful transfection and expression of the LC (figure 5.10B). Analysis of anti-TNF-α staining in eGFP-BoNT.LC/B positive cells stimulated with either DNP or ionomycin and PMA in the absence or presence of BFA and Monensin showed that both stimuli still lead to an increased synthesis of the cytokine, and moreover given the differences observed in the MFI in the BFA and Monensin treated samples, secretion was not abolished (figures 5.11, 5.12). I also reasoned that if eGFP-BoNT.LC/B was inhibiting constitutive secretion in the cells, then the MFI measured in these cells should be higher than those measured in eGFP-transfected control cells, but as shown in (figure 5.12C) this was not the case. Moreover, the increased MFI observed in the presence of BFA and Monensin, are consistent with ongoing secretion of the cytokine under stimulation conditions (figure 5.13).

A

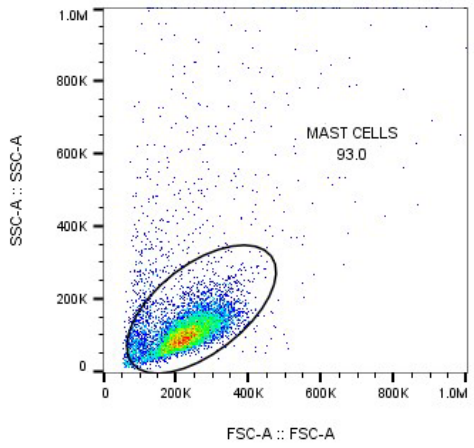

B

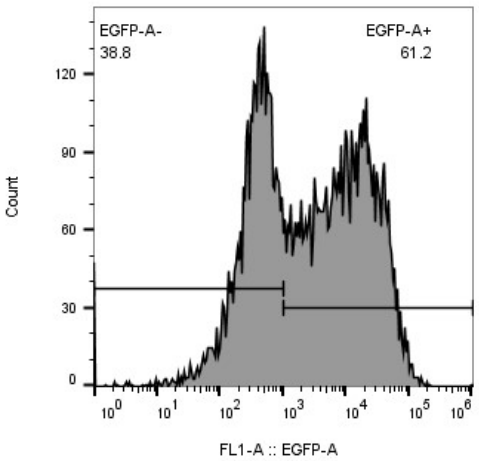

C

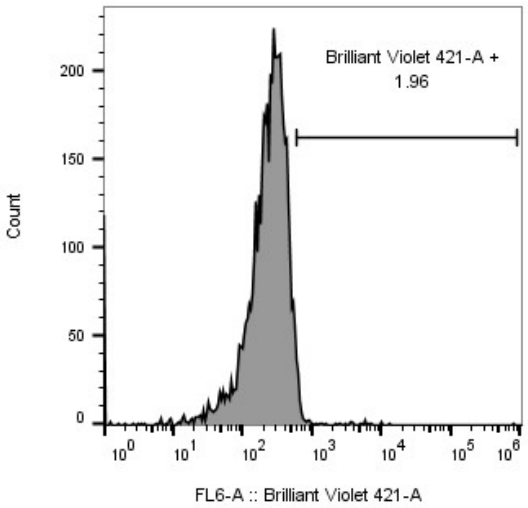

D

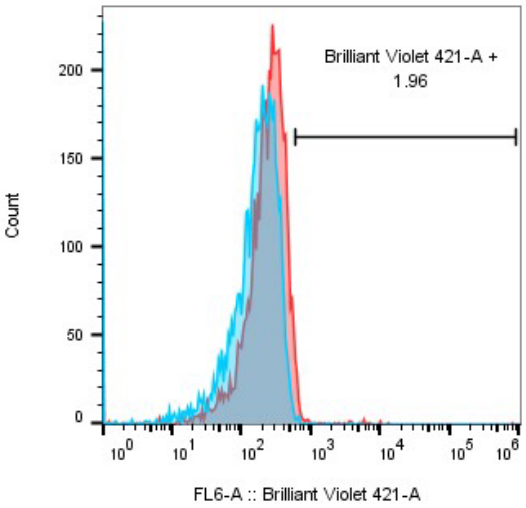

EGFP-A+: **Mean** : *Brilliant Violet 421-A*: 188

EGFP-A+: **Mean** : *Brilliant Violet 421-A*: 420

Figure 5.10: Flow cytometry analysis of TNF-α expression in no stimulus eGFP-BoNT.LC/B-transfected BMMCs. A: Representative example of a gating strategy used to identify single cells. **B:** Representative example of positive eGFP-BoNT.LC/B-transfected BMMCs. **C:** Representative example of TNF-α detected by anti-TNF-α Alexa Fluor 421 in eGFP-BoNT.LC/B-transfected BMMCs. **D:** Representative example of overlapping between unstained with anti-TNF-α in the no stimulus sample in eGFP-BoNT.LC/B-transfected BMMCs.

A

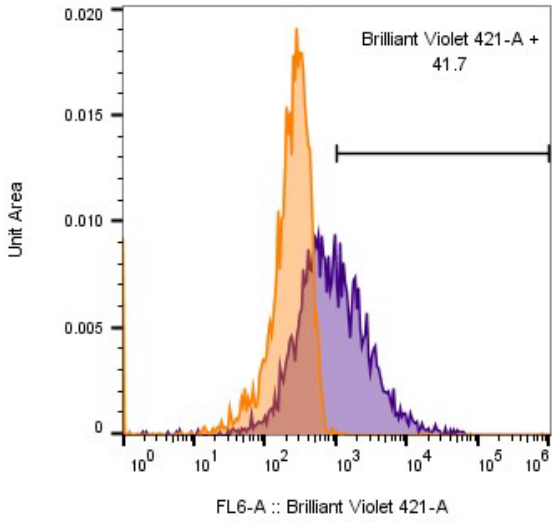

EGFP-A+: **Mean** : *Brilliant Violet 421-A*: 475

EGFP-A+: **Mean** : *Brilliant Violet 421-A*: 1688

B

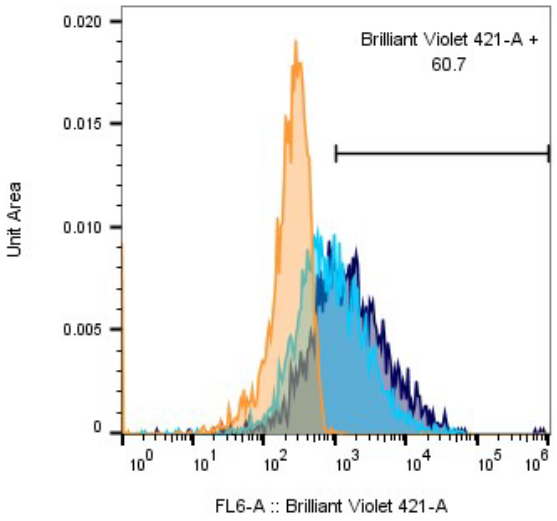

EGFP-A+: **Mean** : *Brilliant Violet 421-A*: 475

EGFP-A+: **Mean** : *Brilliant Violet 421-A*: 1688

EGFP-A+: **Mean** : *Brilliant Violet 421-A*: 3901

C

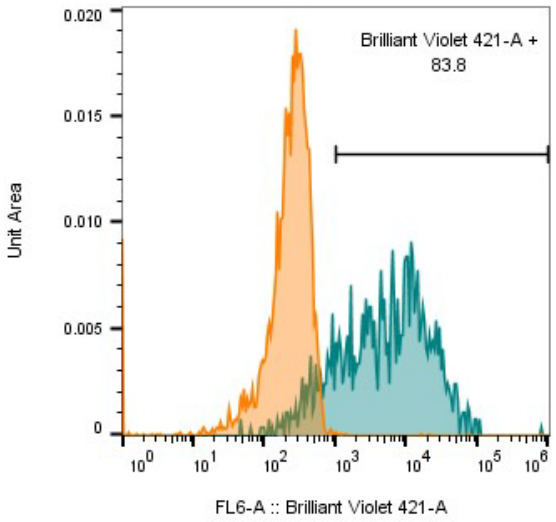

EGFP-A+: **Mean** : *Brilliant Violet 421-A*: 475

EGFP-A+: **Mean** : *Brilliant Violet 421-A*: 10943

D

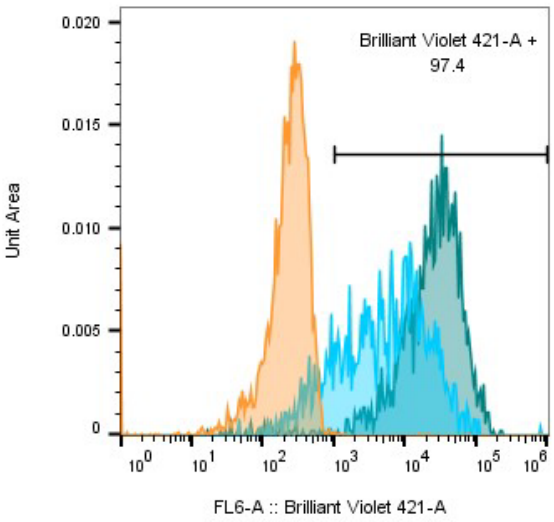

EGFP-A+: **Mean** : *Brilliant Violet 421-A*: 475

EGFP-A+: **Mean** : *Brilliant Violet 421-A*: 10943

EGFP-A+: **Mean** : *Brilliant Violet 421-A*: 32185

Figure 5.11: Flow cytometry analysis of TNF-α expression in stimulated eGFP-BoNT.LC/B-transfected BMMCs. A: Representative example of TNF-α detected by anti-TNF-α Alexa Fluor 421 in eGFP-BoNT.LC/B-transfected BMMCs in response to DNP 100 ng/ml. **B:** Representative example of TNF-α detected by anti- TNF-α Alexa Fluor 421 in eGFP-BoNT.LC/B-transfected BMMCs in response to DNP 100ng/ml in the presence of BFA and Monensin. **C:** Representative example of TNF-α detected by anti-TNF-α Alexa Fluor 421 in eGFP-BoNT.LC/B-transfected BMMCs in response to ionomycin 1μM and PMA 0.1μM. **D:** Representative example of TNF-α detected by anti-TNF-α Alexa Fluor 421 in eGFP-BoNT.LC/B-transfected BMMCs in response to ionomycin 1μM and PMA 0.1μM in the presence of BFA and Monensin.

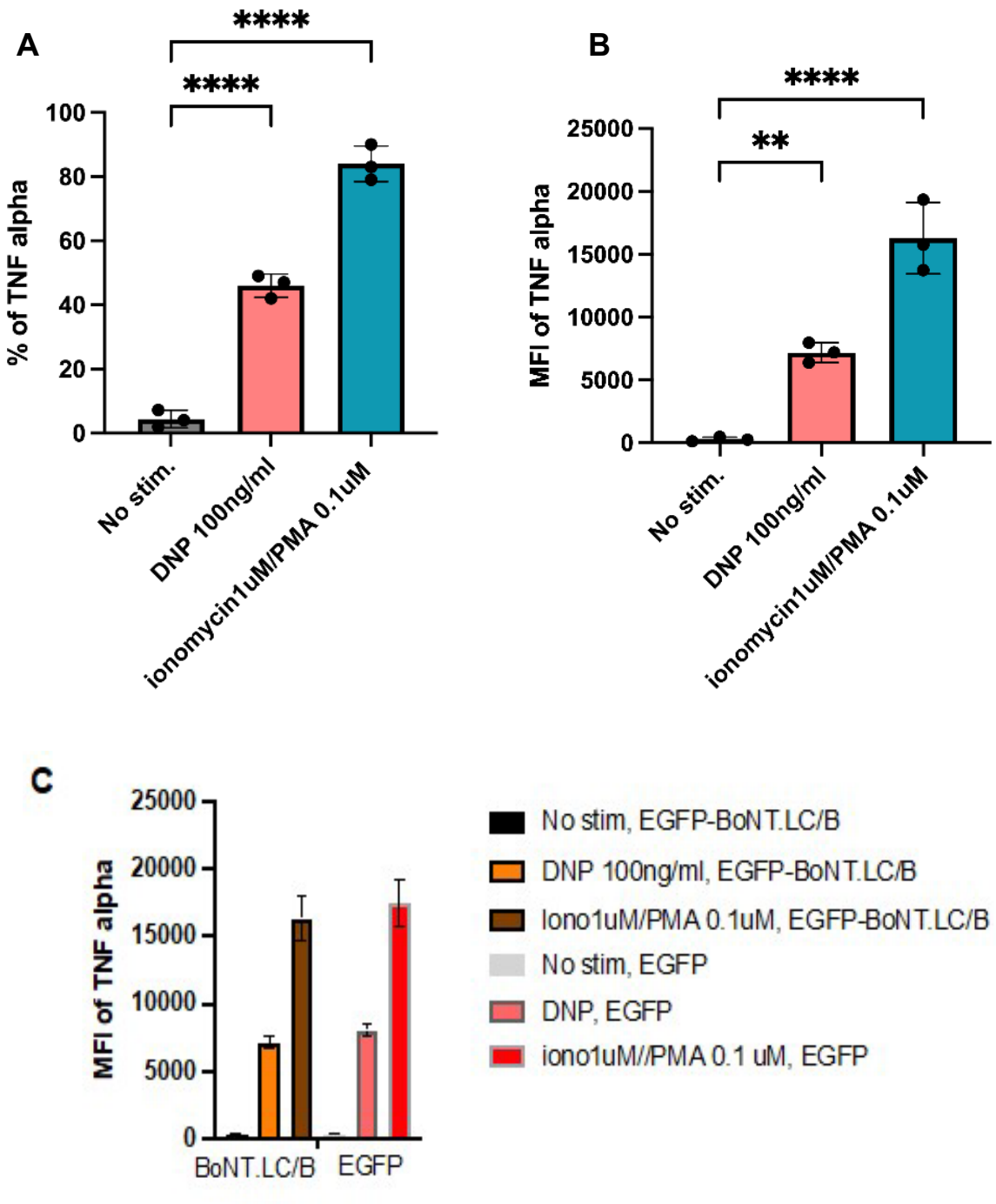
A
****
****
% of TNF alpha
100
80
60
40
20
0
No stim.
DNP 100ng/ml
ionomycin1uM/PMA 0.1uM
B
****
**
MFI of TNF alpha
25000
20000
15000
10000
5000
0
No stim.
DNP 100ng/ml
ionomycin1uM/PMA 0.1uM
C
MFI of TNF alpha
25000
20000
15000
10000
5000
0
BoNT.LC/B
EGFP
No stim, EGFP-BoNT.LC/B
DNP 100ng/ml, EGFP-BoNT.LC/B
Iono1uM/PMA 0.1uM, EGFP-BoNT.LC/B
No stim, EGFP
DNP, EGFP
iono1uM//PMA 0.1 uM, EGFP

Figure 5.12: Statistical analysis of TNF-α expression in eGFP-BoNT.LC/B-transfected BMMCs. A: Summary bar chart showing the analysis of % TNF-α positive cells detected against different stimuli. Values are mean ± SEM N=3, **** indicates $\rho < 0.001$. Data were analyzed using a one-way ANOVA test. **B:** Summary bar chart showing MFI of TNF-α expression in response to different stimuli in eGFP-BoNT.LC/B-transfected BMMCs. Values are mean ± SEM N=3, ** indicates $\rho < 0.01$, **** indicates $\rho < 0.001$. Data were analyzed using a one-way ANOVA test. **C:** Summary data showing comparison of mean ± SEM MFI in BMMCs transfected with either eGFP-BoNT.LC/B or eGFP.

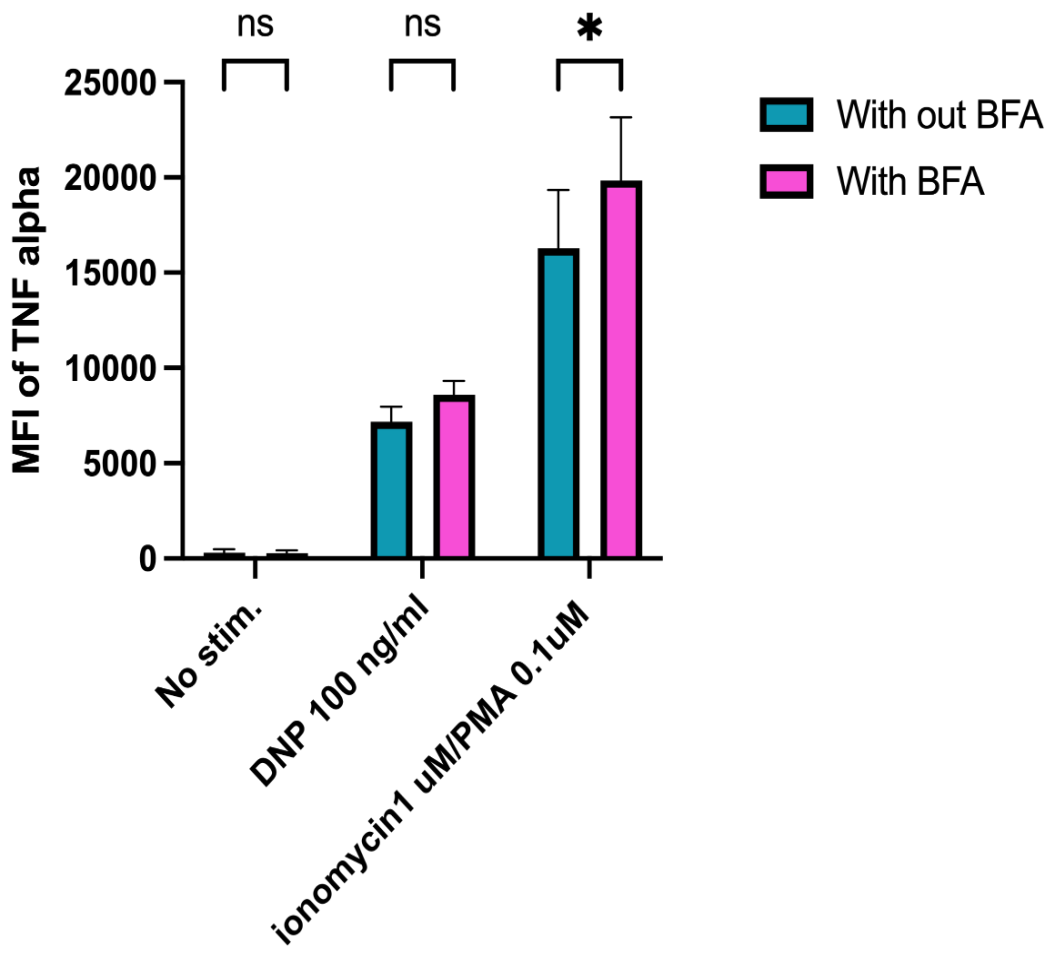

Figure 5.13: Statistical analysis for MFI of TNF-α expression in eGFP-BoNT.LC/B-transfected BMMCs in the presence and absence of BFA and Monensin. Representative bar chart showing the analysis MFI of TNF-α expression in eGFP-BoNT.LC/B-transfected BMMCs against different stimuli, N=3. $*$ indicates $\rho < 0.05$. Data were analyzed using a one-way ANOVA test.

5.2.5 eGFP-BoNT.LC/D-transfected BMMCs

In the final set of these of experiments, I used flow cytometry analysis of TNF-α expression to characterise the consequences of transfection with eGFP-BoNT.LC/D in BMMCs. As before, I used the green fluorescence to gate for cells expressing the LC and then analysed the expression of TNF-α with anti-TNF-α Alexa Fluor 421 (figure 5.14B). Stimulation of transfected cells with either DNP or ionomycin and PMA produced an increase in detected TNF-α (figures 5.15, 5.16). Interestingly, when compared to the eGFP-transfected cells, in cells expressing eGFP-BoNT.LC/D the mean MFI under both stimulus conditions is not significantly increased, suggesting that there was no inhibition of secretion of the cytokine (figure 5.16C). Moreover, the increased MFI observed in the presence of BFA and Monensin, are consistent with ongoing secretion of the cytokine under stimulation conditions (figure 5.17).

A

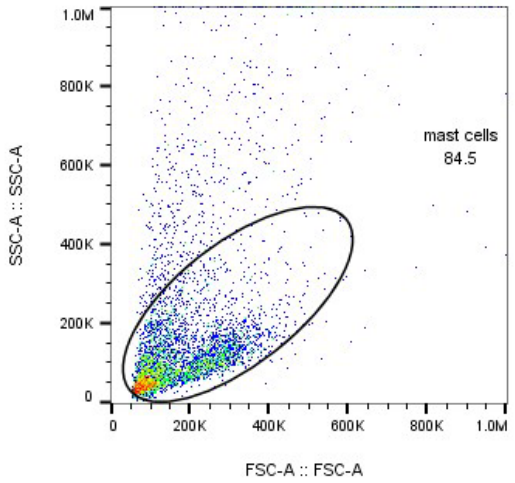

B

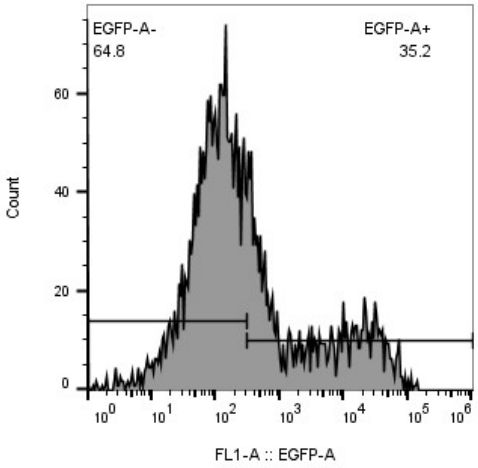

C

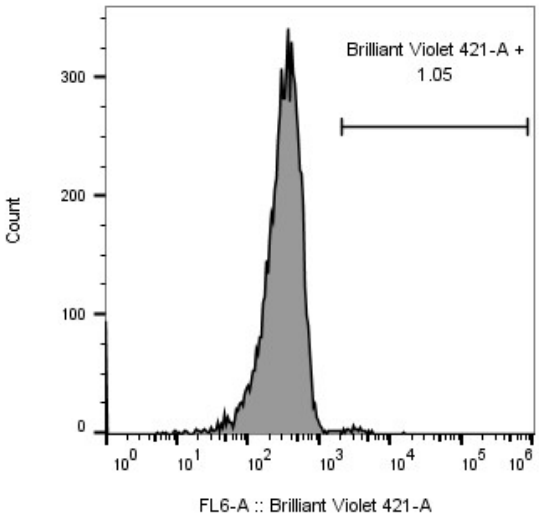

D

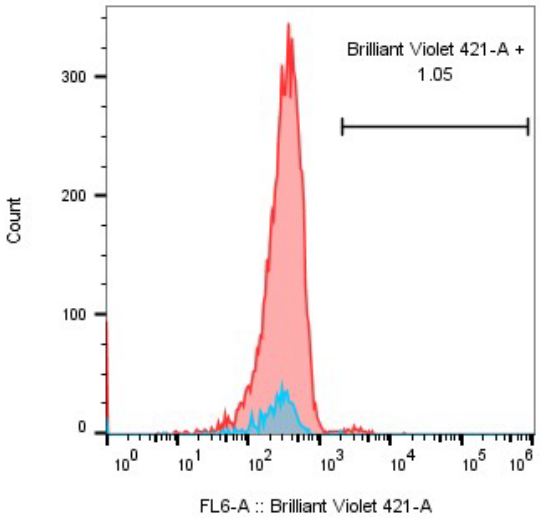

EGFP-A+: **Mean** : *Brilliant Violet 421-A*: 310

EGFP-A+: **Mean** : *Brilliant Violet 421-A*: 388

Figure 5.14: Flow cytometry analysis of TNF-α expression in no stimulus eGFP-BoNT.LC/D-transfected BMMCs. A: Representative example of a gating strategy used to identify single cells. **B:** Representative example of positive eGFP-BoNT.LC/D-transfected BMMCs. **C:** Representative example of TNF-α detected by anti-TNF-α Alexa Fluor 421 in eGFP-BoNT.LC/D-transfected no-stimulus BMMCs. **D:** Representative example of overlapping between unstained with anti-TNF-α in the no stimulus sample in eGFP-BoNT.LC/D-transfected BMMCs.

A

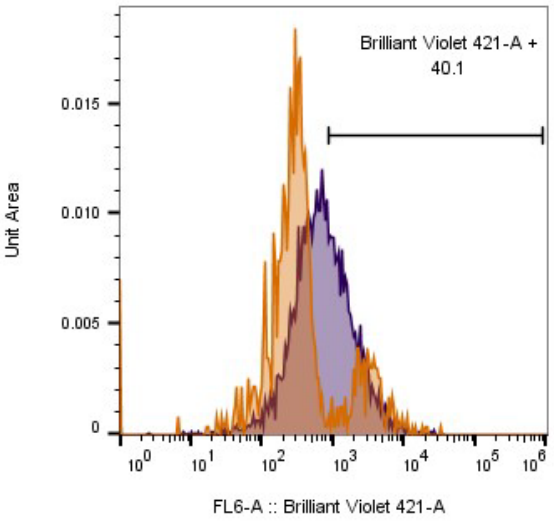

EGFP-A+: **Mean** : *Brilliant Violet 421-A*: 963
EGFP-A+: **Mean** : *Brilliant Violet 421-A*: 1118

B

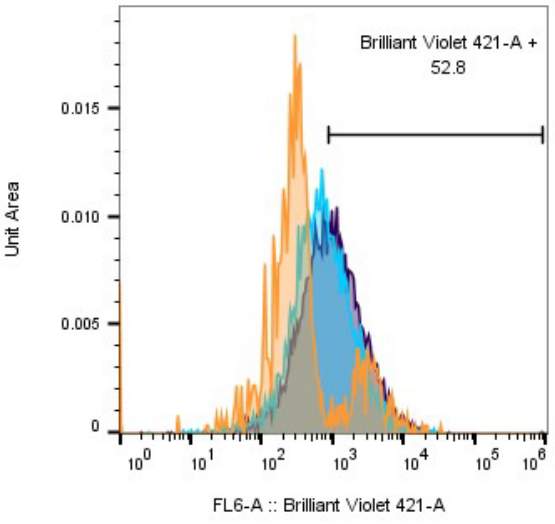

EGFP-A+: **Mean** : *Brilliant Violet 421-A*: 963
EGFP-A+: **Mean** : *Brilliant Violet 421-A*: 1118
EGFP-A+: **Mean** : *Brilliant Violet 421-A*: 1756

C

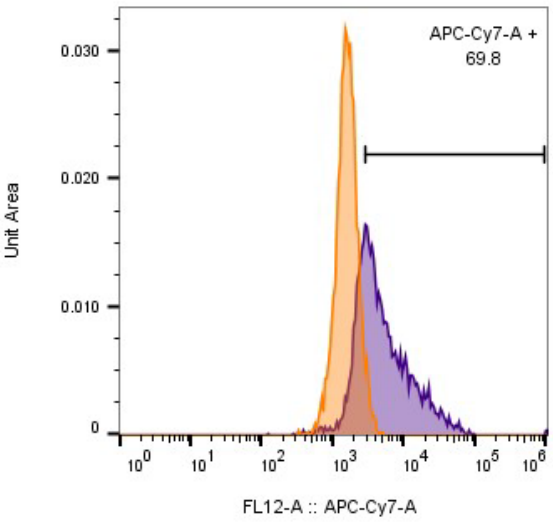

EGFP-A+: **Mean** : *APC-Cy7-A*: 1761
EGFP-A+: **Mean** : *APC-Cy7-A*: 6637

D

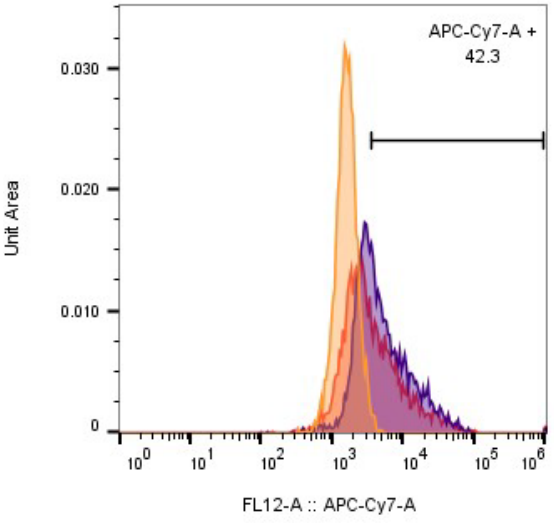

EGFP-A+: **Mean** : *APC-Cy7-A*: 1761
EGFP-A+: **Mean** : *APC-Cy7-A*: 6637
EGFP-A+: **Mean** : *APC-Cy7-A*: 7776

Figure 5.15: Flow cytometry analysis of TNF-α expression in stimulated eGFP-BoNT.LC/D-transfected BMMCs. A: Representative example of TNF-α detected by anti-TNF-α Alexa Fluor 421 in eGFP-BoNT.LC/D-transfected BMMCs in response to DNP 100ng/ml. **B:** Representative example of TNF-α detected by anti-TNF-α Alexa Fluor 421 in eGFP-BoNT.LC/D-transfected BMMCs in response to DNP 100ng/ml in the presence of BFA and Monensin. **C:** Representative example of TNF-α detected by anti- TNF-α Alexa Fluor 421 in eGFP-BoNT.LC/D-transfected BMMCs in response to ionomycin 1μM and PMA 0.1μM. **D:** Representative example of TNF-α detected by anti-TNF-α Alexa Fluor 421 in eGFP-BoNT.LC/D-transfected BMMCs in response to ionomycin 1μM and PMA 0.1μM in the presence of BFA and Monensin.

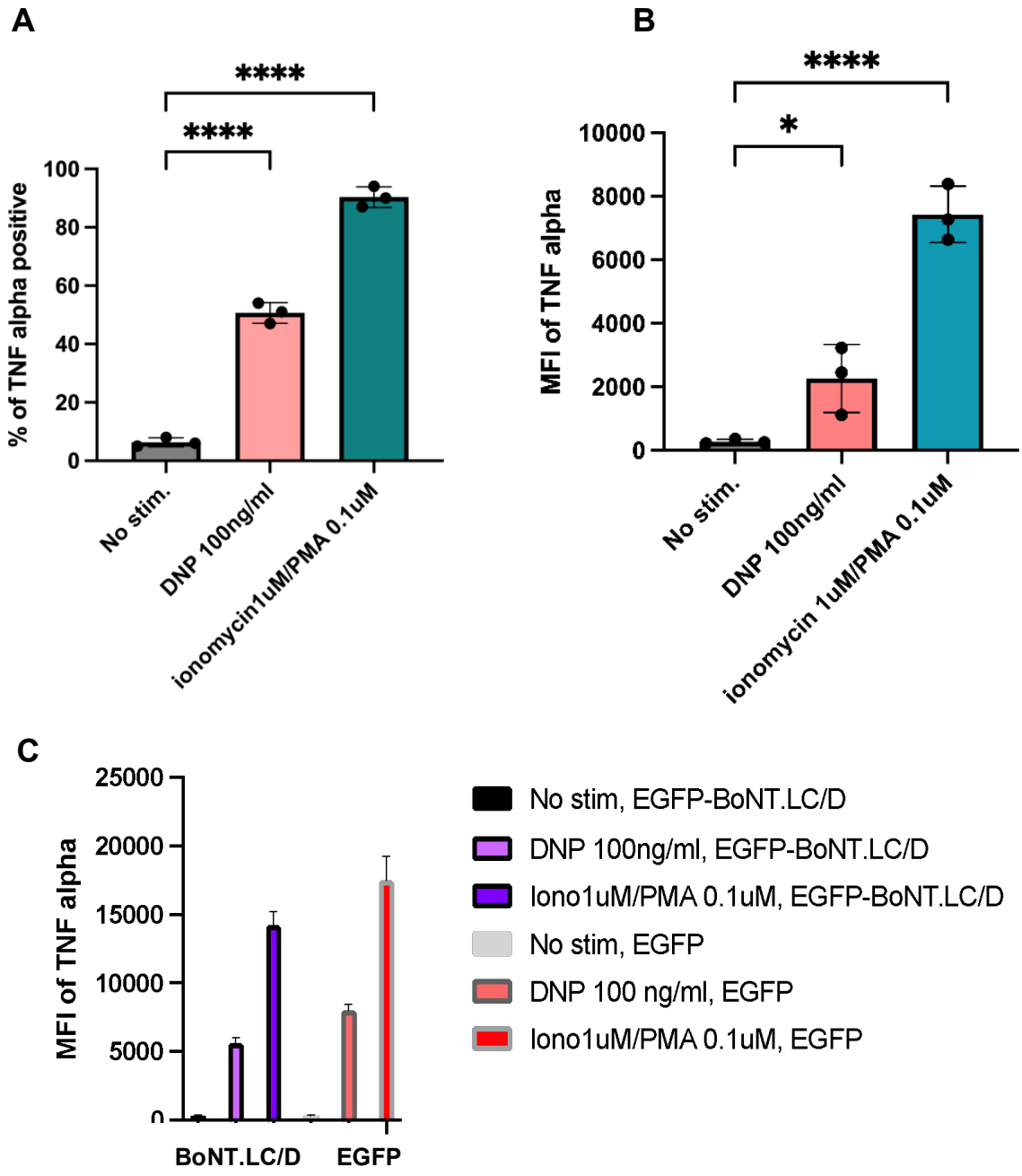
A
****
****
% of TNF alpha positive
100
80
60
40
20
0
No stim.
DNP 100ng/ml
ionomycin1uM/PMA 0.1uM
B
****
*
MFI of TNF alpha
10000
8000
6000
4000
2000
0
No stim.
DNP 100ng/ml
ionomycin 1uM/PMA 0.1uM
C
MFI of TNF alpha
25000
20000
15000
10000
5000
0
BoNT.LC/D
EGFP
No stim, EGFP-BoNT.LC/D
DNP 100ng/ml, EGFP-BoNT.LC/D
Iono1uM/PMA 0.1uM, EGFP-BoNT.LC/D
No stim, EGFP
DNP 100 ng/ml, EGFP
Iono1uM/PMA 0.1uM, EGFP

Figure 5.16: Statistical analysis of TNF-α expression in eGFP-BoNT.LC/D-transfected BMMCs. A: Summary bar chart showing the analysis of % TNF-α positive cells detected against different stimuli. Values are mean ± SEM N=3, **** $\rho < 0.0001$. Data were analyzed using a one-way ANOVA test. **B:** Summary bar chart showing MFI of TNF-α in response to different stimuli in eGFP-BoNT.LC/D-transfected BMMCs. Values are mean ± SEM N=3, * indicates $\rho < 0.05$, **** indicates $\rho < 0.0001$. Data were analyzed using a one-way ANOVA test. **C:** Summary data showing comparison of mean ± SEM MFI in BMMCs transfected with either eGFP-BoNT.LC/D or eGFP.

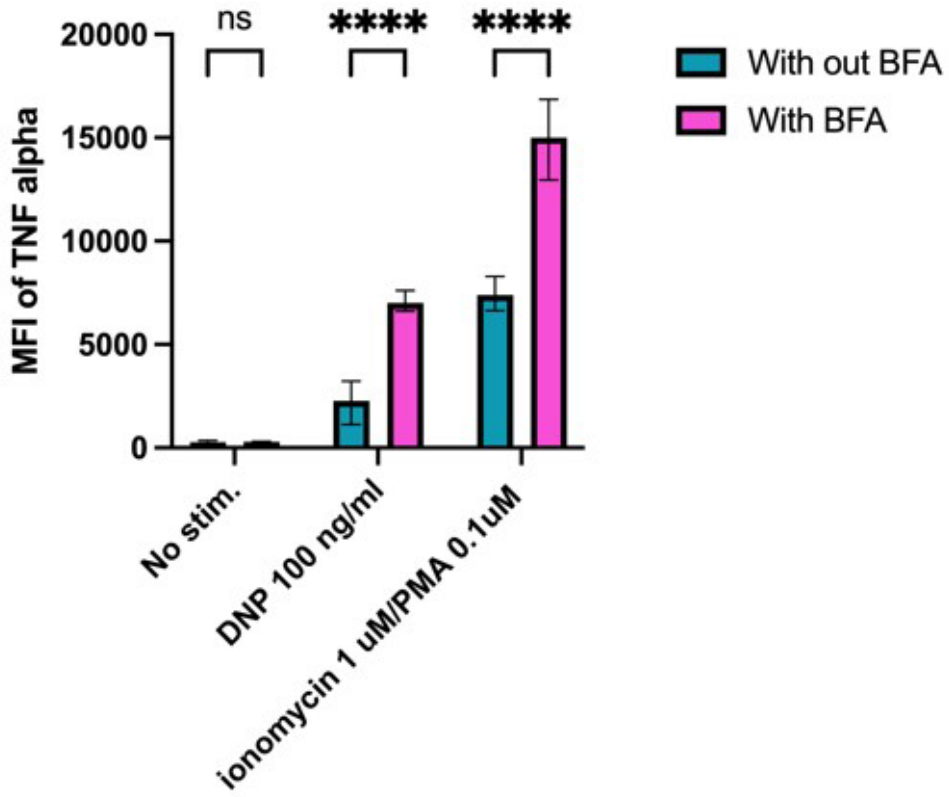

Figure 5.17: Statistical analysis for MFI of TNF-α expression in eGFP-BoNT.LC/D-transfected BMMCs in the presence and absence of BFA and Monensin. Representative bar chart showing the analysis MFI of TNF-α expression in eGFP- BoNT.LC/D-transfected BMMCs against different stimuli. N=3. $***$ $*$ indicates $\rho < 0.0001$. Data were analyzed using a one-way ANOVA test.

5.2.6 Characterisation of BoNTs LC effects on IL-6 by ELISA

Finally, to further characterize the effects of BoNT LCs on the secretion of cytokines, we turned to using ELISAs to measure IL-6, IL-13 and TNF-α. For each cytokine, we compared the amount of secreted cytokine recovered in the media from unstimulated cells and cells stimulated for 6 hours. Comparisons were made between un-transfected, eGFP transfected, eGFP-BoNT.LC/B transfected, and eGFP-BoNT.LC/D transfected BMMCs. Initially I performed experiments with un-transfected cells sensitised overnight with DNP-IgE cells and then stimulated for 6 hours (Kuehn et al., 2010) either with ionomycin 1 μM and PMA 0.1 μM, DNP 100 ng/ml or IL-33 10 ng/ml. IL-33 is an alarmin which has been reported to stimulate cytokine secretion in BMMCs (McCarthy et al., 2019). The stimulation with ionomycin 1 μM and PMA 0.1 μM proved problematic causing toxicity and levels of IL-6 that exceeded the detection limits of the ELISA kit (figure 5.18A (standard curve)) and had to be discarded. Results from a concentration-response experiments showed that stimulation with 100 ng/ml DNP stimulated robust IL-6 secretion (figure 5.18B), in agreement with previous results from PhD student Rania Magadmi from our lab (University of Sheffield) (Magadmi et al., 2019). IL-33 on the other hand proved to be a very weak stimulus under our experimental conditions (figure 5.18C), consistent with recent results reported by (Jordan et al., 2021).

Because ELISA experiments measure mediators secreted from a population of cells, which in transfection experiments would include a mixture of expressing and non-expressing cells, to investigate the effects of the BoNT/LCs on cytokine secretion, I used fluorescence activated cell sorting to isolate transfected cells (figure 5.19), before proceeding with the sensitisation and stimulation. Unfortunately, in two out of the three experiments, results from the ELISA had to be discarded due to levels exceeding the sensitivity of the kit. The results shown in (figure 5.19D) are therefore from 1 experiment. Comparison of IL-6 secreted by BMMCs transfected with eGFP (control) or eGFP-BoNT.LC/D indicate that the toxin LC did not inhibit cytokine secretion in

response to antigen stimulation. Surprisingly, in this experiment expression of eGFP-BoNT.LC/B does appear to inhibit IL-6 secretion, however without further replicates and experiments whether this results from inhibition of the secretory machinery, synthesis or toxicity will require further investigation.

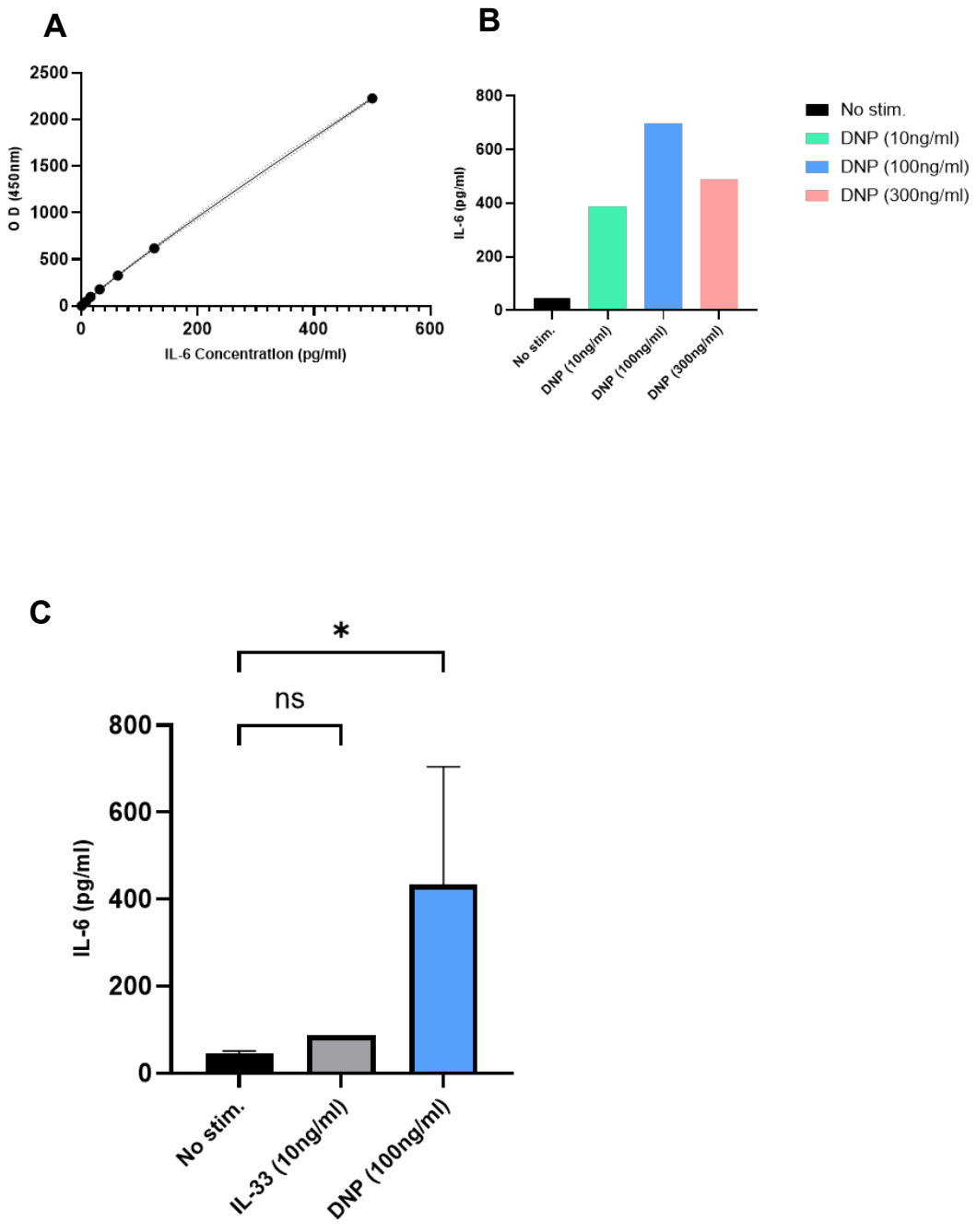

Figure 5.18: ELISA for measuring IL-6 in BMMCs. A: Standard curve of IL-6 in BMMCs. **B:** IL-6 measured from untransfected, DNP-IgE sensitised BMMCs stimulated with (10,100,300 ng/ml) DNP. **C:** Summary data (mean± SEM) from untransfected BMMCs. N=3. $*$ indicates $\rho < 0.05$. Data were analyzed using a one-way ANOVA test.

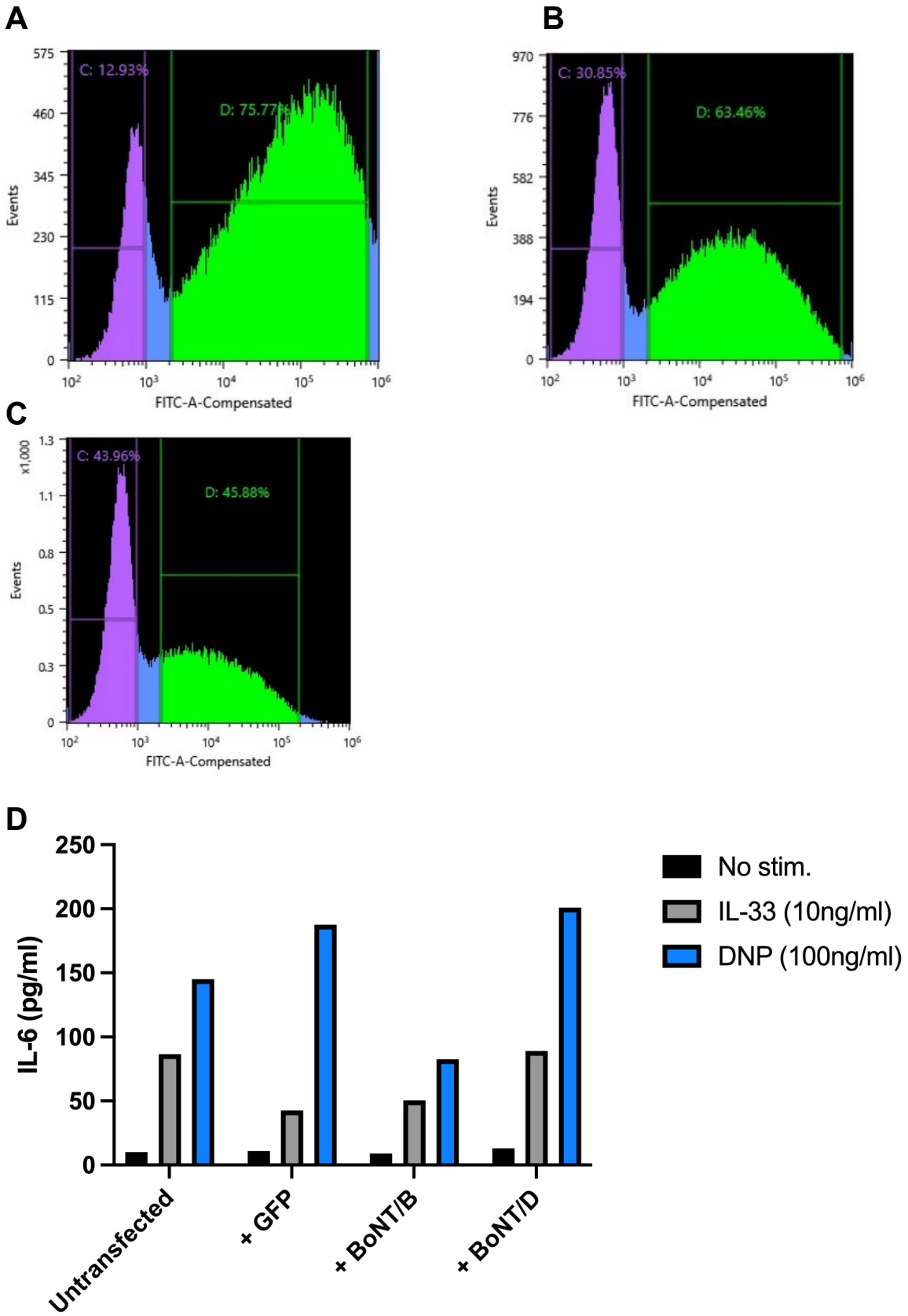
A
C: 12.93%
D: 75.77%
Events
FITC-A-Compensated
B
C: 30.85%
D: 63.46%
Events
FITC-A-Compensated
C
C: 43.96%
D: 45.88%
x1,000
Events
FITC-A-Compensated
D
IL-6 (pg/ml)
No stim.
IL-33 (10ng/ml)
DNP (100ng/ml)
Untransfected
+ GFP
+ BoNT/B
+ BoNT/D

Figure 5.19: IL-6 measurement in Sorting BMMCs using ELISA. A: Representative image by flow cytometry for gating the positive (green) cells used for sorting eGFP-transfected cells. **B:** Representative image by flow cytometry for sorting in eGFP-BoNT.LC/B-transfected cells. **C:** Representative image by flow cytometry for sorting eGFP-BoNT.LC/D-transfected cells. **D:** IL-6 measuring in BMMCs (untransfected and sorted transfected cells) after being stimulated with IL-33 (10ng/ml) and DNP (100ng/ml) compared with no-stimulus group,(N=1).

5.2.7 Characterisation of BoNTs LC effects on IL-13 by ELISA

Given the various technical difficulties experienced measuring IL-6 secretion from BMMCs, I then moved to measure another cytokine (IL-13), which like IL-6 is synthesized *de novo* in response stimulation in BMMCs and is thought to be secreted by the constitutive pathway (Mukai et al., 2018). Summary data from replicate experiments (N=4) obtained from untransfected and sorted, transfected BMMCs are shown in figure 5.20B. Statistical analysis indicates that expression of neither eGFP, nor eGFP-BoNT.LC/B, nor eGFP-BoNT.LC/D inhibited the cells ability to secrete IL-13 in response to antigen-stimulation.

A

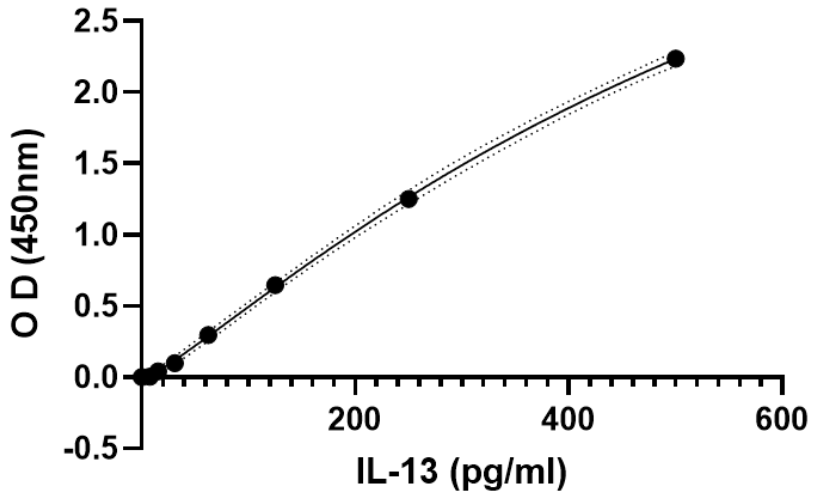

B

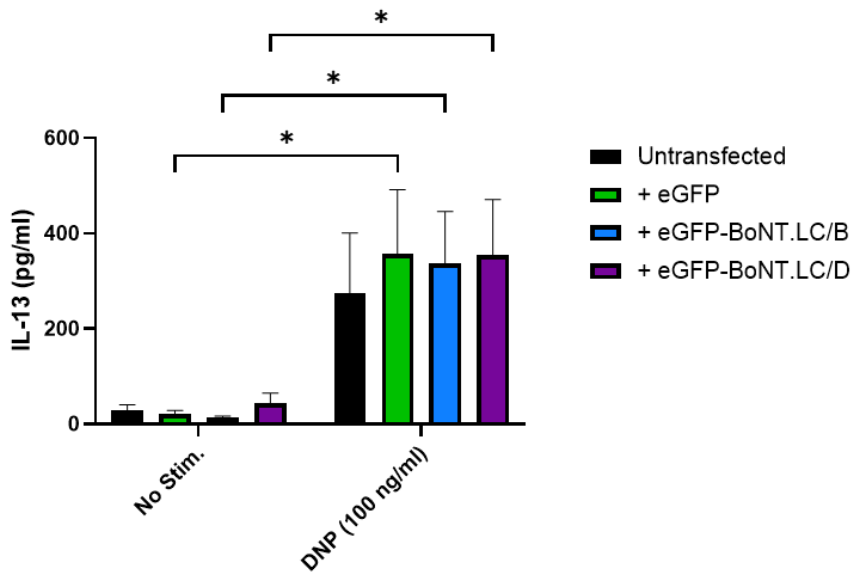

Figure 5.20: IL-13 measurement in BMMCs using ELISA. A: Standard curve of IL-13 in BMMCs. **B:** IL-13 secretion in untransfected and transfected BMMCs when stimulated with DNP 100 ng/ml. N=4. $*$ indicates $\rho < 0.05$ Data were analyzed using a one-way ANOVA test.

5.2.8 Characterisation of BoNTs LC effects on TNF-α by ELISA

In my final set of experiments, I returned to exploring the effects of the BoNT/LCs on secretion of TNF-α. Unlike IL-6 and IL-13, TNF-α is trafficked to both granules and small transport vesicles and its secretion requires proteolytic processing at the plasma membrane (Baumgartner et al., 1994), (Moreira-Tabaka et al., 2012). My previous flow-cytometry based on single cell assay of TNF-α indicated that the BoNT/LCs did not inhibit synthesis or secretion of this cytokine, however it is conceivable that the toxins could affect processing of the pro-cytokine at the plasma membrane. To examine this, I performed ELISAs to measure secreted TNF-α collected from the media of un-transfected and transfected, sorted BMMCs. The results from these experiments are shown in figure 5.21B; comparison of data from eGFP and eGFP-BoNT.LC/B and eGFP-BoNT.LC/D show no significant differences between the levels of TNF-α secreted in response to antigen.

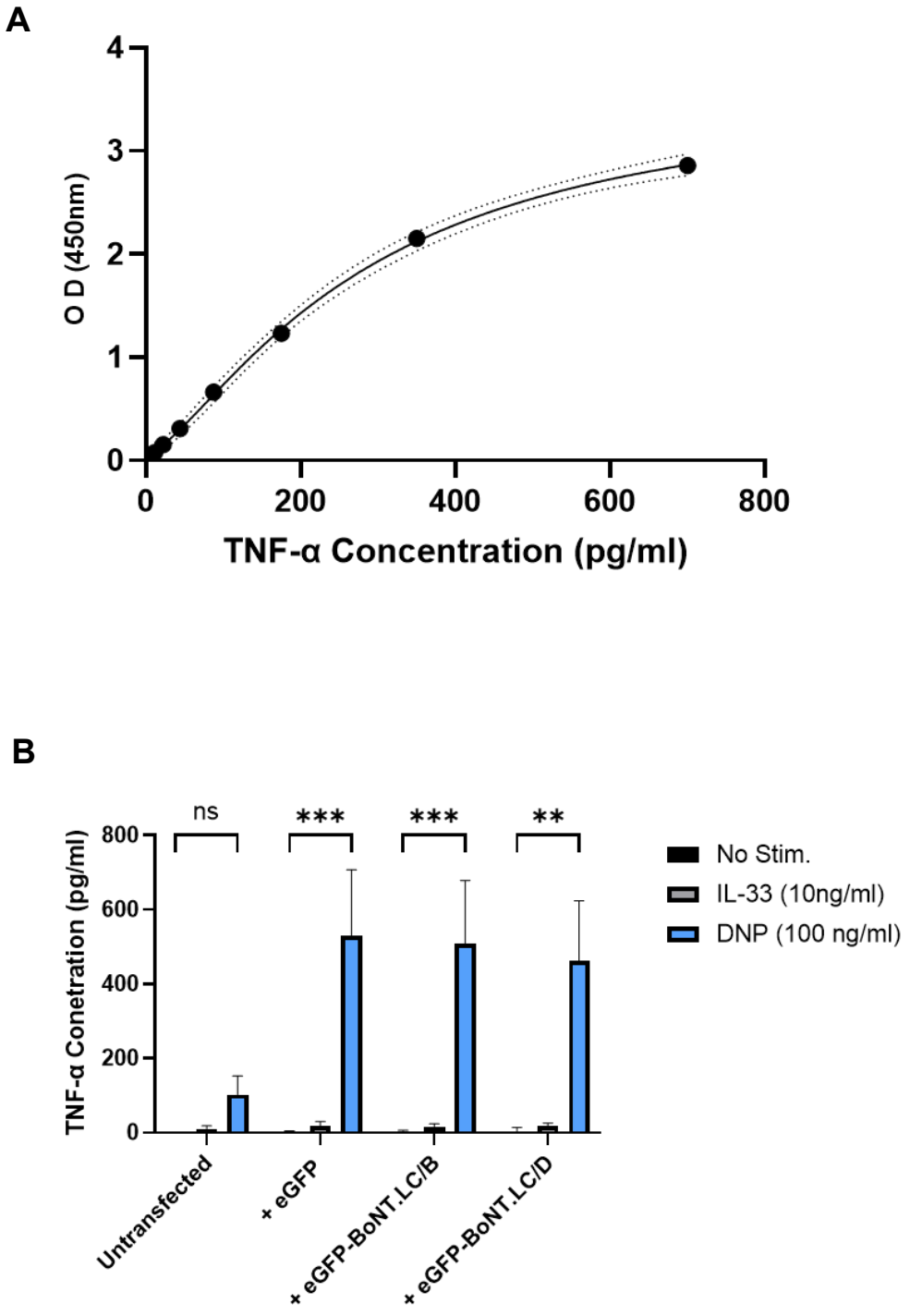

Figure 5.21: ELISA for measuring TNF-α in BMMCs. A: Standard curve of TNF-α in BMMCs. **B:** TNF-α secretion in untransfected and transfected BMMCs when stimulated with IL-33 (10ng/ml) and DNP (100ng/ml). N=4. $**$ indicates $\rho < 0.01$,$***$ indicates $\rho < 0.001$. Data were analyzed using a one-way ANOVA test.

5.3 Discussion

This study aimed to investigate the potential inhibitory effects of BoNT/B and D on MC cytokine secretion, specifically TNF-α, IL-6, and IL-13. Using a combination of single cell based intracellular staining analysis flow cytometry as well as ELISAs to quantify secreted cytokines, I found that the expression of the toxin LC proteases does not markedly inhibit the secretion of TNF-α, IL-6, nor IL-13 following antigen-stimulation. These proteases are known to inactivate VAMP-3, and indeed in Chapter 4, I showed that expression of the LCs lead to a very significant depletion of VAMP-3 in BMMCs. While the molecular mechanisms regulating cytokine secretion in MCs is known to be fundamentally distinct from those controlling classical degranulation, my data suggests that secretion of TNF-α, IL-6, and IL-13 is not strictly dependent on VAMP-3.

Regulated secretion in MCs generally use alternative SNARE proteins such as VAMP-7, VAMP-8, and SNAP-23, in contrast to neurones, which primarily use VAMP-1 or 2 and SNAP-25. This distinction highlights the variations in membrane trafficking pathways and fusion machinery between these cell type (Lorentz et al., 2012). Different SNARE isoforms are co-expressed in MCs, which may facilitate compensation when individual components are inhibited (Lacy and Stow, 2011).

Regarding the cytokines, MCs uniquely contain both pre-formed TNF-α stored in secretory granules and newly synthesised TNF-α released following activation (Theoharides et al., 2007). Pre-formed TNF-α can be released through regulated exocytosis, whereas *de novo* synthesised TNF-α is secreted via post-Golgi or constitutive secretory pathways that may not depend on BoNT/B or BoNT/D sensitive SNARE proteins. These alternative trafficking pathways facilitate TNF-α release even in the absence of functional classical exocytic machinery (Theoharides et al., 2007).

BoNTs require receptor-mediated uptake, membrane translocation and proteolytic cleavage of SNARE substrates to produce biological effects (Guo et al., 1998).

Furthermore, BoNT/B and D specifically cleave VAMPs1-3, whereas cytokine secretion in MCs has been shown depend primarily on VAMP-8 and SNAP-23 especially for the release of TNF-α (Puri and Roche, 2008). Importantly, VAMP-8 does not possess a recognised cleavage site for BoNT/B and D making this way resistant to these serotypes (Lacy and Stow, 2011). Lacy et al demonstrated that VAMP-3 serves as the primary R-SNARE for the recycling endosome-mediated secretion of TNF-α and IL-6, its role definitively established through the intracellular expression of BoNT/B and D LCs, which specifically cleave VAMP-3 to inhibit vesicle fusion.

Previous studies highlight the differentiation of MC secretory pathways and demonstrate that the inhibition of degranulation does not necessarily result in the suppression of cytokine secretion (Theoharides et al., 2007). The failure of BoNT/B and BoNT/D to inhibit TNF-α release highlights the importance of SNARE specificity and the selection of trafficking pathways in MC biology (Theoharides et al., 2007). This differentiation has importance implications for the therapeutic application of BoNTs in inflammatory conditions, as targeting granule exocytosis alone may be insufficient to supress MC derived cytokine-mediated diseases in late stage of their symptoms. Studies investigating other BoNT serotypes such as BoNT/A and /E reported a decrease in cytokine secretion from microglial cells and other immunological cells (Kim et al., 2015), (Chen and Barbieri, 2009), (Filho et al., 2024), confirming the absolute requirement for a functional SNARE complex in supporting cytokine secretion. My research suggests however, that there is not an absolute requirement for VAMP-3 and that other R-SNAREs may contribute to the complex to support secretion.

Chapter 6: General discussion and future works

Inappropriate activation of MCs and subsequent secretion of pro-inflammatory mediators contribute to the symptoms of many diseases including hypersensitivity reactions such as urticaria and life-threatening conditions like anaphylaxis (Puri and Roche, 2008). By virtue of their tissue resident location and expression of FcεRI, MCs are the first cells responding to antigens and contribute to both innate and adaptive immunity, through secretion of pre-synthesized, granule-stored mediators and the synthesis and secretion of *de novo* mediators (Dileepan et al., 2023). With the exception of lipid-derived mediators, all MC mediators are secreted by exocytosis. Distinct molecular pathways and SNARE proteins, however, are used to control secretion of granule-derived versus *de novo* synthesized mediators (Puri and Roche, 2008). BoNTs are composed of a heavy chain domain responsible for binding to cell surface receptors, a prerequisite for internalisation, and BoNT.LC enzymatic domain responsible for SNARE proteolysis; different BoNT.LC serotypes target distinct SNAREs. Recent advances in bioengineering of BoNTs, raise the possibility for developing BoNTs into MC specific inhibitors (Monash et al., 2025).

The main aim of this study was to investigate the effects of BoNT.LC serotypes B and D on mediator release from murine MCs. According on the recognised role of BoNTs in cleaving SNARE proteins to inhibit exocytosis, it was hypothesized that these toxins could similarly interfere with the exocytic machinery of MCs, therefore decreasing the inflammatory reaction. However, the findings of my investigation indicate that neither eGFP-BoNT.LC/B nor eGFP-BoNT.LC/D significantly reduce the exocytosis of MC mediators nor the surface expression of FcεRI, despite effective cleavage of VAMP-3. Although BoNTs are highly effective inhibitors of regulated exocytosis in neurons, this is due to their action on neuronal SNAREs, their efficacy in immune cells is still a part of the debate. The noted absence of inhibition suggests that the VAMP isoforms, particularly VAMP-1,2, and 3 targeted by serotypes B and D, may not be the principal drivers of exocytosis in this murine model cell line. Previous studies have

demonstrated that MCs use a variety of SNARE proteins including VAMP-7 and VAMP-8 which are intrinsically resistant to cleavage by these specific BoNT serotypes (Puri and Roche, 2008), (Lorentz et al., 2012). Thus, the results in this thesis highlight a significant divergence between neuronal and MC secretory pathways, indicating that murine MCs have a robust exocytic mechanism that is independent of eGFP-BoNT.LC/B and eGFP-BoNT.LC/D sensitive proteins. The finding that eGFP-BoNT.LC/B and eGFP-BoNT.LC/D do not inhibit murine MC mediators secretion corresponds with evidence indicating that immune cell exocytosis is specialised and different from neural transmission. While BoNTs are the most potent inhibitors of neurotransmission, their effect on MCs will be significantly serotype-specific. Their effectiveness in immune cells is still a part of debate, the observed lack of inhibition indicates that the VAMP isoforms, notably VAMP-1,2, and 3 targeted by serotype B and D, may not be the principal drivers of exocytosis in this murine model cell line.

The failure of BoNT.LC/B and BoNT/D in this study indicates that their targets proteins-VAMP-1,2, and 3 are not the principal regulators of degranulation in murine MCs. The resistance observed in this study is consistent with the findings of Puri and Roche (2008), who identified VAMP-8 (as also known as Endobrevin) as the principal v-SNARE necessary for MC degranulation. Because VAMP-8 lacks the cleavage sites for BoNT/B and BoNT/D, allowing cells that depend on this protein to maintain functionally despite the presence of BoNTs. Moreover, Ho et al. (2008) described that mice deficient VAMP-8 show significantly impaired MC degranulation, while VAMP-2 and VAMP-3 (the targets of my BoNTs) seem to be less essential for this specific immune process.

Hypersensitivity and immune reactions represent a common cause of tissue dysfunction and reduced quality of life worldwide. The main mechanisms underlying complex hypersensitivity response, including acute and chronic reactions, remain incompletely understood. MCs are key immune effector cells that regulate inflammatory reactions. The main mechanism of MC activation in allergic responses is the cross-linking of antigens with IgE bound to FcεRI on the MC surface. This leads to the release of various preformed and newly synthesised inflammatory mediators

that affect adjacent tissues, including airway smooth muscle, skin, sensory nerve terminals, so inducing the characteristic symptoms associated with allergic responses (Medic et al., 2013). However, dysregulated MC stimulation contributes to the development of inflammatory conditions. These hypersensitivity manifestations continue to cause a marked therapeutic challenges globally. To date, no curative treatments are available for most hypersensitivity disorders and current treatment strategies are mainly focused on symptoms relief. Although several approved therapies target some immune pathways, these treatments are usually associated with severe side effects. Consequently, increasing efforts have focused on MCs as immune regulators with a view to better understand the mechanisms leading to inflammatory reactions and thereby identify novel therapeutic targets. Different promising therapeutic targets have been prescribed in hypersensitivity disorders, such as specific antagonists of some MC mediators such as antihistamine. The present study aimed to determine whether BoNT/LCs might provide an alternative biological therapy for the treatment of hypersensitivity disorders. I focussed on eGFP-BoNT.LC/B and eGFP-BoNT.LC/D, as their target VAMP-3, had been implicated in regulating cytokine secretion and constitutive exocytosis and therefore could in principle attenuate inflammatory responses and be used alongside existing therapies that target the immediate effects of degranulation.

In chapter 3, I reported the results from my investigations to establish the best model for studying MC mediator secretion. I found that BMMCs provide the best model, as they not only express functional FcεRI but also, respond with robust secretion of both pre-stored and *de novo* mediators. Importantly for the purposes of my research, the SNAREs controlling degranulation have been studied extensively in BMMCs (and RBL-2H3) cells and established a requirement for VAMP-7, 8. On the other hand, studies on cytokine secretion are more commonly performed in BMMCs, as RBL-2H3 cells produce more limited responses.

If the BoNTs LC preventing the IgE from being at the surface, then conceivably we would see an impact on the degranulation by antigen. That is why address my question as they do not affect the IgE receptor as this is new finding.

Since BMMCs do not express the neuronal receptors for native botulinum neurotoxins, I sought to introduce the functional proteolytic domains by transient transfection using fluorescently tagged chimeras, eGFP-BoNT.LC/B and eGFP-BoNT.LC/D. As described in Chapter 4, I took advantage of flow cytometry analysis and the possibility of measuring receptors and degranulation at the single cell level, to measure surface expression of CD107a to quantify degranulation. My data showed that expression of the proteases did not significantly impact antigen- or ionomycin and PMA induced degranulation. While the lack of effects on ionomycin induced degranulation are not surprising given the well-known reliance of VAMP-7, 8, it is important to note that the lack of inhibition on antigen-induced degranulation also indicate a lack of effect of the toxins on FcεRI or their downstream signaling which could have indirectly impacted degranulation. This agreed with the lack of change in FcεRI that I observed following expression of eGFP-BoNT.LC/B and eGFP-BoNT.LC/D. My findings contrast with a recent report by (Mishima et al., 2022), who using a VAMP-3 RBL-2H3 knockout cell line, found a role for VAMP-3 in FcεRI and granule biogenesis, both of which resulted in decreased degranulation. From an experimental design point of view, it is unclear whether in generating the knockout cell line, other changes may have taken place which may have also lead to differences between the parent and knockout cells, or whether the shorter time course of my experiments, with functional analysis being performed within 72 hours of transfection, would obscure slow and cumulative effects of VAMP-3 depletion on protein trafficking. Interestingly a recent report by (Weimershaus et al., 2023) showed further a role for a VAMP-3 positive vesicles in trafficking of TNF-α to granules. recent report using a newly generated VAMP-3 knockout RBL-3H3 cell line, reported a role for VAMP-3 in FcεRI trafficking and granule biogenesis (Mishima et al., 2022).

In chapter 5, I reported the results from experiments designed to investigate the effects of the toxin light chains on other MC mediators, focussing on cytokines. I used two

different experimental approaches, flow cytometry to allow for single cell analysis, and ELISA assays of selective secreted mediators. Both assays indicated a lack of effect of either BoNT/B or BoNT/D on antigen-induced TNF-α synthesis and secretion. TNF-a is an unusual cytokine in MCs, as some of it is stored in granules and released rapidly by regulated exocytosis and degranulation, while secretion is maintained by *de novo* synthesis and secretion through constitutive exocytosis. The lack of inhibition of degranulation as measured by CD107a would supports the notion that secretion of granule-derived TNF-α is not inhibited by expression of the toxin LCs. While the lack of inhibition of secreted TNF-α observed following 6 hours of stimulation, also suggests that secretion of *de novo* synthesized TNF-α may proceed in the absence of VAMP-3. In agreement with this, I also found that antigen-stimulated IL-13 and IL-6 secretion, two cytokines synthesized *de novo* and secreted via constitutive exocytosis were also unaffected by expression of eGFP-BoNT.LC/D.

In my project, time and resources limited the number of cytokines and stimulus conditions I could investigate. In future it would interest to extend the research to include other cytokines and chemokines . Because recent studies mention that there are some cytokines there is a possibility that under different stimulation conditions, they use different secretory pathways in MCs has not been investigated.

In future work, extend to look a wide arrays of cytokines using multiplex cytokine assay and also look other stimulation conditions such as MRGPRX2 receptor and study the MCs reactions under infection conditions.

Extend the number of cytokines to include chemokines, it’s possible, because different cytokines have different pathways. Moreover, extend the receptor to include the stimulation of MRGPRX2 and try the new engineering BoNTs. Finally, it might be fruitful to include different cytokines, and different receptors, and use engineering toxins to discover the key role in this pathways and which engineering BoNT serotypes is perfect to use.

Based on the results of my research, I conclude that there is little point in developing BoNT.LC/B or BoNT.LC/D as drugs targeted to MCs for treating hypersensitivity. So, for future studies, recently people have been engineering BoNT to direct them towards other VAMPs like BoNT/F that is re-engineering to cleave VAMP-7 also BoNT/A that

is re-engineering to cleave SNAP-23. It will be interesting to see whether these engineering BoNTs directed at the other SNARE proteins in MCs may be effective.

Conclusion:

In conclusion, the data presented in this thesis revealed an insight measured different group of mediators from stimulated MCs. Our results showed that eGFP-BoNT.LC/B and eGFP-BoNT.LC/D did not inhibit the level of neither β-hexosaminidase nor cytokines (TNF-α,IL-6,IL-13). These findings describe insights into the involvement other mediators and use of engineered BoNTs in future studies.

Bibliography test

ADHIKARI, P., AYO, T. E., VINES, J. C., SUGITA, S. & XU, H. 2023. Exocytic machineries differentially control mediator release from allergen-triggered RBL-2H3 cells. *Inflammation Research,* 72**,** 639-649.

AGLIARDI, C., GUERINI, F. R., ZANZOTTERA, M., BIANCHI, A., NEMNI, R. & CLERICI, M. 2019. SNAP-25 in Serum Is Carried by Exosomes of Neuronal Origin and Is a Potential Biomarker of Alzheimer's Disease. *Mol Neurobiol,* 56**,** 5792-5798.

AGLIARDI, C., MELONI, M., GUERINI, F. R., ZANZOTTERA, M., BOLOGNESI, E., BAGLIO, F. & CLERICI, M. 2021. Oligomeric alpha-Syn and SNARE complex proteins in peripheral extracellular vesicles of neural origin are biomarkers for Parkinson's disease. *Neurobiol Dis,* 148**,** 105185.

AGUADO, F., GOMBAU, L., MAJO, G., MARSAL, J., BLANCO, J. & BLASI, J. 1997. Regulated secretion is impaired in AtT-20 endocrine cells stably transfected with botulinum neurotoxin type A light chain. *J Biol Chem,* 272**,** 26005-8.

AKETANI, S., TESHIMA, R., UMEZAWA, Y. & SAWADA, J. 2001. Correlation between cytosolic calcium concentration and degranulation in RBL-2H3 cells in the presence of various concentrations of antigen-specific IgEs. *Immunol Lett,* 75**,** 185-9.

ALAM, S. B., WANG, F., QIAN, H. & KULKA, M. 2023. Apolipoprotein C3 facilitates internalization of cationic lipid nanoparticles into bone marrow-derived mouse mast cells. *Sci Rep,* 13**,** 431.

ALI, E. A., KALLI, M., WAN, D., NAKAMURA, R., ONION, D., ALANINE, D. G. W., ALCOCER, M. J. C. & FALCONE, F. H. 2019. Characterization of human FcepsilonRIalpha chain expression and gene copy number in humanized rat basophilic leukaemia (RBL) reporter cell lines. *PLoS One,* 14**,** e0221034.

ALMANDOZ-GIL, L., PERSSON, E., LINDSTROM, V., INGELSSON, M., ERLANDSSON, A. & BERGSTROM, J. 2018. In Situ Proximity Ligation Assay Reveals Co-Localization of Alpha-Synuclein and SNARE Proteins in Murine Primary Neurons. *Front Neurol,* 9**,** 180.

AMIN, K. 2012. The role of mast cells in allergic inflammation. *Respir Med,* 106**,** 9-14.

BALLETTA, A., LORENZ, D., RUMMEL, A., GERHARD, R., BIGALKE, H. & WEGNER, F. 2013. Human mast cell line-1 (HMC-1) cells exhibit a membrane capacitance increase when dialysed with high free-Ca(2+) and GTPgammaS containing intracellular solution. *Eur J Pharmacol,* 720**,** 227-36.

BAUMGARTNER, R. A., YAMADA, K., DERAMO, V. A. & BEAVEN, M. A. 1994. Secretion of TNF from a rat mast cell line is a brefeldin A-sensitive and a calcium/protein kinase C-regulated process. *J Immunol,* 153**,** 2609-17.

BEFUS, A. D., MOWAT, C., GILCHRIST, M., HU, J., SOLOMON, S. & BATEMAN, A. 1999. Neutrophil defensins induce histamine secretion from mast cells: mechanisms of action. *J Immunol,* 163**,** 947-53.

BEHRENDORFF, N., DOLAI, S., HONG, W., GAISANO, H. Y. & THORN, P. 2011. Vesicle-associated membrane protein 8 (VAMP8) is a SNARE (soluble N-ethylmaleimide-

sensitive factor attachment protein receptor) selectively required for sequential granule-to-granule fusion. *J Biol Chem,* 286**,** 29627-34.

BEHRENDT, H., ROSENKRANZ, U. & SCHMUTZLER, W. 1978. Ultrastructure of isolated human mast cells during histamine release induced by ionophore A 23187. *Int Arch Allergy Appl Immunol,* 56**,** 188-92.

BEIL, W. J., SCHULZ, M. & WEFELMEYER, U. 2000. Mast cell granule composition and tissue location--a close correlation. *Histol Histopathol,* 15**,** 937-46.

BEILINA, A., BONET-PONCE, L., KUMARAN, R., KORDICH, J. J., ISHIDA, M., MAMAIS, A., KAGANOVICH, A., SAEZ-ATIENZAR, S., GERSHLICK, D. C., ROOSEN, D. A., PELLEGRINI, L., MALKOV, V., FELL, M. J., HARVEY, K., BONIFACINO, J. S., MOORE, D. J. & COOKSON, M. R. 2020. The Parkinson's Disease Protein LRRK2 Interacts with the GARP Complex to Promote Retrograde Transport to the trans-Golgi Network. *Cell Rep,* 31**,** 107614.

BEN DAVID, A., DIAMANT, E., BARNEA, A., ROSEN, O., TORGEMAN, A. & ZICHEL, R. 2013. The receptor binding domain of botulinum neurotoxin serotype A (BoNT/A) inhibits BoNT/A and BoNT/E intoxications in vivo. *Clin Vaccine Immunol,* 20**,** 1266-73.

BENHAMOU, M. & BLANK, U. 2010. Stimulus-secretion coupling by high-affinity IgE receptor: new developments. *FEBS Lett,* 584**,** 4941-8.

BENSKEY, M. J., PEREZ, R. G. & MANFREDSSON, F. P. 2016. The contribution of alpha synuclein to neuronal survival and function - Implications for Parkinson's disease. *J Neurochem,* 137**,** 331-59.

BISCHOFF, S. C. 2007. Role of mast cells in allergic and non-allergic immune responses: comparison of human and murine data. *Nat Rev Immunol,* 7**,** 93-104.

BLANK, U., MADERA-SALCEDO, I. K., DANELLI, L., CLAVER, J., TIWARI, N., SANCHEZ-MIRANDA, E., VAZQUEZ-VICTORIO, G., RAMIREZ-VALADEZ, K. A., MACIAS-SILVA, M. & GONZALEZ-ESPINOSA, C. 2014. Vesicular trafficking and signaling for cytokine and chemokine secretion in mast cells. *Front Immunol,* 5**,** 453.

BLUM, T. R., LIU, H., PACKER, M. S., XIONG, X., LEE, P. G., ZHANG, S., RICHTER, M., MINASOV, G., SATCHELL, K. J. F., DONG, M. & LIU, D. R. 2021. Phage-assisted evolution of botulinum neurotoxin proteases with reprogrammed specificity. *Science,* 371**,** 803-810.

BOYCE, J. A. 2003. Mast cells: beyond IgE. *J Allergy Clin Immunol,* 111**,** 24-32.

BOYCE, J. A. 2022. Advances in mast cell biology. *J Allergy Clin Immunol,* 149**,** 1919-1925.

BROWN, E. E., BLAUWENDRAAT, C., TRINH, J., RIZIG, M., NALLS, M. A., LEVEILLE, E., RUSKEY, J. A., JONVIK, H., TAN, M. M. X., BANDRES-CIGA, S., HASSIN-BAER, S., BROCKMANN, K., INFANTE, J., TOLOSA, E., EZQUERRA, M., BEN ROMDHAN, S., BENMAHDJOUB, M., AREZKI, M., MHIRI, C., HARDY, J., SINGLETON, A. B., ALCALAY, R. N., GASSER, T., GROSSET, D. G., WILLIAMS, N. M., PITTMAN, A., GAN-OR, Z., FERNANDEZ-SANTIAGO, R., BRICE, A., LESAGE, S., FARRER, M., WOOD, N., MORRIS, H. R. & INTERNATIONAL PARKINSON DISEASE GENOMICS, C. 2021. Analysis of DNM3 and VAMP4 as genetic modifiers of LRRK2 Parkinson's disease. *Neurobiol Aging,* 97**,** 148 e17-148 e24.

BURD, P. R., ROGERS, H. W., GORDON, J. R., MARTIN, C. A., JAYARAMAN, S., WILSON, S. D., DVORAK, A. M., GALLI, S. J. & DORF, M. E. 1989. Interleukin 3-dependent and -independent mast cells stimulated with IgE and antigen express multiple cytokines. *J Exp Med,* 170**,** 245-57.

BURGIN, D., PERIER, C., HACKETT, G., ELLIOTT, M., KWAN, D., HORNBY, F., MIR, I., MAIGNEL, J., LIU, S. M. & BEARD, M. 2021. New Modified Recombinant Botulinum Neurotoxin Type F with Enhanced Potency. *Toxins (Basel),* 13.

BURRE, J., SHARMA, M. & SUDHOF, T. C. 2014. alpha-Synuclein assembles into higher-order multimers upon membrane binding to promote SNARE complex formation. *Proc Natl Acad Sci U S A,* 111**,** E4274-83.

BUSTOS, V., PULINA, M. V., BISPO, A., LAM, A., FLAJOLET, M., GORELICK, F. S. & GREENGARD, P. 2017. Phosphorylated Presenilin 1 decreases beta-amyloid by facilitating autophagosome-lysosome fusion. *Proc Natl Acad Sci U S A,* 114**,** 7148-7153.

CAO, J., MA, P., XUE, W., DING, Y., ZHANG, Y. & ZHANG, T. 2018. RBL-2H3 cell model based on VAMP-8-EGFP protein for rapid detection of different allergens. *Acta Biochim Biophys Sin (Shanghai),* 50**,** 1297-1300.

CHEN, C. C., GRIMBALDESTON, M. A., TSAI, M., WEISSMAN, I. L. & GALLI, S. J. 2005. Identification of mast cell progenitors in adult mice. *Proc Natl Acad Sci U S A,* 102**,** 11408-13.

CHEN, S. 2012. Clinical uses of botulinum neurotoxins: current indications, limitations and future developments. *Toxins (Basel),* 4**,** 913-39.

CHEN, S. & BARBIERI, J. T. 2006. Unique substrate recognition by botulinum neurotoxins serotypes A and E. *J Biol Chem,* 281**,** 10906-11.

CHEN, S. & BARBIERI, J. T. 2009. Engineering botulinum neurotoxin to extend therapeutic intervention. *Proc Natl Acad Sci U S A,* 106**,** 9180-4.

CHEN, S. & BARBIERI, J. T. 2011. Association of botulinum neurotoxin serotype A light chain with plasma membrane-bound SNAP-25. *J Biol Chem,* 286**,** 15067-72.

CHEN, S., HALL, C. & BARBIERI, J. T. 2008. Substrate recognition of VAMP-2 by botulinum neurotoxin B and tetanus neurotoxin. *J Biol Chem,* 283**,** 21153-9.

CHOI, B. K., CHOI, M. G., KIM, J. Y., YANG, Y., LAI, Y., KWEON, D. H., LEE, N. K. & SHIN, Y. K. 2013. Large alpha-synuclein oligomers inhibit neuronal SNARE-mediated vesicle docking. *Proc Natl Acad Sci U S A,* 110**,** 4087-92.

CHOI, H. W. & ABRAHAM, S. N. 2015. Mast cell mediator responses and their suppression by pathogenic and commensal microorganisms. *Mol Immunol,* 63**,** 74-9.

CHOI, M. G., KIM, M. J., KIM, D. G., YU, R., JANG, Y. N. & OH, W. J. 2018. Sequestration of synaptic proteins by alpha-synuclein aggregates leading to neurotoxicity is inhibited by small peptide. *PLoS One,* 13**,** e0195339.

COLLACO, C. R., HOCHMAN, D. J., GOLDBLUM, R. M. & BROOKS, E. G. 2006. Effect of sodium sulfite on mast cell degranulation and oxidant stress. *Ann Allergy Asthma Immunol,* 96**,** 550-6.

COSTELA-RUIZ, V. J., ILLESCAS-MONTES, R., PAVON-MARTINEZ, R., RUIZ, C. & MELGUIZO-RODRIGUEZ, L. 2018. Role of mast cells in autoimmunity. *Life Sci,* 209**,** 52-56.

DAHLIN, J. S., DING, Z. & HALLGREN, J. 2015. Distinguishing Mast Cell Progenitors from Mature Mast Cells in Mice. *Stem Cells Dev,* 24**,** 1703-11.

DARIOS, F., RUIPEREZ, V., LOPEZ, I., VILLANUEVA, J., GUTIERREZ, L. M. & DAVLETOV, B. 2010. Alpha-synuclein sequesters arachidonic acid to modulate SNARE-mediated exocytosis. *EMBO Rep,* 11**,** 528-33.

DILEEPAN, K. N., RAVEENDRAN, V. V., SHARMA, R., ABRAHAM, H., BARUA, R., SINGH, V., SHARMA, R. & SHARMA, M. 2023. Mast cell-mediated immune regulation in health and disease. *Front Med (Lausanne),* 10**,** 1213320.

DINGJAN, I., LINDERS, P. T. A., VERBOOGEN, D. R. J., REVELO, N. H., TER BEEST, M. & VAN DEN BOGAART, G. 2018. Endosomal and Phagosomal SNAREs. *Physiol Rev,* 98**,** 1465-1492.

DUGUAY, B. A., HUANG, K. W. & KULKA, M. 2018. Lipofection of plasmid DNA into human mast cell lines using lipid nanoparticles generated by microfluidic mixing. *J Leukoc Biol,* 104**,** 587-596.

EL-LATI, S. G., DAHINDEN, C. A. & CHURCH, M. K. 1994. Complement peptides C3a- and C5a-induced mediator release from dissociated human skin mast cells. *J Invest Dermatol,* 102**,** 803-6.

ELST, J., VAN DER POORTEN, M. L. M., VAN GASSE, A. L., DE PUYSSELEYR, L., HAGENDORENS, M. M., FABER, M. A., VAN HOUDT, M., PASSANTE, E., BAHRI, R., WALSCHOT, M., MERTENS, C., BRIDTS, C. H., SABATO, V. & EBO, D. G. 2021. Mast cell activation tests by flow cytometry: A new diagnostic asset? *Clin Exp Allergy,* 51**,** 1482-1500.

EMMANOUILIDOU, E., MINAKAKI, G., KERAMIOTI, M. V., XYLAKI, M., BALAFAS, E., CHRYSANTHOU-PITEROU, M., KLOUKINA, I. & VEKRELLIS, K. 2016. GABA transmission via ATP-dependent K+ channels regulates alpha-synuclein secretion in mouse striatum. *Brain,* 139**,** 871-90.

ERDEI, A., ANDRASFALVY, M., PETERFY, H., TOTH, G. & PECHT, I. 2004. Regulation of mast cell activation by complement-derived peptides. *Immunol Lett,* 92**,** 39-42.

FILHO, M., ANICETO, G., FERNANDES, P. M., AQUINO, I. G., MENDES, G. D., NAPIMOGA, M. H., CLEMENTE-NAPIMOGA, J. T. & ABDALLA, H. B. 2024. Botulinum toxin A dampened inflammatory response in BV-2 microglial cells. *Toxicon,* 252**,** 108182.

FONFRIA, E., ELLIOTT, M., BEARD, M., CHADDOCK, J. A. & KRUPP, J. 2018a. Engineering Botulinum Toxins to Improve and Expand Targeting and SNARE Cleavage Activity. *Toxins (Basel),* 10.

FONFRIA, E., MAIGNEL, J., LEZMI, S., MARTIN, V., SPLEVINS, A., SHUBBER, S., KALINICHEV, M., FOSTER, K., PICAUT, P. & KRUPP, J. 2018b. The Expanding Therapeutic Utility of Botulinum Neurotoxins. *Toxins (Basel),* 10.

GALLI, S. J., KALESNIKOFF, J., GRIMBALDESTON, M. A., PILIPONSKY, A. M., WILLIAMS, C. M. & TSAI, M. 2005. Mast cells as "tunable" effector and immunoregulatory cells: recent advances. *Annu Rev Immunol,* 23**,** 749-86.

GARCIA-REITBOCK, P., ANICHTCHIK, O., BELLUCCI, A., IOVINO, M., BALLINI, C., FINEBERG, E., GHETTI, B., DELLA CORTE, L., SPANO, P., TOFARIS, G. K., GOEDERT, M. & SPILLANTINI, M. G. 2010. SNARE protein redistribution and synaptic failure in a transgenic mouse model of Parkinson's disease. *Brain,* 133**,** 2032-44.

GAUDENZIO, N., SIBILANO, R., MARICHAL, T., STARKL, P., REBER, L. L., CENAC, N., MCNEIL, B. D., DONG, X., HERNANDEZ, J. D., SAGI-EISENBERG, R., HAMMEL, I., ROERS, A., VALITUTTI, S., TSAI, M., ESPINOSA, E. & GALLI, S. J. 2016. Different activation signals induce distinct mast cell degranulation strategies. *Journal of Clinical Investigation,* 126**,** 3981-3998.

GILFILLAN, A. M. & BEAVEN, M. A. 2011. Regulation of mast cell responses in health and disease. *Crit Rev Immunol,* 31**,** 475-529.

GILFILLAN, A. M. & RIVERA, J. 2009. The tyrosine kinase network regulating mast cell activation. *Immunological Reviews,* 228**,** 149-169.

GILFILLAN, A. M. & TKACZYK, C. 2006. Integrated signalling pathways for mast-cell activation. *Nat Rev Immunol,* 6**,** 218-230.

GORDON, J. R. & GALLI, S. J. 1990. Mast cells as a source of both preformed and immunologically inducible TNF-alpha/cachectin. *Nature,* 346**,** 274-6.

GRIZZI, F., DI CARO, G., LAGHI, L., HERMONAT, P., MAZZOLA, P., NGUYEN, D. D., RADHI, S., FIGUEROA, J. A., COBOS, E., ANNONI, G. & CHIRIVA-INTERNATI, M. 2013. Mast cells and the liver aging process. *Immun Ageing,* 10**,** 9.

GRUENBAUM, Y., STEIN, R., CEDAR, H. & RAZIN, A. 1981. Methylation of CpG sequences in eukaryotic DNA. *FEBS Lett,* 124**,** 67-71.

GRUTZKAU, A., SMORODCHENKO, A., LIPPERT, U., KIRCHHOF, L., ARTUC, M. & HENZ, B. M. 2004. LAMP-1 and LAMP-2, but not LAMP-3, are reliable markers for activation-induced secretion of human mast cells. *Cytometry A,* 61**,** 62-8.

GUO, Z., TURNER, C. & CASTLE, D. 1998. Relocation of the t-SNARE SNAP-23 from Lamellipodia-like Cell Surface Projections Regulates Compound Exocytosis in Mast Cells. *Cell,* 94**,** 537-548.

HAGEMANN, T. L., CONNOR, J. X. & MESSING, A. 2006. Alexander disease-associated glial fibrillary acidic protein mutations in mice induce Rosenthal fiber formation and a white matter stress response. *J Neurosci,* 26**,** 11162-73.

HAN, J., PLUHACKOVA, K. & BOCKMANN, R. A. 2017. The Multifaceted Role of SNARE Proteins in Membrane Fusion. *Front Physiol,* 8**,** 5.

HATSUZAWA, K. & SAKURAI, C. 2020. Regulatory Mechanism of SNAP23 in Phagosome Formation and Maturation. *Yonago Acta Med,* 63**,** 135-145.

HAZZAN, T., GUHL, S., ARTUC, M., FRANKE, K., WORM, M., ZUBERBIER, T. & BABINA, M. 2017. An efficient method for gene knock-down by RNA interference in human skin mast cells. *Exp Dermatol,* 26**,** 1136-1139.

HERNANDEZ-ZIMBRON, L. F. & RIVAS-ARANCIBIA, S. 2016. Syntaxin 5 Overexpression and beta-Amyloid 1-42 Accumulation in Endoplasmic Reticulum of Hippocampal Cells in Rat Brain Induced by Ozone Exposure. *Biomed Res Int,* 2016**,** 2125643.

HOCHMAN, D. J., COLLACO, C. R. & BROOKS, E. G. 2014. Acrolein induction of oxidative stress and degranulation in mast cells. *Environ Toxicol,* 29**,** 908-15.

HOFMANN, A. M. & ABRAHAM, S. N. 2009. New roles for mast cells in modulating allergic reactions and immunity against pathogens. *Curr Opin Immunol,* 21**,** 679-86.

HONG-GELLER, E. & CERIONE, R. A. 2000. Cdc42 and Rac stimulate exocytosis of secretory granules by activating the IP(3)/calcium pathway in RBL-2H3 mast cells. *J Cell Biol,* 148**,** 481-94.

HOSOKAWA, J., SUZUKI, K., NAKAGOMI, D., TAMACHI, T., TAKATORI, H., SUTO, A. & NAKAJIMA, H. 2013. Role of calcium ionophore A23187-induced activation of IkappaB kinase 2 in mast cells. *Int Arch Allergy Immunol,* 161 Suppl 2**,** 37-43.

IDDAMALGODA, A., LE, Q. T., ITO, K., TANAKA, K., KOJIMA, H. & KIDO, H. 2008. Mast cell tryptase and photoaging: possible involvement in the degradation of extra cellular matrix and basement membrane proteins. *Arch Dermatol Res,* 300 Suppl 1**,** S69-76.

JACOBSEN, T., SCHUBOTZ, R. I., HOFEL, L. & CRAMON, D. Y. 2006. Brain correlates of aesthetic judgment of beauty. *Neuroimage,* 29**,** 276-85.

JENSEN, B. M., SWINDLE, E. J., IWAKI, S. & GILFILLAN, A. M. 2006. Generation, isolation, and maintenance of rodent mast cells and mast cell lines. *Curr Protoc Immunol,* Chapter 3**,** Unit 3.23.

JORDAN, P. M., ANDREAS, N., GROTH, M., WEGNER, P., WEBER, F., JÄGER, U., KÜCHLER, C., WERZ, O., SERFLING, E., KAMRADT, T., DUDECK, A. & DRUBE, S. 2021. ATP/IL-33-triggered hyperactivation of mast cells results in an amplified production of pro-inflammatory cytokines and eicosanoids. *Immunology,* 164**,** 541-554.

KALESNIKOFF, J., HUBER, M., LAM, V., DAMEN, J. E., ZHANG, J., SIRAGANIAN, R. P. & KRYSTAL, G. 2001. Monomeric IgE stimulates signaling pathways in mast cells that lead to cytokine production and cell survival. *Immunity,* 14**,** 801-11.

KARIMI, K., KOOL, M., NIJKAMP, F. P. & REDEGELD, F. A. 2004. Substance P can stimulate prostaglandin D2 and leukotriene C4 generation without granule exocytosis in murine mast cells. *Eur J Pharmacol,* 489**,** 49-54.

KAWAMATA, H., NG, S. K., DIAZ, N., BURSTEIN, S., MOREL, L., OSGOOD, A., SIDER, B., HIGASHIMORI, H., HAYDON, P. G., MANFREDI, G. & YANG, Y. 2014. Abnormal intracellular calcium signaling and SNARE-dependent exocytosis contributes to SOD1G93A astrocyte-mediated toxicity in amyotrophic lateral sclerosis. *J Neurosci,* 34**,** 2331-48.

KAWASAKI, H., MIZUSEKI, K., NISHIKAWA, S., KANEKO, S., KUWANA, Y., NAKANISHI, S., NISHIKAWA, S. I. & SASAI, Y. 2000. Induction of midbrain dopaminergic neurons from ES cells by stromal cell-derived inducing activity. *Neuron,* 28**,** 31-40.

KIM, Y. J., KIM, J. H., LEE, K. J., CHOI, M. M., KIM, Y. H., RHIE, G. E., YOO, C. K., CHA, K. & SHIN, N. R. 2015. Botulinum neurotoxin type A induces TLR2-mediated inflammatory responses in macrophages. *PLoS One,* 10**,** e0120840.

KING, C. A., MARSHALL, J. S., ALSHURAFA, H. & ANDERSON, R. 2000. Release of vasoactive cytokines by antibody-enhanced dengue virus infection of a human mast cell/basophil line. *J Virol,* 74**,** 7146-50.

KIRSHENBAUM, A. S., GOFF, J. P., KESSLER, S. W., MICAN, J. M., ZSEBO, K. M. & METCALFE, D. D. 1992. Effect of IL-3 and stem cell factor on the appearance of human basophils and mast cells from CD34+ pluripotent progenitor cells. *J Immunol,* 148**,** 772-7.

KOJIMA, R., OHNO, T., IIKURA, M., NIKI, T., HIRASHIMA, M., IWAYA, K., TSUDA, H., NONOYAMA, S., MATSUDA, A., SAITO, H., MATSUMOTO, K. & NAKAE, S. 2014. Galectin-9 enhances cytokine secretion, but suppresses survival and degranulation, in human mast cell line. *PLoS One,* 9**,** e86106.

KOMIYAMA, H., MIYAKE, K., ASAI, K., MIZUNO, K. & SHIMADA, T. 2014. Cyclical mechanical stretch enhances degranulation and IL-4 secretion in RBL-2H3 mast cells. *Cell Biochem Funct,* 32**,** 70-6.

KRYSTEL-WHITTEMORE, M., DILEEPAN, K. N. & WOOD, J. G. 2015. Mast Cell: A Multi-Functional Master Cell. *Front Immunol,* 6**,** 620.

KUBO, M. 2018. Mast cells and basophils in allergic inflammation. *Curr Opin Immunol,* 54**,** 74-79.

KUEHN, H. S., RADINGER, M. & GILFILLAN, A. M. 2010. Measuring mast cell mediator release. *Curr Protoc Immunol,* Chapter 7**,** Unit7 38.

KULKA, M., ALEXOPOULOU, L., FLAVELL, R. A. & METCALFE, D. D. 2004. Activation of mast cells by double-stranded RNA: evidence for activation through Toll-like receptor 3. *J Allergy Clin Immunol,* 114**,** 174-82.

KULKA, M. & METCALFE, D. D. 2010. Isolation of tissue mast cells. *Curr Protoc Immunol,* Chapter 7**,** Unit 7.25.

KULKA, M., SHEEN, C. H., TANCOWNY, B. P., GRAMMER, L. C. & SCHLEIMER, R. P. 2008. Neuropeptides activate human mast cell degranulation and chemokine production. *Immunology,* 123**,** 398-410.

KUMAR, R. & SINGH, B. R. 2025. Botulinum Toxin: A Comprehensive Review of Its Molecular Architecture and Mechanistic Action. *Int J Mol Sci,* 26.

KUMAR, V. & SHARMA, A. 2010. Mast cells: emerging sentinel innate immune cells with diverse role in immunity. *Mol Immunol,* 48**,** 14-25.

LACY, P. & STOW, J. L. 2011. Cytokine release from innate immune cells: association with diverse membrane trafficking pathways. *Blood,* 118**,** 9-18.

LAI, Y., KIM, S., VARKEY, J., LOU, X., SONG, J. K., DIAO, J., LANGEN, R. & SHIN, Y. K. 2014. Nonaggregated alpha-synuclein influences SNARE-dependent vesicle docking via membrane binding. *Biochemistry,* 53**,** 3889-96.

LAIDLAW, T. M., STEINKE, J. W., TIÑANA, A. M., FENG, C., XING, W., LAM, B. K., PARUCHURI, S., BOYCE, J. A. & BORISH, L. 2011. Characterization of a novel human mast cell line that responds to stem cell factor and expresses functional FcεRI. *J Allergy Clin Immunol,* 127**,** 815-22.e1-5.

LAW, C., SCHAAN PROFES, M., LEVESQUE, M., KALTSCHMIDT, J. A., VERHAGE, M. & KANIA, A. 2016. Normal Molecular Specification and Neurodegenerative Disease-Like Death of Spinal Neurons Lacking the SNARE-Associated Synaptic Protein Munc18-1. *J Neurosci,* 36**,** 561-76.

LIM, C. Y., GRANGER, J. H. & PORTER, M. D. 2019. SERS detection of Clostridium botulinum neurotoxin serotypes A and B in buffer and serum: Towards the development of a biodefense test platform. *Anal Chim Acta X,* 1**,** 100002.

LIPPERT, U., FERRARI, D. M. & JAHN, R. 2007. Endobrevin/VAMP8 mediates exocytotic release of hexosaminidase from rat basophilic leukaemia cells. *FEBS Lett,* 581**,** 3479-3484.

LIU, Y., LI, H., SUGIURA, Y., HAN, W., GALLARDO, G., KHVOTCHEV, M., ZHANG, Y., KAVALALI, E. T., SUDHOF, T. C. & LIN, W. 2015. Ubiquitin-Synaptobrevin Fusion Protein Causes Degeneration of Presynaptic Motor Terminals in Mice. *J Neurosci,* 35**,** 11514-31.

LORENTZ, A., BAUMANN, A., VITTE, J. & BLANK, U. 2012. The SNARE Machinery in Mast Cell Secretion. *Front Immunol,* 3**,** 143.

LOU, X., KIM, J., HAWK, B. J. & SHIN, Y. K. 2017. alpha-Synuclein may cross-bridge v-SNARE and acidic phospholipids to facilitate SNARE-dependent vesicle docking. *Biochem J,* 474**,** 2039-2049.

LYONS, D. O. & PULLEN, N. A. 2020. Beyond IgE: Alternative Mast Cell Activation Across Different Disease States. *Int J Mol Sci,* 21.

MACNEIL, A. J., JUNKINS, R. D., WU, Z. & LIN, T. J. 2014. Stem cell factor induces AP-1-dependent mast cell IL-6 production via MAPK kinase 3 activity. *J Leukoc Biol,* 95**,** 903-15.

MAGADMI, R., MESZAROS, J., DAMANHOURI, Z. A. & SEWARD, E. P. 2019. Secretion of Mast Cell Inflammatory Mediators Is Enhanced by CADM1-Dependent Adhesion to Sensory Neurons. *Frontiers in Cellular Neuroscience,* 13**,** 262.

MALIK, S., LE, L., BOISSY, R. E., BRIDEAU-ANDERSEN, A. & SONDERGAARD, B. 2025. Botulinum neurotoxin type DC (BoNT/DC) cleavage of VAMP3 reduces melanin production in melanocytes. *Toxicon,* 261**,** 108372.

MARGIOTTA, A. 2021. Role of SNAREs in Neurodegenerative Diseases. *Cells,* 10.

MARSHALL, J. S., GOMI, K., BLENNERHASSETT, M. G. & BIENENSTOCK, J. 1999. Nerve growth factor modifies the expression of inflammatory cytokines by mast cells via a prostanoid-dependent mechanism. *J Immunol,* 162**,** 4271-6.

MASUYER, G., ZHANG, S., BARKHO, S., SHEN, Y., HENRIKSSON, L., KOSENINA, S., DONG, M. & STENMARK, P. 2018. Structural characterisation of the catalytic domain of botulinum neurotoxin X - high activity and unique substrate specificity. *Sci Rep,* 8**,** 4518.

MATSUDA, K., PILIPONSKY, A. M., IIKURA, M., NAKAE, S., WANG, E. W., DUTTA, S. M., KAWAKAMI, T., TSAI, M. & GALLI, S. J. 2005. Monomeric IgE enhances human mast cell chemokine production: IL-4 augments and dexamethasone suppresses the response. *J Allergy Clin Immunol,* 116**,** 1357-63.

MCCARTHY, P. C., PHAIR, I. R., GREGER, C., PARDALI, K., MCGUIRE, V. A., CLARK, A. R., GAESTEL, M. & ARTHUR, J. S. C. 2019. IL-33 regulates cytokine production and neutrophil recruitment via the p38 MAPK-activated kinases MK2/3. *Immunol Cell Biol,* 97**,** 54-71.

MCCURDY, J. D., LIN, T. J. & MARSHALL, J. S. 2001. Toll-like receptor 4-mediated activation of murine mast cells. *J Leukoc Biol,* 70**,** 977-84.

MCCURDY, J. D., OLYNYCH, T. J., MAHER, L. H. & MARSHALL, J. S. 2003. Cutting edge: distinct Toll-like receptor 2 activators selectively induce different classes of mediator production from human mast cells. *J Immunol,* 170**,** 1625-9.

MCLELLAND, G. L., LEE, S. A., MCBRIDE, H. M. & FON, E. A. 2016. Syntaxin-17 delivers PINK1/parkin-dependent mitochondrial vesicles to the endolysosomal system. *J Cell Biol,* 214**,** 275-91.

MCNEIL, B. D., PUNDIR, P., MEEKER, S., HAN, L., UNDEM, B. J., KULKA, M. & DONG, X. 2015. Identification of a mast-cell-specific receptor crucial for pseudo-allergic drug reactions. *Nature,* 519**,** 237-41.

MEDIC, N., DESAI, A., OLIVERA, A., ABRAMOWITZ, J., BIRNBAUMER, L., BEAVEN, M. A., GILFILLAN, A. M. & METCALFE, D. D. 2013. Knockout of the Trpc1 gene reveals that TRPC1 can promote recovery from anaphylaxis by negatively regulating mast cell TNF-alpha production. *Cell Calcium,* 53**,** 315-26.

MENASCHE, G., LONGE, C., BRATTI, M. & BLANK, U. 2021. Cytoskeletal Transport, Reorganization, and Fusion Regulation in Mast Cell-Stimulus Secretion Coupling. *Front Cell Dev Biol,* 9**,** 652077.

MENDES, M. A. & PALMA, M. S. 2006. Two new bradykinin-related peptides from the venom of the social wasp Protopolybia exigua (Saussure). *Peptides,* 27**,** 2632-9.

MENDEZ-ENRIQUEZ, E., SALOMONSSON, M., ERIKSSON, J., JANSON, C., MALINOVSCHI, A., SELLIN, M. E. & HALLGREN, J. 2022. IgE cross-linking induces activation of human and mouse mast cell progenitors. *J Allergy Clin Immunol,* 149**,** 1458-1463.

METCALFE, D. D., BARAM, D. & MEKORI, Y. A. 1997. Mast cells. *Physiol Rev,* 77**,** 1033-79.

MINGAZOV, E. R. & UGRUMOV, M. V. 2016. Gene expression of proteins of the vesicle cycle in the striatum and motor cortex under functional failure of nigrostriatal system. *Dokl Biochem Biophys,* 470**,** 313-315.

MISHIMA, S., SAKAMOTO, M., KIOKA, H., NAGATA, Y. & SUZUKI, R. 2022. Multifunctional regulation of VAMP3 in exocytic and endocytic pathways of RBL-2H3 cells. *Front Immunol,* 13**,** 885868.

MONASH, A., TAM, J., ROSEN, O. & SOREQ, H. 2025. Botulinum Neurotoxins: History, Mechanism, and Applications. A Narrative Review. *J Neurochem,* 169**,** e70187.

MOON, T. C., BEFUS, A. D. & KULKA, M. 2014. Mast cell mediators: their differential release and the secretory pathways involved. *Front Immunol,* 5**,** 569.

MOREIRA-TABAKA, H., PELUSO, J., VONESCH, J. L., HENTSCH, D., KESSLER, P., REIMUND, J. M., DUMONT, S. & MULLER, C. D. 2012. Unlike for human monocytes after LPS activation, release of TNF-alpha by THP-1 cells is produced by a TACE catalytically different from constitutive TACE. *PLoS One,* 7**,** e34184.

MUKAI, K., TSAI, M., SAITO, H. & GALLI, S. J. 2018. Mast cells as sources of cytokines, chemokines, and growth factors. *Immunol Rev,* 282**,** 121-150.

MUNCHAU, A. & BHATIA, K. P. 2000. Uses of botulinum toxin injection in medicine today. *BMJ,* 320**,** 161-5.

MUSCH, M. W. & SIEGEL, M. I. 1986. Antigen-stimulated metabolism of inositol phospholipids in the cloned murine mast-cell line MC9. *Biochem J,* 234**,** 205-12.

NABEL, G., GALLI, S. J., DVORAK, A. M., DVORAK, H. F. & CANTOR, H. 1981. Inducer T lymphocytes synthesize a factor that stimulates proliferation of cloned mast cells. *Nature,* 291**,** 332-4.

NARENJKAR, J., MARSH, S. J. & ASSEM, E. S. 1999. The characterization and quantification of antigen-induced Ca2+ oscillations in a rat basophilic leukaemia cell line (RBL-2H3). *Cell Calcium,* 26**,** 261-9.

NIGAM, P. K. & NIGAM, A. 2010. Botulinum toxin. *Indian J Dermatol,* 55**,** 8-14.

NIYONSABA, F., SOMEYA, A., HIRATA, M., OGAWA, H. & NAGAOKA, I. 2001. Evaluation of the effects of peptide antibiotics human beta-defensins-1/-2 and LL-37 on histamine release and prostaglandin D(2) production from mast cells. *Eur J Immunol,* 31**,** 1066-75.

NIYONSABA, F., USHIO, H., HARA, M., YOKOI, H., TOMINAGA, M., TAKAMORI, K., KAJIWARA, N., SAITO, H., NAGAOKA, I., OGAWA, H. & OKUMURA, K. 2010. Antimicrobial peptides human beta-defensins and cathelicidin LL-37 induce the secretion of a pruritogenic cytokine IL-31 by human mast cells. *J Immunol,* 184**,** 3526-34.

OGASAWARA, T., MURAKAMI, M., SUZUKI-NISHIMURA, T., UCHIDA, M. K. & KUDO, I. 1997. Mouse bone marrow-derived mast cells undergo exocytosis, prostanoid generation, and cytokine expression in response to G protein-activating polybasic compounds after coculture with fibroblasts in the presence of c-kit ligand. *J Immunol,* 158**,** 393-404.

OLIVERA, A., BEAVEN, M. A. & METCALFE, D. D. 2018. Mast cells signal their importance in health and disease. *J Allergy Clin Immunol,* 142**,** 381-393.

PALMA, A. M., HANES, M. R. & MARSHALL, J. S. 2021. Mast Cell Modulation of B Cell Responses: An Under-Appreciated Partnership in Host Defence. *Front Immunol,* 12**,** 718499.

PASSANTE, E., EHRHARDT, C., SHERIDAN, H. & FRANKISH, N. 2009. RBL-2H3 cells are an imprecise model for mast cell mediator release. *Inflamm Res,* 58**,** 611-8.

PAUMET, F., LE MAO, J., MARTIN, S., GALLI, T., DAVID, B., BLANK, U. & ROA, M. 2000. Soluble NSF attachment protein receptors (SNAREs) in RBL-2H3 mast cells:

functional role of syntaxin 4 in exocytosis and identification of a vesicle-associated membrane protein 8-containing secretory compartment. *J Immunol,* 164**,** 5850-7.

PELLETT, S., BRADSHAW, M., TEPP, W. H., PIER, C. L., WHITEMARSH, R. C. M., CHEN, C., BARBIERI, J. T. & JOHNSON, E. A. 2018. The Light Chain Defines the Duration of Action of Botulinum Toxin Serotype A Subtypes. *mBio,* 9.

PELLETT, S., YAKSH, T. L. & RAMACHANDRAN, R. 2015. Current status and future directions of botulinum neurotoxins for targeting pain processing. *Toxins (Basel),* 7**,** 4519-63.

PHAM, E., CREWS, L., UBHI, K., HANSEN, L., ADAME, A., CARTIER, A., SALMON, D., GALASKO, D., MICHAEL, S., SAVAS, J. N., YATES, J. R., GLABE, C. & MASLIAH, E. 2010. Progressive accumulation of amyloid-beta oligomers in Alzheimer's disease and in amyloid precursor protein transgenic mice is accompanied by selective alterations in synaptic scaffold proteins. *FEBS J,* 277**,** 3051-67.

PIGNATTI, P., FROSSI, B., PALA, G., NEGRI, S., OMAN, H., PERFETTI, L., PUCILLO, C., IMBRIANI, M. & MOSCATO, G. 2013. Oxidative activity of ammonium persulfate salt on mast cells and basophils: implication in hairdressers' asthma. *Int Arch Allergy Immunol,* 160**,** 409-19.

PILLIOD, J., DESJARDINS, A., PERNEGRE, C., JAMANN, H., LAROCHELLE, C., FON, E. A. & LECLERC, N. 2020. Clearance of intracellular tau protein from neuronal cells via VAMP8-induced secretion. *J Biol Chem,* 295**,** 17827-17841.

PIRAZZINI, M., ROSSETTO, O., ELEOPRA, R. & MONTECUCCO, C. 2017. Botulinum Neurotoxins: Biology, Pharmacology, and Toxicology. *Pharmacol Rev,* 69**,** 200-235.

PIROMCHAI, P., PORNUMNOUY, W., SAESEOW, P. & CHAINANSAMIT, S. 2021. The minimum effective dose of abobotulinum toxin A injection for allergic rhinitis: A dose-escalation randomized controlled trial. *Laryngoscope Investig Otolaryngol,* 6**,** 6-12.

POULAIN, B., LEMICHEZ, E. & POPOFF, M. R. 2020. Neuronal selectivity of botulinum neurotoxins. *Toxicon,* 178**,** 20-32.

PUNDIR, P., CATALLI, A., LEGGIADRO, C., DOUGLAS, S. E. & KULKA, M. 2014. Pleurocidin, a novel antimicrobial peptide, induces human mast cell activation through the FPRL1 receptor. *Mucosal Immunol,* 7**,** 177-87.

PURI, N. & ROCHE, P. A. 2008. Mast cells possess distinct secretory granule subsets whose exocytosis is regulated by different SNARE isoforms. *Proc Natl Acad Sci U S A,* 105**,** 2580-5.

RAMACHANDRAN, R., MARINO, J. M., PAUL, S., WANG, Z., MASCARENHAS, L. N., PELLETT, S., JOHNSON, A. E., DINARDO, A. & YAKSH, L. T. 2018a. A Study and Review of Effects of Botulinum Toxins on Mast Cell Dependent and Independent Pruritus. *Toxins,* 10.

RAMACHANDRAN, R., MARINO, M. J., PAUL, S., WANG, Z., MASCARENHAS, N. L., PELLETT, S., JOHNSON, E. A., DINARDO, A. & YAKSH, T. L. 2018b. A Study and Review of Effects of Botulinum Toxins on Mast Cell Dependent and Independent Pruritus. *Toxins (Basel),* 10.

RAPTIS, A., TORREJON-ESCRIBANO, B., GOMEZ DE ARANDA, I. & BLASI, J. 2005. Distribution of synaptobrevin/VAMP 1 and 2 in rat brain. *J Chem Neuroanat,* 30**,** 201-11.

RASETTI-ESCARGUEIL, C. & PALEA, S. 2024. Embracing the Versatility of Botulinum Neurotoxins in Conventional and New Therapeutic Applications. *Toxins (Basel),* 16.

RAZIN, E., MENCIAHUERTA, J. M., STEVENS, R. L., LEWIS, R. A., LIU, F. T., COREY, E. J. & AUSTEN, K. F. 1983. IGE-MEDIATED RELEASE OF LEUKOTRIENE C-4, CHONDROITIN SULFATE E-PROTEOGLYCAN, BETA-HEXOSAMINIDASE, AND HISTAMINE FROM CULTURED BONE MARROW-DERIVED MOUSE MAST-CELLS. *JOURNAL OF EXPERIMENTAL MEDICINE,* 157**,** 189-201.

REBER, L. L., SIBILANO, R., MUKAI, K. & GALLI, S. J. 2015. Potential effector and immunoregulatory functions of mast cells in mucosal immunity. *Mucosal Immunol,* 8**,** 444-63.

RENDON, W. O., MARTINEZ-ALONSO, E., TOMAS, M., MARTINEZ-MARTINEZ, N. & MARTINEZ-MENARGUEZ, J. A. 2013. Golgi fragmentation is Rab and SNARE dependent in cellular models of Parkinson's disease. *Histochem Cell Biol,* 139**,** 671-84.

REYNIER-REBUFFEL, A. M., MATHIAU, P., CALLEBERT, J., DIMITRIADOU, V., FARJAUDON, N., KACEM, K., LAUNAY, J. M., SEYLAZ, J. & ABINEAU, P. 1994. Substance P, calcitonin gene-related peptide, and capsaicin release serotonin from cerebrovascular mast cells. *Am J Physiol,* 267**,** R1421-9.

ROY, S., CHOMPUNUD NA AYUDHYA, C., THAPALIYA, M., DEEPAK, V. & ALI, H. 2021. Multifaceted MRGPRX2: New insight into the role of mast cells in health and disease. *J Allergy Clin Immunol,* 148**,** 293-308.

SANDER, L. E., FRANK, S. P., BOLAT, S., BLANK, U., GALLI, T., BIGALKE, H., BISCHOFF, S. C. & LORENTZ, A. 2008. Vesicle associated membrane protein (VAMP)-7 and VAMP-8, but not VAMP-2 or VAMP-3, are required for activation-induced degranulation of mature human mast cells. *Eur J Immunol,* 38**,** 855-63.

SANTOS, T. C., WIERDA, K., BROEKE, J. H., TOONEN, R. F. & VERHAGE, M. 2017. Early Golgi Abnormalities and Neurodegeneration upon Loss of Presynaptic Proteins Munc18-1, Syntaxin-1, or SNAP-25. *J Neurosci,* 37**,** 4525-4539.

SAUVOLA, C. W. & LITTLETON, J. T. 2021. SNARE Regulatory Proteins in Synaptic Vesicle Fusion and Recycling. *Front Mol Neurosci,* 14**,** 733138.

SCHAEFER, T. M., DESOUZA, K., FAHEY, J. V., BEAGLEY, K. W. & WIRA, C. R. 2004. Toll-like receptor (TLR) expression and TLR-mediated cytokine/chemokine production by human uterine epithelial cells. *Immunology,* 112**,** 428-36.

SHALIT, M., RUBINOW, A., GRANIT, L. & BAR-SELA, S. 1987. Codeine-induced mast cell degranulation in human skin: effect of calcium channel blockers. *Ann Allergy,* 59**,** 461-3.

SHEEN, C. H., SCHLEIMER, R. P. & KULKA, M. 2007. Codeine induces human mast cell chemokine and cytokine production: involvement of G-protein activation. *Allergy,* 62**,** 532-538.

SICK, E., BREHIN, S., ANDRE, P., COUPIN, G., LANDRY, Y., TAKEDA, K. & GIES, J. P. 2010. Advanced glycation end products (AGEs) activate mast cells. *Br J Pharmacol,* 161**,** 442-55.

SIKORRA, S., DONALD, S., ELLIOTT, M., SCHWEDE, S., COKER, S. F., KUPINSKI, A. P., TRIPATHI, V., FOSTER, K., BEARD, M. & BINZ, T. 2020. Engineering an Effective Human SNAP-23 Cleaving Botulinum Neurotoxin A Variant. *Toxins (Basel),* 12.

SIRAGANIAN, R. P., ZHANG, J., SUZUKI, K. & SADA, K. 2002. Protein tyrosine kinase Syk in mast cell signaling. *Mol Immunol,* 38**,** 1229-33.

SMITH, S. K., ANDERSON, H. A., YU, G., ROBERTSON, A. G., ALLEN, S. J., TYLER, S. J., NAYLOR, R. L., MASON, G., WILCOCK, G. W., ROCHE, P. A., FRASER, P. E. & DAWBARN, D. 2000. Identification of syntaxin 1A as a novel binding protein for presenilin-1. *Brain Res Mol Brain Res,* 78**,** 100-7.

SMRŽ, D., BANDARA, G., BEAVEN, M. A., METCALFE, D. D. & GILFILLAN, A. M. 2013. Prevention of F-actin assembly switches the response to SCF from chemotaxis to degranulation in human mast cells. *European Journal of Immunology,* 43**,** 1873-1882.

SOLIMANDO, A. G., DESANTIS, V. & RIBATTI, D. 2022. Mast Cells and Interleukins. *Int J Mol Sci,* 23.

SOULE, B. P., BROWN, J. M., KUSHNIR-SUKHOV, N. M., SIMONE, N. L., MITCHELL, J. B. & METCALFE, D. D. 2007. Effects of gamma radiation on FcepsilonRI and TLR-mediated mast cell activation. *J Immunol,* 179**,** 3276-86.

SUBRAMANIAN, H., GUPTA, K., LEE, D., BAYIR, A. K., AHN, H. & ALI, H. 2013. beta-Defensins activate human mast cells via Mas-related gene X2. *J Immunol,* 191**,** 345-52.

SUDO, N., TANAKA, K., KOGA, Y., OKUMURA, Y., KUBO, C. & NOMOTO, K. 1996. Extracellular ATP activates mast cells via a mechanism that is different from the activation induced by the cross-linking of Fc receptors. *J Immunol,* 156**,** 3970-9.

SUGA, K., SAITO, A., MISHIMA, T. & AKAGAWA, K. 2015. ER and Golgi stresses increase ER-Golgi SNARE Syntaxin5: Implications for organelle stress and betaAPP processing. *Neurosci Lett,* 604**,** 30-5.

SUGA, K., TOMIYAMA, T., MORI, H. & AKAGAWA, K. 2004. Syntaxin 5 interacts with presenilin holoproteins, but not with their N- or C-terminal fragments, and affects beta-amyloid peptide production. *Biochem J,* 381**,** 619-28.

SUN, J., WANG, L., BAO, H., PREMI, S., DAS, U., CHAPMAN, E. R. & ROY, S. 2019. Functional cooperation of alpha-synuclein and VAMP2 in synaptic vesicle recycling. *Proc Natl Acad Sci U S A,* 116**,** 11113-11115.

SUNDSTROM, J. B., HAIR, G. A., ANSARI, A. A., SECOR, W. E., GILFILLAN, A. M., METCALFE, D. D. & KIRSHENBAUM, A. S. 2009. IgE-FcepsilonRI interactions determine HIV coreceptor usage and susceptibility to infection during ontogeny of mast cells. *J Immunol,* 182**,** 6401-9.

SWINDLE, E. J. 2020. Generation of Mast Cells from Murine Stem Cell Progenitors. *Methods Mol Biol,* 2163**,** 85-89.

SWINDLE, E. J., COLEMAN, J. W., DELEO, F. R. & METCALFE, D. D. 2007. FcepsilonRI- and Fcgamma receptor-mediated production of reactive oxygen species by mast cells is lipoxygenase- and cyclooxygenase-dependent and NADPH oxidase-independent. *The Journal of Immunology,* 179**,** 7059-7071.

TANG, M., MENG, J. & WANG, J. 2019. New Engineered-Botulinum Toxins Inhibit the Release of Pain-Related Mediators. *Int J Mol Sci,* 21.

THAYANIDHI, N., HELM, J. R., NYCZ, D. C., BENTLEY, M., LIANG, Y. & HAY, J. C. 2010. Alpha-synuclein delays endoplasmic reticulum (ER)-to-Golgi transport in mammalian cells by antagonizing ER/Golgi SNAREs. *Mol Biol Cell,* 21**,** 1850-63.

THEOHARIDES, T. C., ALYSANDRATOS, K. D., ANGELIDOU, A., DELIVANIS, D. A., SISMANOPOULOS, N., ZHANG, B., ASADI, S., VASIADI, M., WENG, Z., MINIATI, A. & KALOGEROMITROS, D. 2012. Mast cells and inflammation. *Biochim Biophys Acta,* 1822**,** 21-33.

THEOHARIDES, T. C. & KALOGEROMITROS, D. 2006. The critical role of mast cells in allergy and inflammation. *Ann N Y Acad Sci,* 1088**,** 78-99.

THEOHARIDES, T. C., KEMPURAJ, D., TAGEN, M., CONTI, P. & KALOGEROMITROS, D. 2007. Differential release of mast cell mediators and the pathogenesis of inflammation. *Immunol Rev,* 217**,** 65-78.

TIWARI, N., WANG, C.-C., BROCHETTA, C., KE, G., VITA, F., QI, Z., RIVERA, J., SORANZO, M. R., ZABUCCHI, G., HONG, W. & BLANK, U. 2008a. VAWP-8 segregates mast cell-preformed mediator exocytosis from cytokine trafficking pathways. *BLOOD,* 111**,** 3665-3674.

TIWARI, N., WANG, C. C., BROCHETTA, C., KE, G., VITA, F., QI, Z., RIVERA, J., SORANZO, M. R., ZABUCCHI, G., HONG, W. & BLANK, U. 2008b. VAMP-8 segregates mast cell-preformed mediator exocytosis from cytokine trafficking pathways. *Blood,* 111**,** 3665-74.

TOMAS, M., MARTINEZ-ALONSO, E., MARTINEZ-MARTINEZ, N., CARA-ESTEBAN, M. & MARTINEZ-MENARGUEZ, J. A. 2021. Fragmentation of the Golgi complex of dopaminergic neurons in human substantia nigra: New cytopathological findings in Parkinson's disease. *Histol Histopathol,* 36**,** 47-60.

TOMIOKA, M., STEAD, R. H., NIELSEN, L., COUGHLIN, M. D. & BIENENSTOCK, J. 1988. Nerve growth factor enhances antigen and other secretagogue-induced histamine release from rat peritoneal mast cells in the absence of phosphatidylserine. *J Allergy Clin Immunol,* 82**,** 599-607.

TSVILOVSKYY, V., SOLIS-LOPEZ, A., OHLENSCHLAGER, K. & FREICHEL, M. 2018. Isolation of Peritoneum-derived Mast Cells and Their Functional Characterization with Ca2+-imaging and Degranulation Assays. *J Vis Exp*.

UNGAR, D. & HUGHSON, F. M. 2003. SNARE protein structure and function. *Annu Rev Cell Dev Biol,* 19**,** 493-517.

VALENT, P., AKIN, C., HARTMANN, K., REITER, A., GOTLIB, J., SOTLAR, K., SPERR, W. R., DEGENFELD-SCHONBURG, L., SMILJKOVIC, D., TRIGGIANI, M., HORNY, H. P., AROCK, M., GALLI, S. J. & METCALFE, D. D. 2022. Drug-induced mast cell eradication: A novel approach to treat mast cell activation disorders? *J Allergy Clin Immunol,* 149**,** 1866-1874.

VARRICCHI, G., ROSSI, F. W., GALDIERO, M. R., GRANATA, F., CRISCUOLO, G., SPADARO, G., DE PAULIS, A. & MARONE, G. 2019. Physiological Roles of Mast Cells: Collegium Internationale Allergologicum Update 2019. *Int Arch Allergy Immunol,* 179**,** 247-261.

WAGNER, A., ALAM, S. B. & KULKA, M. 2023. The effects of age, origin, and biological sex on rodent mast cell (BMMC and MC/9) and basophil (RBL-2H3) phenotype and function. *Cell Immunol,* 391-392**,** 104751.

WANG, X. S., SAM, S. W., YIP, K. H. & LAU, H. Y. 2006. Functional characterization of human mast cells cultured from adult peripheral blood. *Int Immunopharmacol,* 6**,** 839-47.

WANG, Y., CHEN, Z., BA, T., PU, J., CHEN, T., SONG, Y., GU, Y., QIAN, Q., XU, Y., XIANG, K., WANG, H. & JIA, G. 2013. Susceptibility of young and adult rats to the oral toxicity of titanium dioxide nanoparticles. *Small,* 9**,** 1742-52.

WEIMERSHAUS, M., CARVALHO, C., RIGNAULT, R., WAECKEL-ENEE, E., DUSSIOT, M., VAN ENDERT, P., MACIEL, T. T. & HERMINE, O. 2023. Mast cell-mediated

inflammation relies on insulin-regulated aminopeptidase controlling cytokine export from the Golgi. *J Allergy Clin Immunol,* 151**,** 1595-1608 e6.
WELLER, C. L., COLLINGTON, S. J., WILLIAMS, T. & LAMB, J. R. 2011. Mast cells in health and disease. *Clin Sci (Lond),* 120**,** 473-84.
WENDELER, M. & SANDHOFF, K. 2009. Hexosaminidase assays. *Glycoconj J,* 26**,** 945-52.
WOLFREYS, K. & OLIVEIRA, D. B. 1997. Alterations in intracellular reactive oxygen species generation and redox potential modulate mast cell function. *Eur J Immunol,* 27**,** 297-306.
WOSKA, J. R., JR. & GILLESPIE, M. E. 2011. Small-interfering RNA-mediated identification and regulation of the ternary SNARE complex mediating RBL-2H3 mast cell degranulation. *Scand J Immunol,* 73**,** 8-17.
WOSKA, J. R., JR. & GILLESPIE, M. E. 2012. SNARE complex-mediated degranulation in mast cells. *J Cell Mol Med,* 16**,** 649-56.
WU, L. C. 2011. Immunoglobulin E receptor signaling and asthma. *J Biol Chem,* 286**,** 32891-7.
XIA, Y. C., SUN, S., KUEK, L. E., LOPATA, A. L., HULETT, M. D. & MACKAY, G. A. 2011. Human mast cell line-1 (HMC-1) cells transfected with FcepsilonRIalpha are sensitive to IgE/antigen-mediated stimulation demonstrating selectivity towards cytokine production. *Int Immunopharmacol,* 11**,** 1002-11.
XU, Y. & CHEN, G. 2015. Mast cell and autoimmune diseases. *Mediators Inflamm,* 2015**,** 246126.
YAMAMOTO, H., IDA, T., TSUTSUKI, H., MORI, M., MATSUMOTO, T., KOHDA, T., MUKAMOTO, M., GOSHIMA, N., KOZAKI, S. & IHARA, H. 2012. Specificity of botulinum protease for human VAMP family proteins. *Microbiol Immunol,* 56**,** 245-53.
YANG, B. G., KIM, A. R., LEE, D., AN, S. B., SHIM, Y. A. & JANG, M. H. 2023. Degranulation of Mast Cells as a Target for Drug Development. *Cells,* 12.
YANG, W., LEE, S., LEE, J., BAE, Y. & KIM, D. 2010. Silver nanoparticle-induced degranulation observed with quantitative phase microscopy. *J Biomed Opt,* 15**,** 045005.
YANG, Y., KIM, J., KIM, H. Y., RYOO, N., LEE, S., KIM, Y., RHIM, H. & SHIN, Y. K. 2015. Amyloid-beta Oligomers May Impair SNARE-Mediated Exocytosis by Direct Binding to Syntaxin 1a. *Cell Rep,* 12**,** 1244-51.
YANG, Y., KONG, B., JUNG, Y., PARK, J. B., OH, J. M., HWANG, J., CHO, J. Y. & KWEON, D. H. 2018. Soluble N-Ethylmaleimide-Sensitive Factor Attachment Protein Receptor-Derived Peptides for Regulation of Mast Cell Degranulation. *Front Immunol,* 9**,** 725.
YANG, Z. & MARSHALL, J. S. 2009. Zymosan treatment of mouse mast cells enhances dectin-1 expression and induces dectin-1-dependent reactive oxygen species (ROS) generation. *Immunobiology,* 214**,** 321-30.
YUN, H. J., PARK, J., HO, D. H., KIM, H., KIM, C. H., OH, H., GA, I., SEO, H., CHANG, S., SON, I. & SEOL, W. 2013. LRRK2 phosphorylates Snapin and inhibits interaction of Snapin with SNAP-25. *Exp Mol Med,* 45**,** e36.
ZHANG, H., THERRIAULT, J., KANG, M. S., NG, K. P., PASCOAL, T. A., ROSA-NETO, P., GAUTHIER, S. & ALZHEIMER'S DISEASE NEUROIMAGING, I. 2018. Cerebrospinal fluid synaptosomal-associated protein 25 is a key player in synaptic degeneration

in mild cognitive impairment and Alzheimer's disease. *Alzheimers Res Ther,* 10**,** 80.

ZHANG, S., MASUYER, G., ZHANG, J., SHEN, Y., LUNDIN, D., HENRIKSSON, L., MIYASHITA, S. I., MARTINEZ-CARRANZA, M., DONG, M. & STENMARK, P. 2017. Identification and characterization of a novel botulinum neurotoxin. *Nat Commun,* 8**,** 14130.